CHAPTER 6

FRACTAL PHYSIOLOGY, COMPLEXITY, AND THE FRACTIONAL CALCULUS

BRUCE J. WEST

Mathematical & Information Sciences Directorate, U.S. Army Research Office, Research Triangle Park, NC 27709, USA

CONTENTS

Fractals, Diffusion, and Relaxation in Disordered Complex Systems: A Special Volume of Advances in Chemical Physics, Volume 133, Part B, edited by William T. Coffey and Yuri P. Kalmykov. Series editor Stuart A Rice.

I. INTRODUCTION

The title of this chapter targets two central themes. The first theme is a modern view of physiology that explicitly takes into account the complexity of living systems, since physiology is that branch of biology that deals with the functions and activities of life and of living matter such as organs, tissues, or cells. Complexity in this context incorporates the recent advances in physiology concerned with the applications of the concepts ranging from fractal geometry, fractal statistics, and nonlinear dynamics to the formation of a new kind of understanding in the life sciences. The second theme has to do with a parallel development on understanding the dynamics of fractal processes. For a number of years the study of fractals was restricted to the determination of the fractal dimension of structure—in particular, the static structure of objects and the stationary structure of time series. However, now we explore the dynamics of fractal processes using the fractional calculus, applying this dynamical approach to both regular and stochastic processes. In our discussion we motivate the applications of the fractional calculus using physiological time series.

The fractal concept was formally introduced into the physical sciences by Benoit Mandelbrot over 20 years ago and has since then captured the imagination of a generation of scientists. Mandelbrot had, of course, been working on the development of the idea for over a decade before he was finally willing to expose his brainchild to the scrutiny of the scientific community at large. His monograph [1] brought together mathematical, experimental, and physical arguments that undermined the traditional picture of the physical world. It has been accepted that celestial mechanics and physical phenomena are, by and large, described by smooth, continuous, and unique functions, since before the time of Lagrange (1736–1813). This belief is part of the conceptual infrastructure of the physical sciences. The changes in physical processes are modeled by systems of dynamical equations, and the solutions to such equations are continuous and differentiable at all but a finite number of points. Therefore the phenomena being described by these equations were thought to have these properties of continuity and differentiability as well. Thus, the solutions to the equations of motion such as the Euler–Lagrange equations, or Hamilton's equations, are analytic functions, and such functions were thought to represent physical phenomena in general.

At the turn of the last century, there were two opposing points of view in physics regarding continuity: those held by the atomists and those held by the anti-atomists. The latter camp believed in the continuity of nature and saw no reason why matter should stop being divisible at the level of the atom and should, they reasoned, continue indefinitely to smaller and smaller scales. The

atomists, on the other hand, with the successes of the periodic table and the kinetic theory of gases, had Boltzmann as their chief proponent. Boltzmann was such an ''extreme'' atomist that he did not even accept the continuity of time. In his St. Louis lecture in 1904 he stated [2] the following:

> Perhaps our equations are only very close approximations to average values that are made up of much finer elements and are not strictly differentiable.

It is the atomist's view of the classical microscopic world and its influence on the macroscopic world that we endorse in this chapter.

From the phenomenological side, Mandelbrot called the accuracy of the traditional perspective into question, by pointing to the failure of the equations of physics to explain such familiar phenomena as turbulence and phase transitions. In his books [1,3], Mandelbrot catalogued and described dozens of physical, social, and biological phenomena that cannot be properly described using the familiar tenets of dynamics from physics. The functions required to explain these complex phenomena have properties that for 100 years had been thought to be mathematically pathological. Mandelbrot argued that, rather than being pathological, these functions capture essential properties of reality and are therefore better descriptors of the physical world than the traditional analytic functions of theoretical physics.

Living organisms are immeasurably more complicated than inanimate objects, so we do not have available fundamental laws and principles governing biological phenomena equivalent to those in physics. Some may object to this harsh characterization, but there are no equivalents of Newton's Laws, Maxwell's equations, and Boltzmann's Principle in physiology. Part of the goal of biophysics, in fact, is to seek out and establish the existence of such biological laws and relate them to known physical laws, so that both the physical and biological aspects of living matter can be better understood. In this chapter our aim is much more modest than identifying such fundamental biophysical principles; it is merely to present a strategy for understanding a diverse set of complex phenomena in physiology and suggest that this strategy reveals an underlying symmetry that can be exploited.

Schrödinger, in his book *What is Life?* [4], laid out his understanding of the connection between the world of microscopic and macroscopic based on the principles of equilibrium statistical physics. In that discussion he asked why atoms are so small relative to the dimension of the human body. The answer to this question is both immediate and profound. The high level of organization necessary for life is only possible in a macroscopic system; otherwise the order would be destroyed by microscopic (thermal) fluctuations. A living system must be sufficiently large to maintain its integrity in the presence of thermal fluctuations that disrupt its constitutive elements. Thus, macroscopic phenomena are characterized by averages over ensemble distribution functions characterizing

microscopic fluctuations. Consequently, any strategy for understanding physiology must be based on the probabilistic description of complex phenomena and, as we shall see, on our understanding of phenomena lacking characteristic scales.

There are three types of fractals that appear in the life sciences: geometrical fractals, which determine the spatial properties of the tree-like structures of the mammalian lung, arterial, and venous systems and other ramified structures [5]; statistical fractals, which determine the properties of the distribution of intervals in the beating of the mammalian heart, in breathing, in walking, and in the firing of certain neurons; and finally dynamical fractals, which determine the dynamical properties of systems having a large number of characteristic time scales. In the complex systems found in physiology, the distinctions between these three kinds of fractals blur, but we focus our attention on the dynamical rather than the geometrical fractals, in part, because the latter have been reviewed in a number of places and we have little to add to that understanding.

In this chapter we lay the foundation for how such concepts as complexity, fractals, diverging moments, nonlinear dynamics, and other related mathematical topics are used in understanding physiology. Of course, a number of books have been written about any one of these ideas—books for the research expert, books for the informed teacher, books for the struggling graduate student, and books for the intelligent lay person. Different authors stress different characteristics of complex phenomena, from the erratic data collected by clinical researchers to the fluctuations generated by deterministic dynamical equations used to model such systems. Some authors have painted with broad brushstrokes, indicating only the panorama that these concepts reveal to us, whereas others have sketched with painstaking detail the structure of such phenomena and have greatly enriched those that could follow the arguments. Herein we view our efforts midway between the two because *fractal physiology* is still a work in progress and much of what we present may prove to be irrelevant, whereas some of it might be even more significant than we can now appreciate.

II. SCALING IN PHYSIOLOGICAL TIME SERIES

We begin our discussion of physiological processes with an empirical study of the scaling behavior of time series obtained from the quantitative measurements of certain physiologic systems—for example, the cardiovascular and respiratory systems. We pursue this approach in order to convince the reader of the ubiquity of scaling in physiological time series. Once this property is established, we turn to the mathematical modeling of the mechanisms that generate such scaling. The attention is on scaling statistics because physiological measures are usually given to us in the form of time series. Whether it is the electrocardiogram (ECG) for the beating heart from which the interbeat intervals are extracted to determine heart rate variability (HRV) [6–8], the electrogastrogram (EGG) for gastric activity of

the stomach in which the contraction intervals are used to determine the gastric rate variability (GRV) [9], the stride intervals during walking that determines the stride rate variability (SRV) [10–13], or the interbreath interval which determines the breathing rate variability (BRV) [14], they all appear at first sight to be random processes with no underlying pattern. However, upon processing the data, they reveal long-term memory indicative of fractal time series, as we review in Section III.

A. Allometric Aggregation Data Analysis

Note that the term *scaling* denotes a power-law relation between two variables x and y,

$$y = Ax^{\alpha} \tag{1}$$

as Barenblatt [15] explained in his excellent inaugural lecture delivered before the University of Cambridge on May 3, 1993. He points out that such scaling laws are not merely special cases of more general relations; they never appear by accident; they always reveal self-similarity, a very important property of the phenomenon being studied. In biology, Eq. (1) is historically referred to as an allometric relation between the two observables.

Allometric relations are not new in science. Such relations were introduced into biology in the nineteenth century. Typically, an allometric relation interrelates two properties of a given organism. For example, the total mass of a deer y is proportional to the mass of the deer's antlers x raised to a specific power α. Thus, on doubly logarithmic graph paper, this relation would yield a straight line with a slope given by the power-law index. Huxley summarized the experimental basis for this relation in his 1931 book, *Problems of Relative Growth* [16], and developed the mathematics to describe and explain allometric growth laws. In biological systems, he reasoned, two parts of an organism grow at different rates, but the rates are proportional to one another. Consequently, how rapidly one part of the organism grows can be related to how rapidly the other part of the organism grows, and the ratio of the two rates is constant.

In this section the notion of an allometric relation is generalized to include measures of time series. In this view, y is interpreted to be the variance and x the average value of the quantity being measured. The fact that these two central measures of a time series satisfy an allometric relation implies that the underlying time series is a fractal random process and therefore scales. It was first determined empirically that certain statistical data satisfy a power-law relation of the form given by Taylor [17] in Eq. (1), and this is where we begin our discussion of the allometric aggregation method of data analysis.

Taylor was a scientist interested in biological speciation. For example, he was curious about how many species of beetle can be found over a given area of

land. He answered this question by sectioning off a large field into plots and in each plot sampling the soil for the variety of beetles that were present. This enabled him to determine the distribution in the number of new species of beetle spatially distributed across the field. From the distribution he could then determine the average number of species $\bar{X}$ and the variance in the number of species Var X. After this first calculation, he partitioned his field into smaller plots and redid his sampling, again determining the mean and standard deviation in the number of species at this increased resolution. This process was repeated a number of times, yielding a set of values of means and variances. In the ecological literature a graph of the logarithm of the variance versus the logarithm of the average value is called a *power curve*, which is linear in the logarithms of the two variables, and b is the slope of the curve. The algebraic form of the relation between the variance and mean is

$$\operatorname{Var} X = a\bar{X}^b \tag{2}$$

where the two parameters a and b determine how the variance and mean are related to one another.

Taylor was able to exploit the curves obtained from data in a number of ways using the slope and intercept parameters [17]. If the slope of the curve and the intercept are both equal to one, $a = b = 1$, then the variance and mean are equal to one another. This equality is only true for a Poisson distribution, which, when it occurred, allowed him to interpret the number of species as being randomly distributed over the field, with the number of species in any one plot being completely independent of the number of species in any other plot. If, however, the slope of the curve was less than unity, the number of species appearing in the plots was interpreted to be quite regular. The spatial regularity of the number of species, in this case, was compared with the trees in an orchard and given the name *evenness*. Finally, if the slope of the variance versus mean curve was greater than one, the number of new species was interpreted as being clustered in space, like disjoint herds of sheep grazing in a meadow.

Of particular interest to us here was the mechanism that Taylor and Taylor [18] postulated to account for the experimentally observed allometric relation:

> We would argue that all spatial dispositions can legitimately be regarded as resulting from the balance between two fundamental antithetical sets of behaviour always present between individuals. These are, repulsion behaviour, which results from the selection pressure for individuals to maximise their resources and hence to separate, and attraction behaviour, which results from the selection pressure to make the maximum use of available resources and hence to congregate wherever these resources are currently most abundant.

Consequently, they postulated that it is the conflict between the attraction and repulsion, migration and congregation, which produces the interdependence (scaling) of the spatial variance and the average population density.

We can now interpret Taylor's observations more completely because the kind of clustering he observed in the spatial distribution of species number, when the slope of the power curve is greater than one, is consistent with an asymptotic inverse power-law distribution of the underlying data set. Furthermore, the clustering or clumping of events is due to the fractal nature of the underlying dynamics. Willis, some 40 years before Taylor, established the inverse power-law form of the number of species belonging to a given genus [19]. Willis used an argument associating the number of species with the size of the area they inhabit. It was not until the decade of the 1990s that it became clear to more than a handful of experts that the relationship between an underlying fractal process and its space filling character obeys a scaling law [1,3]. It is this scaling law that is reflected in the allometric relation between the variance and mean.

It is possible to test the allometric relation of Taylor using computer-generated data. But before we do so, we note that Taylor and Woiwod [20] were able to extend the discussion from the stability of the population density in space, independent of time, to the stability of the population density in time, independent of space. Consequently, just as spatial stability, as measured by the variance, is a power function of the mean population density over a given area at all times, so too the temporal stability, as measured by the variance, is a power function of the mean population density over time at all locations. With this generalization in hand we can apply Taylor's ideas to time series.

The correlation of discrete time series data is here determined by grouping the data into aggregates of two or more of the original data points and calculating the mean and variance at each level of aggregation. Consider the jth data element of an aggregation of n-adjacent data points:

$$Y_j^{(n)} = \sum_{k=1}^{n-1} Y_{nj-k} \tag{3}$$

In terms of these new data the average is defined by

$$\bar{Y}^{(n)} \equiv \frac{1}{[N/n]} \sum_{j=1}^{[N/n]} Y_j^{(n)} = n\bar{Y}^{(1)} \tag{4}$$

For example, when $n = 3$ each value of the new variable, defined by Eq. (3), consists of the sum of three non-overlapping original data points, and the number

of new data points is given by [$N/3$], where the brackets denote the closest integer value and N is the original number of data points. The variance, for a mono-fractal random time series, is similarly given by [21]

$$\text{Var } Y^{(n)} = n^{2H}\text{Var } \bar{Y}^{(1)} \tag{5}$$

where the superscript (1) on the average variable indicates that it was determined using all the original data without aggregation, and the superscript (n) on the average variable indicates that it was determined using the aggregation of n-adjacent data points and H is referred to as the Hurst exponent. Thus, comparing Eq. (5) with Eq. (4), we obtain the allometric relation given by Eq. (2):

$$\begin{aligned}\text{Var } Y^{(n)} &\equiv \left(\frac{\bar{Y}^{(n)}}{\bar{Y}^{(1)}}\right)^{2H} \bar{Y}^{(1)} \\ &= a\bar{Y}^{(n)^b}\end{aligned} \tag{6}$$

with the parameters given by the theoretical values

$$a = \frac{\text{Var } Y^{(1)}}{\left(\bar{Y}^{(1)}\right)^b} \quad \text{and} \quad b = 2H \tag{7}$$

It is well established that the exponent in such scaling equations is related to the fractal dimension [21] D of the underlying time series by $D = 2 - H$, so that

$$D = 2 - b/2 \tag{8}$$

A simple mono-fractal time series, therefore, satisfies the power-law relation of the allometric form given by Eq. (2).

This allometric aggregation technique has been applied to a number of data sets implementing the method of linear regression using the equation

$$\log \text{Var } Y^{(n)} = \log \alpha + \beta \log \bar{Y}^{(n)} \tag{9}$$

Fitting the parameters α and β in Eq. (9) to time series data gives the best least-squares estimates of the parameters a and b in the allometric relation, respectively.

We find that the Gaussian distribution is a more useful exemplar for time series than is the Poisson distribution used by Taylor. In Fig. 1 we apply Eq. (9) to one million computer-generated data points with Gaussian statistics. The far left dot in Fig. 1 contains all the data in the calculation of the aggregated mean and variance so that $n = 1$ in Eq. (9); the next point to the right in the figure

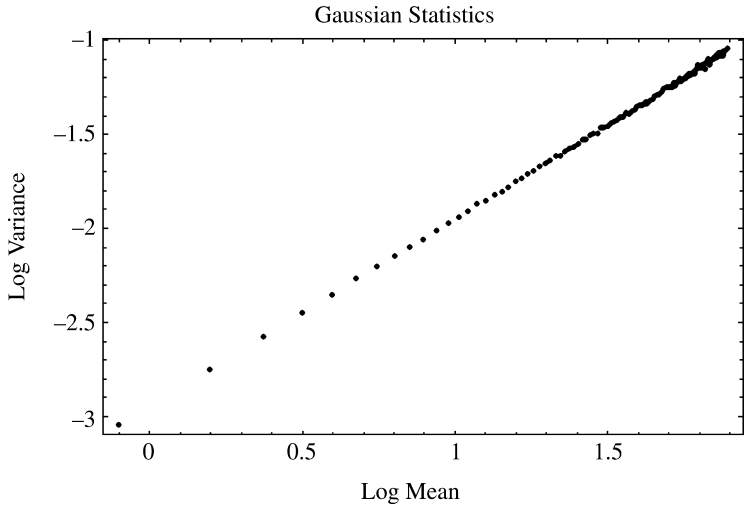

Figure 1. The logarithm of the variance is plotted versus the logarithm of the mean for the successive aggregation of 10^6 computer-generated random data points with Gaussian statistics. The slope of the curve is essentially one, determined by a linear regression using Eq. (9), so the fractal dimension of the time series is 1.5 using Eq. (8).

contains the nearest-neighbor data points added together to define a data set with 500,000 data points from which to calculate the aggregated mean and variance. Next we take the original data and add the three nearest-neighbor data points to define a data set with 333,333 data, and so on. The jth data element after aggregating n nearest-neighbor data points is given by Eq. (3). Consequently, this process of aggregating the data is equivalent to decreasing the resolution of the time series, and as the resolution is systematically decreased, the adopted measure, the relationship between the mean and variance, reveals an underlying property of the time series. The increase in the variance with increasing mean for increasing aggregation number shown in the figure is not an arbitrary pattern. The relationship indicates that the aggregated uncorrelated data points are interconnected. The original data points are not necessarily correlated, but the addition of data in the aggregation process induces a correlation, one that is completely predictable. The induced correlation is linear if the original data are uncorrelated, but not linear if the original data are correlated.

The aggregated variance versus the aggregated mean falls along a straight line in Fig. 1 with a slope of $b = 1$ for the uncorrelated random process with computer-generated Gaussian statistics. Therefore, in the case of Gaussian statistics, with $b = 1$, we have $D = 1.5$ corresponding to the fractal dimension of Brownian motion. In the same way, a completely correlated time series would

have $b = 2$, so that $D = 1$. The fractal dimension for most time series fall somewhere between the two extremes; the closer the fractal dimension is to one, the more regular the process; the closer the fractal dimension is to 1.5, the more it is like an uncorrelated random process. The Gaussian process depicted in Fig. 1 is certainly a mono-fractal in the sense we have defined it here; that is, the computer-generated time series is characterized by a single fractal dimension.

We point out here that the allometric aggregation method is just one of many procedures designed to take advantage of the scaling properties of the central moments of time series. We refer to such methods collectively as finite variance statistical methods (FVSM). However, it should be emphasized that not all time series that scale have finite variance. Time series having Lévy α-stable statistics exemplify processes with diverging variance, but they are described by probability density functions that scale. We review these matters after some discussion of the scaling properties of physiological time series.

B. Fractal Heartbeats

The mechanisms producing the observed variability in the size of a heart's interbeat intervals apparently arise from a number of sources. The sinus node (the heart's natural pacemaker) receives signals from the autonomic (involuntary) portion of the nervous system which has two major branches: the parasympathetic, whose stimulation decreases the firing rate of the sinus node, and the sympathetic, whose stimulation increases the firing rate of the sinus node pacemaker cells. The influence of these two branches produces a continual tug-of-war on the sinus node, one decreasing and the other increasing the heart rate. It has been suggested that it is this tug-of-war that produces the fluctuations in the heart rate of healthy subjects, but alternate suggestions will be pursued subsequently. Consequently, heart rate variability (HRV) provides a window through which we can observe the heart's ability to respond to normal disturbances that can affect its rhythm. The clinician focuses on retaining the balance in regulatory impulses from the vagus nerve and sympathetic nervous system and in this effort requires a robust measure of that balance [22]. A quantitative measure of HRV time series, such as the fractal dimension, serves this purpose.

HRV time series have become very well known over the past two decades as a quantitative indicator of autonomic activity. The medical community became interested in developing such an indicator of heart rate because experiments indicated a relationship between lethal arrhythmias and such activity. The importance of HRV to medicine became widely apparent when a task force was formed by the *Board of the European Society of Cardiology* and the *North American Society of Pacing and Electrophysiology* and was charged with the responsibility of developing the standards of measurement, physiological interpretation and clinical use of HRV. The task force published their findings in

1996 [22]. It is one of the few times that the members of such a task force were drawn from the fields of mathematics, engineering, physiology and clinical medicine in recognition of the complexity of the phenomenon they were charged to investigate and actually worked together.

When heart rate is atypical, say 120 bpm, in contrast to its usual 60 bpm, quantifying the variation in heart rate becomes very important. The degree of deviation from normality is determined by the interpretation of the size of the variation and how it is used to identify associated patterns. There are a number of ways to assess HRV, some 16 in all, each related to scaling in one way or another and most being FVSM, but we do not want to go into all of them here. Instead we identify the quantity that is the most revealing of the nature of HRV, but again we shall not go into a detailed discussion of the many ways of estimating this quantity. Instead we present a single explanatory technique that is relatively straightforward and that allows us to introduce the measure of interest. We use the allometric aggregation technique on real data to relate the variance and mean, as we discussed.

Now we apply the allometric aggregation approach to the beat-to-beat intervals shown in Fig. 2, a typical HRV time series for a healthy young adult male. The data points in the figure are connected to aid in visualizing how the time intervals between heartbeats are changing. It is evident that the variation in the time intervals between heartbeats is relatively small, the mean being 1.0 s and the standard deviation being 0.06 s. This modest variance supports the frequently used

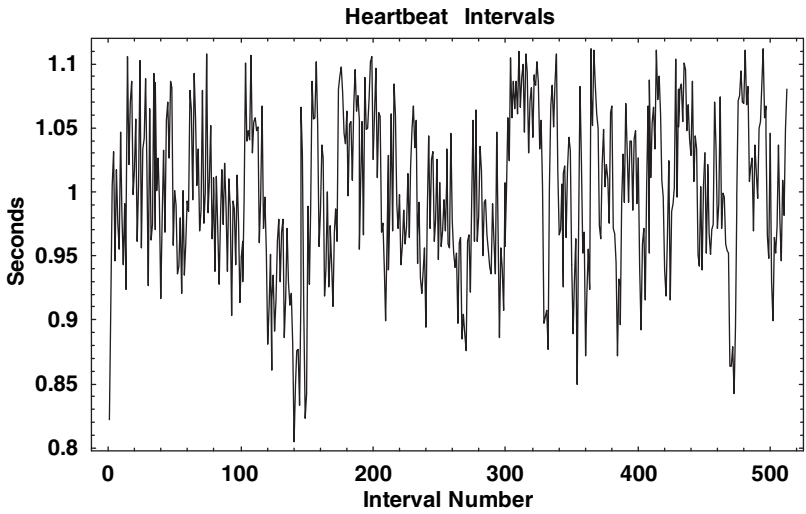

Figure 2. The time series of heartbeat intervals of a healthy young adult male is shown. It is clear that the variation in the time interval between beats is relatively modest, but certainly not negligible.

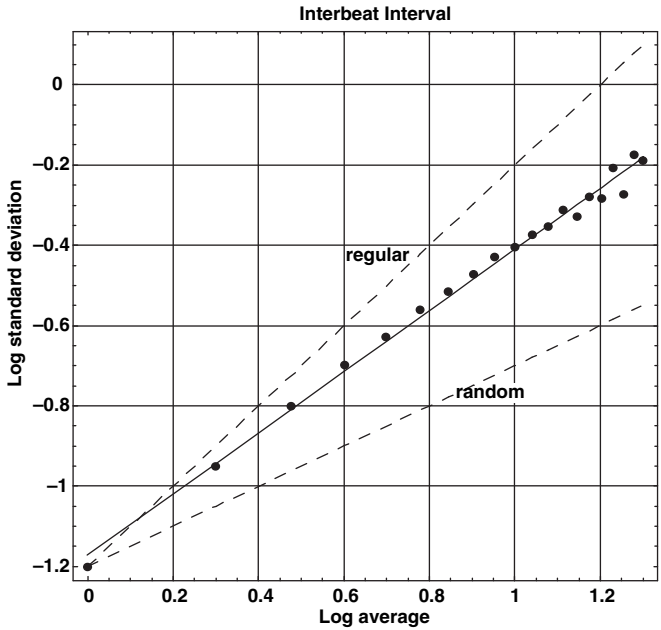

Figure 3. The logarithm of the standard deviation is plotted versus the logarithm of the average value for the heartbeat interval time series for a young adult male, using sequential values of the aggregation number. The solid line is the best fit to the aggregated data points and yields a fractal dimension of $D = 1.24$ midway between the curve for a regular process and that for an uncorrelated random process as indicated by the dashed curves.

medical term "normal sinus rhythm." So the question of what is learned by applying the allometric aggregation technique to these data and constructing the standard deviation and mean as a function of aggregation number, becomes important.

In Fig. 3 the logarithm of the standard deviation is plotted versus the logarithm of the mean value for the HRV time series depicted in Fig. 2. Note that we use the standard deviation in the figure and not the variance used in the discussion of Taylor's Law. We use the standard deviation because we are primarily interested in whether the time series is fractal or not and not particularly in the actual value of the fractal dimension. At the leftmost position the data point indicates the standard deviation and mean, using all the data points. Moving from left to right, the next data point is constructed from the time series with two nearest-neighbor data points added together, and the procedure is repeated moving right until the rightmost data point has 20 nearest-neighbor data points added together. The solid line is the best linear representation of the scaling and intercepts most of the data points with a positive slope of 0.76. We can see that the slope of the HRV data is *midway*

between the dashed curves depicting an uncorrelated random process (slope = 1/2) and one that is deterministically regular (slope = 1).

We emphasize that the conclusions we draw here are not from this single figure or set of data presented; these are only representative of a much larger body of work. The conclusions are based on a large number of similar observations [23,24] made using a variety of data processing techniques, all of which yield results consistent with the scaling of the HRV time series indicated in Fig. 3. So we conclude that the heartbeat intervals do not form an uncorrelated random sequence. Instead we see that the HRV time series is a statistical fractal, indicating that the heartbeats have a long-time memory. The implications of this long-time memory concerning the underlying physiological control system will be taken up later when we discuss the mathematical models of these phenomena.

Phenomena obeying a scaling relation, such as shown for the HRV time series data in Fig. 3, are said to be self-similar. The fact that the standard deviation and mean values change as a function of aggregation number implies that the magnitudes of the standard deviation and mean values depend on the size of the ruler used to measure the time interval. Recall that this is one of the defining characteristics of fractal curves; the length of the curve becomes infinite as the size of the ruler goes to zero. The dependence of the mean and standard deviation on the ruler size, for a self-similar time series, implies that the statistical process is fractal and consequently defines a fractal dimension for the HRV time series.

The average scaling exponent obtained by Peng et al. [25] for a group of 10 healthy subjects having a mean age of 44 years, using 10,000 data points for each subject, was $\alpha = 0.19$ for the difference in heartbeat interval time series. They interpreted this value to be consistent with a theoretical value of $\alpha = 0$, which they conjectured would be obtained for an infinitely long time series. The latter scaling implies that the scaling exponent for the beat intervals themselves would be 1.0. However, all data sets are finite, and it was determined that the asymptotic scaling coefficients for the heartbeat interval time series of healthy young adults lie in the interval $0.7 \leq \alpha \leq 1.0$. The value of the scaling coefficient obtained using much shorter time series and the relatively simple processing technique of allometric aggregation is consistent with these results.

We also comment on certain speculations made by Peng et al. [25] regarding their analysis of the set of HRV time series; speculations that have been supported by subsequent research. They suggested that the scaling behavior is adaptive for two reasons:

(i) The long-range correlations serve as an organizing principle for highly complex, nonlinear processes that generate fluctuations on a wide range of time scales.

(ii) The lack of a characteristic scale helps prevent excessive mode-locking that would restrict the functional responsiveness of the organism.

C. Fractal Breathing

Breathing is a function of the lungs, whereby the body takes in oxygen and expels carbon dioxide. The smooth muscles in the bronchial tree are innervated by sympathetic and parasympathetic fibers, much like the heart, and produce contractions in response to stimuli such as increased carbon dioxide, decreased oxygen, and deflation of the lungs. Fresh air is transported through some 20 generations of bifurcating airways of the lung, during inspiration, down to the alveoli in the last four generations of the bronchial tree. At this tiny scale there is a rich capillary network that interfaces with the bronchial tree for the purpose of exchanging gases with the blood.

In this section we are interested in the dynamics of breathing; the apparently regular breathing as you sit quietly reading this paper. Here evolution's design of the lung may be closely tied to way in which the lung carries out its function. It is not by accident that the cascading branches of the bronchial tree become smaller and smaller, nor is it good fortune alone that ties the dynamics of our every breath to this biological structure. We argue that, like the heart, the lung is made up of fractal processes, some dynamic and others now static. However, both kinds of processes lack a characteristic scale, and a simple argument establishes that such lack of scale has evolutionary advantages [26].

An early application of fractal analysis was made by Szeto et al. [27] to fetal lamb breathing. The changing patterns of breathing in 17 fetal lambs and the clusters of faster breathing rates, interspersed with periods of relative quiescence, suggested to them that the breathing process was self-similar. The physiological property of self-similarity implies that the structure of the mathematical function describing the time series is repeated on progressively finer time scales. Clusters of faster rates were seen within the fetal breathing data, what Dawes et al. [28] called breathing episodes. When the time series were examined on even finer time scales, clusters could be found within these clusters, and the signature of this scaling behavior emerged as an inverse power-law distribution of time intervals. Consequently, the fractal scaling was found to reside in the statistical properties of the fluctuations and not in the geometrical properties of the dynamic variable.

As with the heart, the variability of breathing rate using breath-to-breath time intervals is denoted by breathing rate variability (BRV), to maintain a consistent notation. Examples of HRV and BRV time series data on which scaling calculations are based are shown in Fig. 4. A typical BRV time series for a senior citizen at rest is shown at the top of the figure; the simultaneous HRV time series for the same person is depicted at the bottom of the figure. Because

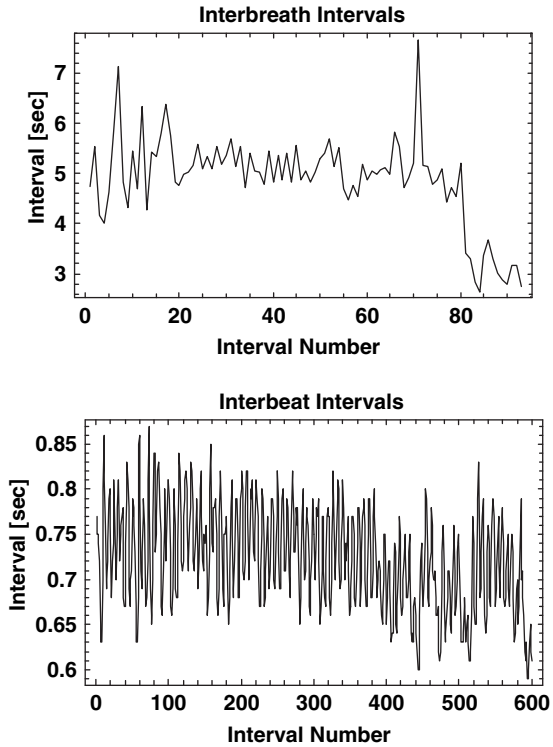

Figure 4. Typical time series from one of the 18 subjects in the study conducted by West et al. [14], while at rest, is shown for the interbreath intervals (BRV) and the interbeat intervals (HRV) time series.

heart rate is higher than respiration rate, in the same measurement epoch there is a factor of five more data for the HRV time series than there is for the BRV time series. These data were collected under the supervision of Dr. Richard Moon, the Director of the Hyperbaric Laboratory at Duke Medical Center. Looking at these two time series together, one is struck by how different they appear. It is not apparent that both physiological phenomena scale in essentially the same way, but they do [14].

The allometric aggregation method applied to the various time series obtained by West et al. [14] yields the typical results depicted in Fig. 5, where the logarithms of the aggregated variance versus the aggregated means are plotted for the HRV and BRV data depicted in Fig. 4. At the extreme left of each graph in Fig. 5 ($m = 1$), all the data points are used to calculate the variance and mean, and at the extreme right the aggregated quantities use $m = 10$ data points. Note that we stop the aggregation at 10 points because of

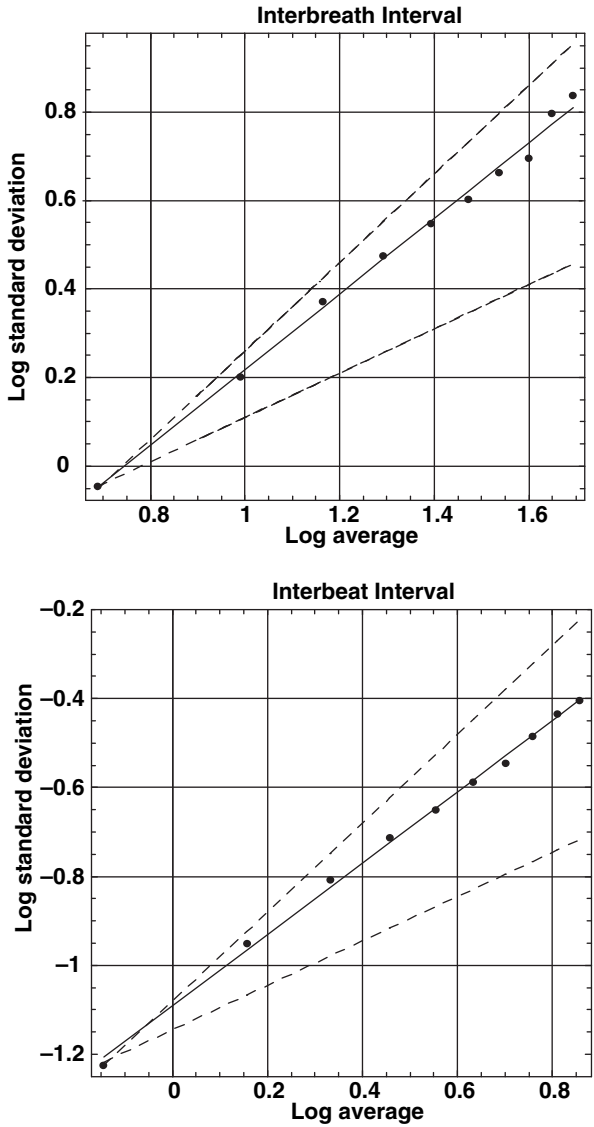

Figure 5. A typical fit to the aggregated variance versus the aggregated mean for BRV and HRV time series obtained by West et al. [14]. The points are calculated from the data and the solid curve is the best least-square fit to the data. The upper curve is the fit to the BRV data (slope = 0.86), and the lower curve is the best fit to the HRV data (slope = 0.80). It is evident from these two graphs that the allometric relation given by Eq. (9) does indeed fit both data sets extremely well and lies well within the regular and random boundaries, indicated by the dashed curves.

the small number of data in the breathing sequence. The solid curve at the top of Fig. 5 is the best least-square fit to the aggregated BRV data and has a slope of 0.86, which is the scaling index. A similar graph is constructed for the HRV data in the lower curve, where we obtain a slope of 0.80 for the scaling index.

The scaling index of both the HRV and BRV time series increase with increasing levels of exercise, but the data are not shown here, mainly because we can't show everything all the time. The 18 subjects in the experiment rode a stationary bicycle with various levels of load on the wheels to mimic cycling uphill. The breathing rate, breathing volume, and heart rate were monitored for each of the individuals in the study. The consistent result was that as the level of exercise increased, the amount of variability in both HRV and BRV decreased, indicating that the associated time series were becoming more ordered. This increase in scaling index was determined to be statistically significant [14]. The scaling indices and fractal dimensions obtained from these curves are consistent with the results obtained by other researchers.

Such observations regarding the self-similar nature of breathing time series have been used in a medical setting to produce a revolutionary way of utilizing mechanical ventilators. Historically, ventilators have been used to facilitate breathing after an operation and have a built-in frequency of ventilation. The single-frequency ventilator design has recently been challenged by Mutch et al. [29], who have used an inverse power-law spectrum of respiratory rate to drive a variable ventilator. They demonstrated that this way of supporting breathing produces an increase in arterial oxygenation over that produced by conventional control-mode ventilators. This comparison indicates that the fractal variability in breathing is not the result of happenstance, but is an important property of respiration. A reduction in variability of breathing reduces the overall efficiency of the respiratory system.

Altemeier et al. [30] measured the fractal characteristics of ventilation and determined that not only are local ventilation and perfusion highly correlated, but they scale as well. Finally, Peng et al. [31] analyzed the BRV time series for 40 healthy adults and found that under supine, resting, and spontaneous breathing conditions, the time series scale. This result implies that human BRV time series have "long-range (fractal) correlations across multiple time scales."

Some particularly long records of breathing were made by Kantelhardt et al. [32], for 29 young adults participating in a sleep study where their breathing was recorded during REM sleep, non-REM sleep, and periods of being awake. They showed that the stages of healthy sleep (deep, light, and REM) have different autonomic regulation of breathing. During deep or light sleep, both of which are non-REM, the scaling index was determined to be $\alpha = 1/2$ and consequently the BRV time series was essentially an uncorrelated random process. On the other hand, during REM sleep and during periods of wakefulness, the scaling index was

found to be in the interval $0.9 \leq \alpha \leq 0.8$, so that the BRV time series has a long-time memory.

Webber [33] also investigated the nonlinear physiology of breathing, pointing out that the central rhythm and pattern generators within the brainstem/spinal cord are subject to afferent feedback and suprapontine feed-forward inputs of varying coupling strengths. In short, there are multiple signals that influence one another in the respiratory controller, and the dynamics are nonlinear; that is, a given response is not proportional to a given stimulus. But putting this aside for the moment, Webber applied a number of techniques from nonlinear dynamics systems theory to the analysis of breathing. He recorded 4500 consecutive respiratory cycles for the spontaneous breathing patterns of anaesthetized, unrestrained rats (10 in all). He then constructed phase-space plots using continuous thoracic pressure fluctuations. His plots reveal patterns in the breathing data that are consistent with chaos and fractal time series.

D. Fractal Gait

Walking is one of those things we do without giving it much thought, day in and day out. We walk confidently with a smooth pattern of strides and without apparent variation in gait. This seeming lack of pattern is remarkable considering that the motion of walking is created by the loss of balance, as pointed out by Leonardo da Vinci (1452–1515) in his treatise on painting. da Vinci considered walking to be a sequence of fallings; consequently, it should come as no surprise that there is variability in this sequence of falling intervals, even if such variability is usually masked.

The regular gait cycle, so apparent in everyday experience, is not as regular as we believed. Gait is no more regular than is normal sinus rhythm or breathing. The subtle variability in the stride characteristics of normal locomotion were first discovered by the nineteenth-century experimenter Vierordt [34], but his findings were not exploited for over 120 years. The random variability he observed was so small that the biomechanical community has historically considered these fluctuations to be an uncorrelated random process. In practice this means that the fluctuations in gait were thought to contain no information about the underlying motorcontrol process. The follow-up experiments to quantify the degree of irregularity in walking was finally done in the middle of the last decade by Hausdorff et al. [35] and involved observations of healthy individuals, as well as of subjects having certain diseases that affect gait and also the elderly. Additional experiments and analyses that both verified and extended the earlier results were subsequently done by West and Griffin [11,36].

Human gait is a complex process, since the locomotor system synthesizes inputs from the motor cortex, the basal ganglia, and the cerebellum, as well as

feedback from vestibular, visual, and proprioceptive sources. The remarkable feature of this complex phenomenon is that although the stride pattern is stable in healthy individuals, the duration of the gait cycle is not fixed. Like normal sinus rhythm in the beating of the heart, where the intervals between successive beats change, the time interval for a gait cycle fluctuates in an erratic way from step to step. The gait studies carried out to date concur that the fluctuations in the stride-interval time series exhibit long-time inverse power-law correlations indicating that the phenomenon of walking is a self-similar fractal activity.

Walking consists in a sequence of steps, and the corresponding time series is made up of the time intervals for these steps. These steps may be partitioned into two phases: a stance phase and a swing phase. It has been estimated, using blood flow to skeletal muscles, that the stance phase muscles consume three times the energy as do the swing phase muscles, independently of speed [37]. The stance phase is initiated when a foot strikes the ground and ends when it is lifted. The swing phase is initiated when the foot is lifted and ends when it strikes the ground again. The time to complete each phase varies with the stepping speed. A stride interval is the length of time from the start of one stance phase to the start of the next stance phase. It is the variability in the time series made from these intervals that is probed in this analysis of the stride interval time series.

One definition of the gait cycle or stride interval is the time between successive heel strikes of the same foot [10]. An equivalent definition of the stride interval uses successive maximum extensions of the knee of either leg [36]. The stride interval time series for a typical subject is shown in Fig. 6, where it is seen that the variation in time interval is on the order of 3–4%, indicating that the stride pattern is very stable. The stride interval time series is referred to as stride rate variability (SRV) for name consistency with the other two time series we have discussed. It is the stability of SRV that has historically led investigators to decide that not much could go wrong by assuming that the stride interval is constant and that the fluctuations are merely biological noise. The second set of data in Fig. 6 is computer-generated Gaussian noise, having the same mean and standard deviation as the experimental data. Note that it is not easy to distinguish between the two data sets. However, the experimental data fluctuate around the mean gait interval and, although small, are non-negligible because they indicate an underlying complex structure and, as we show, these fluctuations cannot be treated as an uncorrelated random noise.

Using a 15-minute SRV time series, from which the data depicted in Fig. 6 were taken, we apply the allometric aggregation procedure to determine the relation between the standard deviation and mean of the time series as shown in Fig. 7. In the latter figure, the curve for the SRV data is, as we did with the other data sets, contrasted with an uncorrelated random process (slope $= 0.5$) and a regular deterministic process (slope $= 1.0$). The slope of the data curve is 0.70,

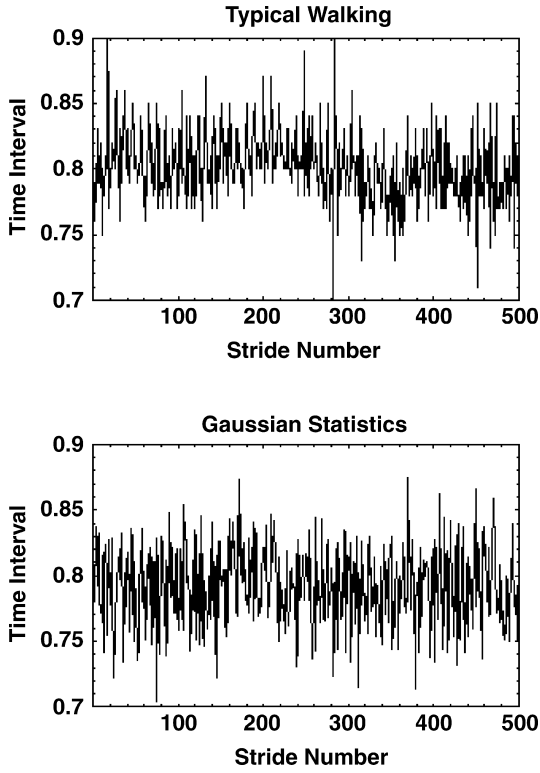

Figure 6. Real data compared with computer-generated data. At the top, the time interval between strides for the first 500 steps made by a typical walker in an experiment [36] is depicted. At the bottom a computer-generated time series having uncorrelated Gaussian statistics is shown, with the same mean and variance as in the data shown at the top.

midway between the two extremes of regularity and uncorrelated randomness. So, as in the cases of HRV and BRV time series, we again find the erratic physiological time series to represent a random fractal process.

In a previous section we argued that if the power-law index, the slope of the aggregated variance versus aggregated average curve on a log–log graph, is greater than one, then the data are clustered. In the SRV context, indicated by a slope greater than the random dashed line, this clustering indicates that the intervals between strides change in clusters and not in a statistically uniform manner over time. This result suggests that the walker does not smoothly adjust his/her stride from step to step. Rather, there are a number of steps over which adjustments are made followed by a number of steps over which the changes in stride are completely random. The number of steps in the adjustment process and the number of steps between adjustment periods are not independent. The

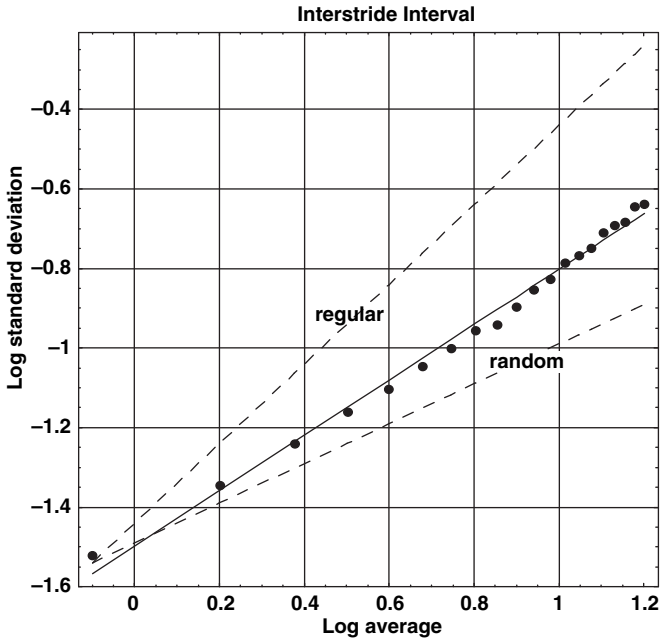

Figure 7. The SRV data for a typical walker in the experiment [36] is used to construct the aggregated variance and mean as indicated by the dots. The logarithm of the aggregated variance is plotted versus the logarithm of the aggregated mean, starting with all the data points at the lower left to the aggregation of 20 data points at the upper right. The SRV data curve lies between the extremes of uncorrelated random noise (lower dashed curve) and a regular deterministic process (upper dashed curve) with a fractal dimension of $D = 1.30$.

results of a substantial number of stride interval experiment supports the universality of this interpretation.

The SRV time series for 16 healthy adults were downloaded from *PhysioNet* and the allometric aggregation procedure carried out. Each of the curves looked more or less like that in Fig. 7, with the experimental curve being closer to the indicated regular or the random limits (dashed curves). On average, the 16 individuals have fractal dimensions for gait in the interval $1.2 \leq D \leq 1.3$ and an average correlation on the order of 40% [38]. The fractal dimension obtained from the analysis of an entirely different dataset, obtained using a completely different protocol, yields consistent results [36]. The narrowness of the interval around the fractal dimension suggests that this quantity may be a good quantitative measure of an individual's dynamical variability. We suggest the use of the fractal dimension as a quantitative measure of how well the motor control system is doing in regulating locomotion. Furthermore, excursions

outside the narrow interval of fractal dimension values for apparently healthy individuals may be indicative of hidden pathologies.

Further analysis was done on the SRV time series of 50 children, also downloaded from *PhysioNet*. One of the features of the time series were large excursions in the fractal dimension for children under the age of five, $1.12 \leq D \leq 1.36$, unlike the narrower range of values for mature adults. The interval expands from 0.08 for adults to 0.24 for children, a factor of three decrease of the interval from childhood to adulthood. It is clear that the average fractal dimension over each group is the same, approximately 1.24, but the range of variation in the fractal dimension decreases significantly with age [38]. This would seem to make the fractal dimension an increasingly reliable indicator of the health of the motorcontrol system with advancing age.

It should not go unnoticed that people use pretty much the same control system when they are standing still, maintaining balance, as they do when they are walking. This observation would lead one to suspect that the body's slight movements around the center of mass of the body—that fictitious point at which all of the body's mass is located in any simple model of locomotion—would have the same statistical behavior as that observed during walking. These tiny movements are called postural sway in the literature and have given rise to papers with such interesting titles as "Random walking during quiet standing" by Collins and De Lucca [39]. It has been determined that postural sway is really chaotic [40], so one might expect that there exists a relatively simple dynamical model for balance regulation that can be used in medical diagnosis. Here again the fractal dynamics can be determined from the scaling properties of postural sway time series, and it is determined that a decrease of postural stability is accompanied by an increase of fractal dimension.

E. Fractal Neurons

Up to this point the discussion has been focused primarily on time series generated by various complex physiological phenomena. Now let us examine a class of basic building blocks used to construct these phenomena, the individual neurons in the various control systems of the body. The neuron is in most respects quite similar to other cells in that it contains a nucleus and cytoplasm. However, it is distinctive in that long, threadlike tendrils emerge from the cell body, and those numerous projections branch out into still finer extensions. These are the dendrites that form a branching tree of ever more slender threads not unlike the fractal trees discussed by West and Deering [5]. One such thread does not branch and often extends for several meters even though it is still part of a single cell. This is the axon that is the nerve fiber in the typical nerve. Excitations in the dendrites always travel toward the cell body in a living system, whereas excitations in the axon always travel away from the cell body.

The activity of a nerve is invariably accompanied by electrical phenomena. The first systematic observation of this effect was made by Luigi Galvani in 1791. He observed that when a muscle (frog's leg) was touched with a scalpel and a spark was drawn nearby, but not in direct physical contact with the scalpel, the muscle contracted. In 1852 the German physician/physicist Helmholtz first measured the speed of the nerve impulse by stimulating a nerve at different points and recording the time it took the muscle to which it was connected to respond. Electrical impulses are observed along the corresponding axon, whether it is an external excitation of a nerve or the transmission of a message from the brain. The properties of individual nerves seem to be ubiquitous because there is apparently no fundamental difference in structure, chemistry, or function between the neurons and their interconnections in humans and those in a squid, a snail, or a leach. However, neurons do vary in size, position, shape, pigmentation, firing patterns, and chemical substances by which they transmit information to other cells.

There are two different ways in which neurons can be fractal. The first way is through their geometrical structure. The shape of nerve cells may be fractal in space just as observed for the cardiac conduction system and the architecture of the lung [5]. The fractal dimension has been used to classify the different shapes of neurons and to suggest mechanisms of growth responsible for these shapes. The second way neurons can be fractal is through the time intervals between the action potentials recorded from nerves, again as was observed for the interbeat interval distribution in cardiac time series, the interbreath interval distribution for breathing, and the interstride interval for walking discussed herein. The statistical properties of these time intervals have the same strange properties observed earlier, in that collecting more data does not improve the accuracy of the statistical distribution of the intervals measured for some neurons as characterized by the width of the distribution. The realization that the statistics of these intervals are fractal helps in understanding these surprising properties. Bassingthwaighte et al. [21] review how the fractal dimension can be used to classify neurons into different functional types.

The statistical properties of the time intervals between action potentials display three different types of distributions: (1) Some neurons are well described by a *Poisson process*, in which the probability that there is an action potential in a time interval Δt is proportional to Δt. The durations of subsequent intervals between action potentials are statistically independent of one another. (2) Some neurons fire almost, but not exactly, at a constant rhythm. The time series for the action potentials in this case are well described by a *Gaussian model*, where the intervals have a small dispersion around the mean value. (3) Some neurons show self-similar fractal patterns on the *scaled interval distributions*. In the last case, neurons occasionally have very long intervals between action potentials. These long intervals occur with sufficient frequency

so that they can be the most important in the determination of the average interval length. As more and more data are collected, longer and longer intervals are found. Thus, the average interval increases with the duration of the data record analyzed, in such a way that if an infinitely long record could be analyzed, then the average interval would be infinite. Such infinite moments are characteristic of a type of stable statistical fractal process called a Lévy process [5].

Gernstein and Mandelbrot [41] were the first to quantitatively analyze the scaling properties of neuronal action potentials, and from their analysis a number of conclusions were drawn. The first conclusion concerns the fact that, as more data were analyzed, the values found for the average interval and the variance in the average increase. That is, in the limit of an infinitely long data record, both the mean and its variance could become infinite. Since the variance is, in principle, infinite, the averages measured for different segments of the same data record may be markedly different. It is commonly thought that if moments, such as the average, measured from data are constant in time, then the parameters of the process that generate the data are constant, and that if these moments vary, then the parameters that generate the data also vary. This commonly held notion is wrong, as stressed by Gernstein and Mandelbrot. Processes, especially fractal processes, where the generating mechanism remains unchanged can yield time series whose moments, such as the average, vary with time. The second conclusion concerns the fact that as additional data are analyzed, increasingly long intervals are found. Hence the inclusion of these intervals increases rather than decreases the variance in the measured distribution. That is, the statistical irregularities in the measured distribution become larger as more data are collected. As stated by Gernstein and Mandelbrot [41]:

> Thus, in contradiction to our intuitive feelings, increasing the length of available data for such processes does not reduce the irregularity and does not make the sample mean or sample variance converge.

Action potentials can be recorded from the primary auditory neurons that transmit information about sound and from the pulse vestibular neurons that transmit information about head position to the brain. Fractal behavior is ubiquitous in these and other such sensory systems [42]. Without including the references given by Teich et al. [42], we quote their review of the evidence for this observation:

> Its presence has been observed in cat striate-cortex neural spike trains, and in the spike train of a locust visual interneuron, the descending contralateral movement detector. It is present in the auditory system of a number of species; primary auditory (VIII-nerve) nerve fiber in the cat, the chinchilla, and the chicken all exhibit fractal behavior. It is present at many biological levels, from the

microscopic to the macroscopic; examples include ion-channel behavior, neurotransmitter exocytosis at the synapse, spike trains in rabbit somatosensory-cortex neurons, spike trains in mesencephalic reticular-formation neurons, and even the sequence of human heartbeats. In almost all cases the upper limit of the observed time over which fractal correlations exist is imposed by the duration of the recording.

It would probably be considered bad form in a discussion of neurons and action potentials if we did not comment on the electrical properties of the human brain. It has been known for well over a century that the activity of a nerve is based on electrical phenomena and that the mammalian brain generates a small but measurable electrical signal. The electroencephalograms (EEGs) of small animals were measured by Caton in 1875, and those of humans were measured by Berger in 1925. The mathematician N. Wiener thought that *generalized harmonic analysis* would provide the mathematical tools necessary to penetrate the mysterious relations between EEG time series and the functioning of the brain. The progress along this path has been slow, and the understanding and interpretation of EEG's remains quite elusive. After 130 years, one can only determine intermittent correlations between the activity of the brain and that found in EEG records. There is no taxonomy of EEG patterns that delineates the correspondence between those patterns and brain activity.

It probably bears repeating that the traditional methods of analyzing EEG time series rely on the paradigm that all temporal variations consist of a superposition of harmonic and periodic vibrations, in the tradition of Wiener. The attractor reconstruction technique reinterprets the time series as a multidimensional geometrical object generated by a deterministic dynamical process in phase space. If the dynamics are reducible to deterministic laws, then the phase portraits of the system converge toward a finite region of phase space containing an attractor. Figure 8 shows EEG time series for a variety of brain states, including quiet resting with eyes open and closed, three stages of sleep, and a petit mal epileptic seizure. Adjacent to each of these time series is depicted a projection of the EEG attractor onto a two-dimensional subspace using the attractor reconstruction technique [43].

The brain wave activity of an individual during various stages of sleep is depicted in Fig. 8. Here the standard division of sleeping into four stages is used. In stage one, the individual drifts in and out of sleep. In stage two, the slightest noise will arouse the sleeper, whereas in stage three a loud noise is required. The final stage, level four, is one of deep sleep. This is the normal first sequence of stages one goes through during a sleep cycle. Afterwards the cycle is reversed back through stages three and two, at which time dreams set in and the individual manifests rapid eye movement (REM). The dream state is followed by stage two, after which the initial sequence begins again. It is clear that whatever the form of the cognitive attractor, if such an object exists, it is not static but varies with the

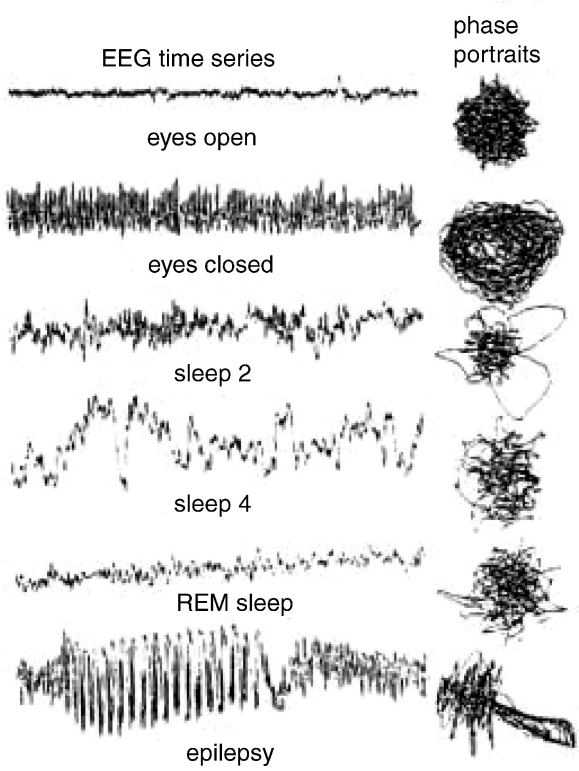

Figure 8. Typical episodes of the electrical activity of the human brain as recorded from the electroencephalogram (EEG) time series together with the corresponding phase space portraits. The portraits are two-dimensional projections of the actual attractors. (From Babloyantz and Destexhe [43] with permission.)

level of sleep. In fact, the fractal dimension decreases as sleep deepens, from a fractal dimension of eight during REM to half that in deep sleep level four [43]. The dimension drops further, to a value of approximately two, during petit mal epileptic seizure. The seizure corresponds to highly organized discharges between the right and left hemispheres of the brain.

III. DYNAMICAL MODELS OF SCALING

The physiological time series processed in the previous section clearly show that the complex phenomena supporting life, although they appear to be random, do in fact scale in time. This scaling indicates that the fluctuations that occur on multiple time scales are tied together, and the way we understand such interdependency in the physical sciences is through underlying mechanisms

that are coupled one to the other. This coupling is typically done through the equations of motion governing the dynamical description of the process. Unfortunately, we do not have the dynamic equations to describe the physiologic phenomena in which we are interested. Therefore we must take a more phenomenological tack and develop mathematical models to explain the data based on heuristic reasoning. However, to start we need to know the formal properties of the models we propose to use.

The best physical model is the simplest one that can "explain" all the available experimental time series, with the fewest number of assumptions. Alternative models are those that make predictions and which can assist in formulating new experiments that can discriminate between different hypotheses. We start our discussion of models with a simple random walk, which in its simplest form provides a physical picture of diffusion—that is, a dynamic variable with Gaussian statistics in time. Diffusive phenomena are shown to scale linearly in time and generalized random walks including long-term memory also scale, but they do so nonlinearly in time, as in the case of anomalous diffusion. Fractional diffusion operators are used to incorporate memory into the dynamics of a diffusive process and leads to fractional Brownian motion, among other things. The continuum form of these fractional operators is discussed in Section IV.

The continuous limit of a simple random walk model leads to a stochastic dynamic equation, first discussed in physics in the context of diffusion by Paul Langevin. The random force in the Langevin equation [44], for a simple dichotomous process with memory, leads to a diffusion variable that scales in time and has a Gaussian probability density. A long-time memory in such a random force is shown to produce a non-Gaussian probability density for the system response, but one that still scales.

Finally we show that physiologic time series are not mono-fractal, but have a fractal dimension that changes over time. The time series are multifractal, and as such they have a spectrum of dimensions. We review the procedure for constructing the multifractal spectrum and apply the technique to the SRV time series data obtained in our walking experiment [36] as a typical example of physiologic variability.

A. Scaling in Time Series

Time series analysis is the backdrop against which most theoretical models are developed in the life sciences and their analysis employs the traditional engineering assumption of signal plus noise. The signal plus noise model postulates that the time series variable $X(t)$ consists of a slowly varying part $S(t)$ and a randomly fluctuating part $\xi(t)$:

$$X(t) = S(t) + \xi(t) \tag{10}$$

The slow, regular variation of the time series S is called the *signal*, and the rapid erratic fluctuations represented by ξ is called the *noise*. The implication of this separation of effects is that $S(t)$ contains only information about the system of interest, whereas $\xi(t)$ is a property of the environment and does not contain any information about the system. In this model the noise can therefore be removed, by means of such techniques as filtering, without influencing what can be learned about the system.

In more complex phenomena the separation of effects implied by Eq. (10) may no longer be appropriate. The low-frequency, slowly varying part of the spectrum may be coupled to, and exchange energy with, the high-frequency, rapidly varying part of the spectrum; a fact that often results in fractal statistical processes. For these latter processes the traditional view of a deterministic, predictable signal given by the smooth part of the time series, on which random, unpredictable noise is superposed, distorts the dynamics of the underlying process, see, for example, *Biodynamics* [38] for a complete discussion. Herein we study techniques that purport to isolate and separate the deterministic part from the scaling part of the time series, without distorting the mutual influence of the low-frequency and high-frequency components of the same time series.

The science of complexity, in so far as it can be said to be a science, has relinquished the signal plus noise paradigm for a different perspective. Physiological time series invariably contain fluctuations, so that when sampled N times the data set $\{X_j\}, j = 1, \ldots, N$, appears to be a sequence of random points. Examples of such data are the interbeat intervals of the human heart, interstride intervals of human gait, brain wave data from EEGs and interbreath intervals, to name a few. The processing of time series in each of these cases has made use of random walk concepts in both the processing of the data and in the interpretation of the results. So let us review some of what is known about random walks.

1. *Simple Random Walks and Scaling*

We define the variable of interest as X_j, where $j = 0,1,2, \ldots$ indexes the time step, and in the simplest model a step is taken in each increment of time, which for convenience we set to one. The operator B lowers the index by one unit such that $BX_j = X_{j-1}$ so that a simple random walk can be written

$$(1 - B)X_j = \xi_j \tag{11}$$

where ξ_j is $+1$ or -1 and is selected according to some random process characterized by the probability density $p(\xi)$. The solution to this discrete equation is given by the position of the walker after N steps, the sum over the sequence of steps

$$X(N) = \sum_{j=1}^{N} \xi_j \tag{12}$$

and the total number of steps N can be interpreted as the total time t over which the walk unfolds, since we have set the time increment to one. For N sufficiently large and a symmetric probability density $p(\xi)$ with a finite width, the central limit theorem determines that the statistics of the dynamic variable $X(t)$ are Gaussian:

$$p_N(x) = \frac{1}{\sqrt{2\pi\langle X(N)^2\rangle}} e^{-\frac{-x^2}{2\langle X(N)^2\rangle}} \tag{13}$$

Assuming that the random steps are statistically independent $\langle \xi_j \xi_k \rangle = \langle \xi^2 \rangle \delta_{jk}$, we have for the second moment of the diffusion variable

$$\langle X(t)^2 \rangle = \sum_{j=1}^{N} \sum_{k=1}^{N} \langle \xi_j \xi_k \rangle = \langle \xi^2 \rangle N \rightarrow 2Dt \tag{14}$$

In the continuum limit the second moment increases linearly with time and in direct proportion to the diffusion coefficient, so that the probability density becomes the familiar Gaussian distribution for Einstein diffusion:

$$p(x,t) = \frac{1}{\sqrt{4\pi Dt}} e^{-x^2/2Dt} \tag{15}$$

Of particular interest to us here is the scaling property of the Gaussian distribution, Eq. (15). The joint probability distribution for two statistically independent processes X_1 and X_2, occurring in sequential time intervals, each of length τ, is the product of the separate probability densities. Consequently the probability density for the aggregate process $X = X_1 + X_2$, occurring in the time interval 2τ, is obtained by integrating over the two-variable constrained integral:

$$P(x, 2\tau) = \int_{-\infty}^{\infty} dx_1 \int_{-\infty}^{\infty} dx_2 P(x_1, \tau) P(x_2, \tau) \delta(x - x_1 - x_2) \tag{16}$$

Integrating out the delta function constraint and substituting the Gaussian distribution from Eq. (15) into Eq. (16) yields

$$p(x, 2\tau) = \int_{-\infty}^{\infty} dx_1 \frac{e^{-(x-x_1)^2/2D\tau}}{\sqrt{4\pi D\tau}} \frac{e^{-x_2^2/2D\tau}}{\sqrt{4\pi D\tau}} = \frac{e^{-x^2/2D(2\tau)}}{\sqrt{4\pi D(2\tau)}} \tag{17}$$

Thus, when viewed with only half the time resolution, that being 2τ rather than τ, the increments of the Brownian particle position are still zero-centered Gaussian random. More generally, whatever the number of the microscopic time steps between observations M, one always finds that the increments in the particle position constitute a zero-centered Gaussian process with a variance that increases linearly with M.

The above property means that one can sample the process of Brownian motion at any level of resolution and still observe a zero-centered Gaussian process. The time series obtained by sampling the process at every time τ, or at every time $b\tau$, where b is an integer, would be statistically indistinguishable. This is the scale invariance of Brownian motion. This scaling property is manifest by writing $\hat{x} = \lambda^{1/2}x$ and $\hat{t} = \lambda t$, yielding the scaling result

$$p(\hat{x}, \hat{t}) = \lambda^{-1/2} p(x, t) \tag{18}$$

so that the distribution for the random variable $\lambda^{1/2}X(\lambda t)$ is the same as that for $X(t)$. This scaling relation establishes that the random irregularities are generated at each scale in a statistically identical manner; that is, if the fluctuations are known in a given time interval, they can be determined in a second larger time interval by scaling. This is the property manifest in the allometric aggregation method used in the previous section.

In the simple random walk the steps are statistically independent of one another. The simplest generalization of this model is to make each step dependent on the preceding step in such a way that the second moment is

$$\langle X(t)^2 \rangle = 2Dt^{2H} \tag{19}$$

where $H \neq 1/2$ corresponds to anomalous diffusion. A value of $H < 1/2$ is interpreted as an antipersistent process in which case a step in one direction is preferentially followed by a reversal of direction. A value of $H > 1/2$ is interpreted as a persistent process in which case a step in one direction is preferentially followed by another step in the same direction. A value of $H = 1/2$ is interpreted as ordinary diffusion in which case the steps are statistically independent of one another. This interpretation of anomalous diffusion would be compatible with the concept of environmental noise and the signal plus noise paradigm.

In the science of complexity the system response $X(t)$ is expected to depart from the totally random condition of the simple random walk model, since such fluctuations are expected to have memory and correlation. In the physics literature, anomalous diffusion has been associated with phenomena with long-time memory such that the autocorrelation function is

$$C(t_1, t_2) = \langle X(t_1)X(t_2) \rangle \propto |t_1 - t_2|^{\beta} \tag{20}$$

and the brackets denote an average over an ensemble of realizations of fluctuations in the random variable. Here the power-law index is given by $\beta = 2H - 2$. Note that the two-point correlation function depends only on the time difference, thus, the underlying process is stationary in time. The Fourier transform of the autocorrelation function yields the spectrum, which in this case has the inverse power-law form

$$S(\omega) \propto \frac{1}{\omega^{\beta+1}} \tag{21}$$

and could also have been determined by applying a Tauberian theorem to Eq. (20). These power-law properties of the spectrum and the autocorrelation function, as well as a number of other properties involving long-time memory, are clearly discussed for discrete time series by Beran [45].

2. *Fractional Random Walks and Scaling*

One way of introducing long-term memory into a random walk model is by means of fractional differences. The concept of fractional differences is most readily introduced through the shift operator introduced in the previous subsection. Following Hosking [46], we define a fractional difference process as

$$(1 - B)^{\alpha} X_j = \xi_j \tag{22}$$

and the exponent α is not an integer. As it stands, Eq. (22) is just a formal definition without content. To make this equation usable, we must determine how to represent the operator acting on X_j, and this is done using the binomial expansion [45,46]. The inverse operator in the formal solution of Eq. (22),

$$X_j = (1 - B)^{-\alpha} \xi_j \tag{23}$$

has the binomial series expansion

$$(1 - B)^{-\alpha} = \sum_{k=0}^{\infty} \binom{-\alpha}{k} (-1)^k B^k \tag{24}$$

Expressing the binomial coefficient as the ratio of gamma function in the solution given in Eq. (23), we obtain after some algebra [23]

$$\begin{aligned} X_j &= \sum_{k=0}^{\infty} \frac{\Gamma(k + \alpha)}{\Gamma(k + 1)\Gamma(\alpha)} B^k \xi_j \\ &= \sum_{k=0}^{\infty} \Theta_k \xi_{j-k} \end{aligned} \tag{25}$$

The solution to the fractional diffusion equation is clearly dependent on fluctuations that have occurred in the remote past; note the time lag k in the index on the fluctuations and the fact that it can be arbitrarily large. The extent of the influence of these distant fluctuations on the system response is determined by the relative size of the coefficients in the series. Using Stirling's approximation on the gamma functions determines the size of the coefficients in Eq. (25) as the fluctuations recede into the past, that is, as $k \to \infty$ we obtain

$$\Theta_k \approx \frac{(k+\alpha-1)^{k+\alpha-1}}{k^k(\alpha-1)^k} = \frac{k^{\alpha-1}}{(\alpha-1)!} \tag{26}$$

since $k \gg \alpha$. Thus, the strength of the contributions to Eq. (25) decrease with increasing time lag as an inverse power law asymptotically in the time lag as long as $\alpha < 1/2$.

The spectrum of the time series in Eq. (25) is obtained using its discrete Fourier transform

$$X_k = \frac{1}{2\pi}\int_{-\pi}^{\pi} e^{ik\omega}\hat{X}_\omega d\omega \tag{27}$$

in the discrete convolution form of the solution, Eq. (25), to obtain

$$\hat{X}_\omega = \hat{\Theta}_\omega \hat{\xi}_\omega \tag{28}$$

yielding the power spectrum

$$S(\omega) = \left\langle |\hat{X}_\omega|^2 \right\rangle = \left\langle |\hat{\xi}_\omega|^2 \right\rangle |\hat{\Theta}_\omega|^2 \tag{29}$$

The strength of the fluctuations is assumed to be constant—that is, independent of the frequency. On the other hand, the Fourier transform of the strength parameter is given by

$$\begin{aligned}\Theta_\omega &= \sum_{k=0}^{\infty} \Theta_k e^{-ik\omega} = \sum_{k=0}^{\infty} \frac{(k+\alpha-1)!}{k!(\alpha-1)!}(e^{-i\omega})^k \\ &= \frac{1}{(1-e^{-i\omega})^\alpha}\end{aligned} \tag{30}$$

so that rearranging terms in Eq. (30) and substituting that expression into Eq. (29), we obtain

$$S(\omega) \propto \frac{1}{(2\sin\omega/2)^{2\alpha}} \tag{31}$$

for the spectrum of the fractional-differenced white noise process. In the low-frequency limit we therefore obtain the inverse power-law spectrum

$$S(\omega) \propto \frac{1}{\omega^{2\alpha}} \tag{32}$$

Thus, since the fractional-difference dynamics are linear, the system response is Gaussian, the same as the statistics for the white noise process on the right-hand side of Eq. (22). However, whereas the spectrum of fluctuations is flat, since it is white noise, the spectrum of the system response is inverse power law. From these analytic results we conclude that X_j is analogous to fractional Brownian motion. The analogy is complete if we set $\alpha = H - 1/2$ so that the spectrum in Eq. (32) can be expressed as

$$S(\omega) \propto \frac{1}{\omega^{2H-1}} \quad \text{as} \quad \omega \to 0 \tag{33}$$

Taking the inverse Fourier transform of the exact expression in Eq. (31) yields the autocorrelation coefficient [23]

$$\begin{aligned} r_k &\equiv \frac{\langle X_j X_{j+k} \rangle}{\langle X_j^2 \rangle} \approx \frac{\Gamma(1-\alpha)}{\Gamma(\alpha)} k^{2\alpha-1} \\ &= \frac{\Gamma(1.5-H)}{\Gamma(H-0.5)} k^{2H-2} \end{aligned} \tag{34}$$

as the lag time increases without limit $k \to \infty$.

The probability density function (pdf) for the fractional-difference diffusion process in the continuum limit *p(x,t)* satisfies the scaling condition

$$p(x,t) = \frac{1}{t^{\delta}} F\left(\frac{x}{t^{\delta}}\right) \tag{35}$$

where $\delta = H = \alpha - 1/2$. The deviation from ordinary statistical mechanics, and consequently the manifestation of complexity, is indicated by two distinct quantities. The first indicator is the scaling parameter δ departing from the ordinary value $\delta = 0.5$, which it would have for a simple diffusion process. But for fractional Brownian motion the value of the scaling index can be quite different. A second indicator of the deviation from ordinary statistical mechanics is the function *F(y)* in Eq. (35) departing from the conventional Gaussian form. The scaling index is usually determined by calculating the second moment of a time series. This method of analysis is reasonable only when *F(y)* has the Gaussian form, or some other distribution with a finite second moment—that is, if it is a member of the FVSM class. If the scaling condition Eq. (35) is realized,

it is convenient to measure the scaling parameter δ by the method of Diffusion Entropy Analysis (DEA) [47], which, in principle, works independently of whether the second moment is finite or not. The DEA method affords many advantages, including that of being totally independent of a constant bias. However, before we review the DEA method, let us examine another way in which the diffusion variable may scale—that is, another mechanism to generate long-time memory.

3. *Various Inverse Power-Law Autocorrelation Functions*

Consider the following form of the autocorrelation function,

$$C(\tau) = \langle X(t)X(t+\tau)\rangle = \frac{1}{(1+|\tau|^{\alpha})^{\beta/\alpha}} \tag{36}$$

where the random process $X(t)$ is still Gaussian, see Gneiting and Schlather [48] for a complete discussion of this correlation function and its implications. Any combination of parameters $0 < \alpha \leq 2$ and $\beta > 0$ is allowed, in which case (36) is referred to as the Cauchy class of correlation functions. Now consider the two asymptotic limits.

In the short time limit $\tau \to 0$ we expand the autocorrelation function in a Taylor series and obtain the power-law form

$$\lim_{\tau\to 0} C(\tau) \approx 1 - |\tau|^{\alpha} \tag{37}$$

for $0 < \alpha \leq 2$. The autocorrelation function in this case indicates realizations of the random function $X(t)$ in an E-dimensional Euclidian space that has a fractal dimension given by

$$D = E + 1 - \alpha/2 \tag{38}$$

with probability one [48]. In the one-dimensional case ($E = 1$) the power spectrum corresponding to Eq. (25) is the inverse power law

$$S(\omega) \propto \frac{1}{|\omega|^{\alpha+1}} \quad \text{as} \quad \omega \to \infty \tag{39}$$

Consequently the inverse power-law spectrum obtained in this way has a slope related to the fractal dimension by $\alpha + 1 = 5 - 2D$.

At the long time extreme, the autocorrelation function can again be expanded in a Taylor series to yield the long-time memory indicated by the inverse power-law correlation function

$$\lim_{\tau\to\infty} C(\tau) \approx |\tau|^{-\beta} \tag{40}$$

when $0 < \beta < 1$. In this case we obtain, as found earlier, $2H = 2 - \beta$, relating the scaling index with the Hurst exponent. Here again the Fourier transform of the autocorrelation function yields the power spectrum

$$S(\omega) \propto |\omega|^{\beta-1} = \frac{1}{|\omega|^{2H-1}} \qquad \text{as } \omega \to 0 \tag{41}$$

which is still an inverse power law for the index in the range $0 < \beta < 1$, or equivalently the Hurst exponent in the same range.

It cannot be too strongly emphasized that the fractal dimension and the Hurst exponent can vary independently of one another. From the example presented we see that the fractal dimension is a local property of time series ($\tau \to 0$), whereas the Hurst exponent is a global property of time series ($\tau \to \infty$) and, although not proven here, these are general properties of D and H [48]. Therefore, returning to our DEA argument, the scaling behavior $\delta = H$ would be the exception and not the rule for fractal stochastic processes. Note that these two scaling exponents are obtained by comparing the scaling of the second moment with that of the probability distribution (DEA). Most methods for determining the scaling index of time series, including the allometric aggregation method, rely on the central moments of the time series having finite values (FVSM). So let us consider the case where such moments do not exist and therefore are of no help in determining the scaling exponents.

B. Dichotomous Fluctuations with Memory

The time interval between steps were assumed to be a constant finite value in the simple random walk model. If, however, we explicitly take the limit where the time interval vanishes, then the discrete walk is replaced with a continuous rate. We begin our discussion of the scaling of statistical processes by considering one of the simplest stochastic rate equations and follow the development of Allegrini et al. [49].

$$\frac{dX(t)}{dt} = \xi(t) \tag{42}$$

where $\xi(t)$ is a two-state random process taking the values $\pm W$. If $\phi(x, \xi, \mathbf{R}, t)$ is the phase-space distribution function, then the equation of evolution corresponding to the dynamical equation (42) is

$$\frac{\partial \phi(x, \xi, \mathbf{R}, t)}{\partial t} = \left(-\hat{\xi} \frac{\partial}{\partial x} + \hat{\Gamma} \right) \phi(x, \xi, \mathbf{R}, t) \tag{43}$$

where we are adopting a quantum-like formalism. Thus, $\hat{\Gamma}$ is an operator characterizing the dynamics of the ξ-process and $\hat{\xi}$ is an operator having the eigenvalues $\pm W$, namely,

$$\hat{\xi}|\pm\rangle = \pm W|\pm\rangle. \tag{44}$$

The underlying process generating $\xi(t)$ need not be specified, but one realization of it could be a Hamiltonian system with a set of variables $\mathbf{R}$. These latter variables can be infinitely many so as to result in the relaxation of the correlation properties of the system.

At equilibrium, the two states $|+\rangle$ and $|-\rangle$ must have the same statistical weight. Thus we assume that the bath equilibrium corresponds to the state

$$|p_0\rangle = \frac{1}{\sqrt{2}}\{|+\rangle + |-\rangle\}\Pi(\mathbf{R}) \tag{45}$$

where $\Pi(\mathbf{R})$ denotes the equilibrium distribution of the variables responsible for the stochastic dynamics of the variable ξ. The state $|p_0\rangle$ is one of the eigenstates of the operator $\hat{\Gamma}$. In fact, we set

$$\hat{\Gamma}|\mu\rangle = -\Lambda_\mu|\mu\rangle \tag{46}$$

and $|p_0\rangle = |\mu = 0\rangle$, $\Lambda_0 = 0$. Within this quantum-like formalism the variable $\xi(t)$, as mentioned earlier, corresponds to the operator $\hat{\xi}$. This operator, applied to the equilibrium state $|p_0\rangle$, yields the excited state

$$|p_1\rangle = \frac{\hat{\xi}|p_0\rangle}{W}\Pi(\mathbf{R}) \tag{47}$$

Thus the operator $\hat{\xi}$ does not affect the distribution of $\mathbf{R}$ but has the effect of making the transitions $|+\rangle + |-\rangle \to |+\rangle - |-\rangle$ and $|+\rangle - |-\rangle \to |+\rangle + |-\rangle$, without affecting the other bath variables. The ''excited'' state $|p_1\rangle$ is not an eigenstate of $\hat{\Gamma}$, but it is a linear combination of the states $|\mu\rangle$, with $\mu \neq 0$. The operator $\hat{\Gamma}$ applied to the ''excited'' state $|p_1\rangle$ has the effect of relaxing it through coupling the state $|p_1\rangle$ to infinitely many other eigenstates $|\mu\rangle$. The autocorrelation function $\langle\xi\xi(t)\rangle$, within this quantum-like formalism, reads

$$\langle\xi\xi(t)\rangle = \langle p_0|\hat{\xi}\exp\big(\hat{\Gamma}t\big)\hat{\xi}|p_0\rangle \tag{48}$$

On the basis of the properties of the operators $\hat{\xi}$ and $\hat{\Gamma}$, this correlation function can also be expressed as

$$\langle\xi\xi(t)\rangle = W^2\sum_{\mu\neq 0}\langle p_1|\mu\rangle\langle\mu|p_1\rangle\exp\big(-\Lambda_\mu t\big) \tag{49}$$

It is convenient to define the phase space distribution function

$$\sigma_\mu(t) \equiv \langle \mu | \phi(x, \xi, \mathbf{R}, t) \rangle \tag{50}$$

with $\mu = 0,1,2,\ldots$. We are interpreting the distribution ϕ of Eq. (43) as a sort of ket vector $|\phi\rangle$. By multiplying Eq. (43) on the left by the states $|\mu\rangle$, we obtain

$$\frac{\partial \sigma_0(x,t)}{\partial t} = -W \sum_{\mu \neq 0}^{\infty} a_\mu \frac{\partial \sigma_\mu(x,t)}{\partial x} \tag{51}$$

and, for $\mu > 0$,

$$\frac{\partial \sigma_\mu(x,t)}{\partial t} = -W \sum_{\mu \neq 0}^{\infty} a_\mu^* \frac{\partial \sigma_0(x,t)}{\partial x} - \Lambda_\mu \sigma_\mu(x,t) \tag{52}$$

with $a_\mu = \langle \mu | \hat{\xi} | p_0 \rangle$.

Let us make the assumption that at $t = 0$ all the σ_μ's but the one with $\mu = 0$ vanish. This condition is equivalent to assuming the spatial distribution is statistically independent of the "velocity" distribution and results in an equation of motion without an inhomogeneous term. By solving Eq. (52) and placing the solution into Eq. (51), we obtain

$$\frac{\partial \sigma_0(x,t)}{\partial t} = W^2 \sum_{\mu \neq 0}^{\infty} a_\mu \frac{\partial}{\partial x} |a_\mu|^2 \int_0^t dt' \exp[-\Lambda_\mu (t - t')] \frac{\partial^2 \sigma_0(x,t)}{\partial x^2} \tag{53}$$

From now on we shall focus on the reduced density matrix $\sigma_0(x,t)$ and for the sake of simplicity we omit the subscript zero. Using Eq. (48), we can rewrite Eq. (53) in the form

$$\frac{\partial \sigma(x,t)}{\partial t} = \int_0^t dt' \langle \xi(t) \xi(t') \rangle \frac{\partial^2 \sigma(x,t')}{\partial x^2} \tag{54}$$

where again the brackets denote an average over an ensemble of realizations of the statistical fluctuations. In Section IV the form of Eq. (54) is determined to be that for a fractional diffusion equation when the two-point correlation function is appropriately chosen.

In the case where the correlation function in Eq. (54) is an exponential

$$\langle \xi(t) \xi(t') \rangle = \langle \xi^2 \rangle e^{-\gamma t} \tag{55}$$

taking the time derivative of Eq. (54) yields

$$\frac{\partial^2\sigma(x,t)}{\partial t^2}+\gamma\frac{\partial\sigma(x,t)}{\partial t}-\langle\xi^2\rangle\frac{\partial^2\sigma(x,t)}{\partial x^2}=0 \tag{56}$$

This is the celebrated telegrapher's equation, whose phenomenological pedigree dates back to Maxwell. His (Maxwell's) argument was to include relaxation into the wave equation and did not require the invocation of microscopic dynamics. However, his use of dissipation was compatible with the action of infinitely many degrees of freedom in the medium supporting the wave motion.

The equation of motion for the Liouville density from Eq. (54) is

$$\frac{\partial\sigma(x,t)}{\partial t}=\int_0^t dt'\Phi_\xi(t-t')\frac{\partial^2\sigma(x,t')}{\partial x^2}=\int_0^t dt'\Phi_\xi(t')\frac{\partial^2\sigma(x,t-t')}{\partial x^2} \tag{57}$$

In the case when the correlation function Φ_ξ is integrable, using the last term of the equality of Eq. (57), we can make use of the Markov approximation. This approximation is based on replacing the second derivative in space containing the time argument $(t-t')$ with the second derivative in space containing the time argument t and extending the upper bound of the time integration from t to infinity. This can be justified by expanding the probability density in a Taylor series in time and neglecting all but the first term. In this, the Markov approximation in Eq. (57) reduces to the ordinary diffusion equation

$$\frac{\partial\sigma(x,t)}{\partial t}=D\frac{\partial^2\sigma(x,t)}{\partial x^2} \tag{58}$$

where the diffusion coefficient D is given by

$$D=W^2\tau_C \tag{59}$$

and the correlation time is given by

$$\tau_C=\int_0^\infty dt'\Phi(t') \tag{60}$$

Notice that in the Continuous-Time Random Walk (CTRW) as used in Klafter et al. [50], in the case where the waiting time distribution is exponential, $\psi(t)=a\,\exp[-at]$, the same evolution for the probability density $p(x,t)$ and the phase-space distribution $\sigma(x,t)$ occurs as that resulting from Eq. [57]. This can

be established by noticing that in the case of the dichotomous variable ξ used here, the waiting-time distribution is related to the correlation function by the exact relation [51]

$$\Phi_\xi(t) = \frac{1}{\tau_W} \int_t^\infty (t' - t)\psi(t')dt' \tag{61}$$

where τ_W denotes the mean sojourn time. In the exponential case this sojourn time becomes identical to the correlation time; that is, since $\Phi_\xi(0) = 1$, in the exponential case $a = 1/\tau_W$ and $\tau_C = \tau_W$.

1. *The Exact Solution*

Here we are interested in the asymptotic behavior of the exact solution to Eq. (57) and we follow the analysis of Bologna et al. [52]. The most direct way to determine these properties is to take the Laplace transform in time and Fourier transform in space to obtain the Fourier–Laplace transform of the Liouville density

$$\hat{\tilde{\sigma}}(k, s) = \frac{1}{s + \tilde{\Phi}_\xi(s)k^2} \tag{62}$$

where we have imposed the initial conditions

$$\sigma(x, t)|_{t=0} = \delta(x) \quad \text{and} \quad \left.\frac{\partial\sigma(x, t)}{\partial t}\right|_{t=0} = 0 \tag{63}$$

The inverse Fourier transform of Eq. (62) yields

$$\tilde{\sigma}(x, s) = \sqrt{\frac{s}{\tilde{\Phi}_\xi(s)}} \frac{e^{-|x|\sqrt{\frac{s}{\tilde{\Phi}_\xi(s)}}}}{2s} \tag{64}$$

which we can integrate over space to obtain

$$\int_{-\infty}^{\infty} \tilde{\sigma}(x, s)dx = \frac{1}{s} \tag{65}$$

indicating the conservation of normalization over time. To go beyond the formal solution in Eq. (64), we must specify the autocorrelation function. We select an inverse power-law autocorrelation function,

$$\Phi_\xi(t) = W^2 \frac{T^\beta}{(T + t)^\beta} \tag{66}$$

with $0 < \beta < 1$ and T is a positive constant. The Laplace transform of the autocorrelation function given by Eq. (66) becomes

$$\tilde{\Phi}_\xi(s) = \frac{\Gamma(1-\beta)TW^2}{(sT)^{1-\beta}}[e^{sT} - E^{sT}_{\beta-1}] \tag{67}$$

where the generalized exponential function is defined by [23,53]

$$E^x_\gamma \equiv \sum_{n=0}^{\infty} \frac{x^{n-\gamma}}{\Gamma(n+1-\gamma)} \tag{68}$$

and we subsequently define the generalized exponential using the fractional derivative operator.

2. *Early Time Behavior*

Let us first consider the behavior of the autocorrelation function at early times. In this domain, $t \to 0$, we have $s \to \infty$, so that the generalized exponential becomes

$$E^{sT}_{\beta-1} \approx e^{sT} - \frac{1}{\Gamma(1-\beta)(sT)^\beta} \tag{69}$$

which when substituted into Eq. (67) yields $\tilde{\Phi}_\xi(s) \approx W^2/s$ so that the Laplace transform of the early time solution for the phase-space equation of evolution is

$$\tilde{\sigma}(x,s) \approx \frac{e^{-|x|s/W}}{2W} \tag{70}$$

The inverse Laplace transform of Eq. (70) yields the delta function for the phase-space distribution function

$$\sigma(x,t) \approx \frac{1}{2W}\delta\left(t - \frac{|x|}{W}\right) \tag{71}$$

Thus, for times shorter than T, the evolution of the Liouville density consists of two peaks traveling in opposite directions at the same speed, W. Note that this is the same early-time solution one would obtain for the solution to the telegrapher's equation [51].

3. *Late Time Behavior*

Now let us now consider the time asymptotic behavior of the exact solution. In the late time domain $t \to \infty$, we have $s \to 0$, so examining the behavior of

Eq. (67) in this domain we obtain

$$\tilde{\Phi}_{\xi}(s) \approx \frac{\Gamma(1-\beta)TW^2}{(sT)^{1-\beta}}\left[1-\frac{(sT)^{1-\beta}}{\Gamma(1-\beta)}\right] \tag{72}$$

Note that as $s \to 0$ the leading term in this expansion diverges for $\beta < 1$, corresponding to the fact that there is no correlation time for this process. Inserting this expression for the Laplace transform of the correlation function into Eq. (64), keeping only the diverging term, yields

$$\tilde{\sigma}(x,s) = \frac{\exp\left[-\dfrac{|x|s^{1-\beta/2}}{\Gamma(1-\beta)WT^{\beta/2}}\right]}{2\Gamma(1-\beta)W(sT)^{\beta/2}} \tag{73}$$

The inverse Laplace transform of Eq. (73) yields the phase-space distribution function

$$\sigma(x,t) \approx \frac{1}{2\langle x\rangle t^{1-\beta/2}}\sum_{n=0}^{\infty}\frac{(-1)^n}{n!\Gamma(1-(n+1)(1-\beta/2))}\left(\frac{|x|}{\langle x\rangle t^{1-\beta/2}}\right)^n \tag{74}$$

where the average of the system variable is

$$\langle x\rangle = WT^{\beta/2}\Gamma(1-\beta) \tag{75}$$

as had been obtained previously [54]. Straightforward dimensional analysis indicates that the space variable in Eq. (74) scales as $x \sim t^{\alpha}$ where

$$\alpha = 1-\beta/2 \tag{76}$$

as had also been found by other authors [55].

To further support this conclusion, note that in the asymptotic limit $s \to 0$, Eq. (62) yields

$$\hat{\tilde{\sigma}}(k,s) = \frac{1}{s+\text{constant } s^{\beta-1}k^2} \tag{77}$$

The scaling condition $x \sim t^{\alpha}$ implies $k = s^{\alpha}$, which when inserted into the right-hand-side term of Eq. (77) makes the left-hand side of the same equation proportional to $1/s$ when the scaling condition of (76) applies. We note that $1/s$ is the Laplace transform of a constant in accordance with the fact that scaling is a reflection of stationarity. For this reason we are inclined to believe that the density perspective yields in the asymptotic limit a unique scaling and that our solution correctly reflects this condition.

C. Fractals, Multifractals, and Data Processing

The salient property of mathematical random fractals processes is the existence of long-time correlations, here measured by the correlation index r, which can be related to the fractal dimension by [21]

$$r = 2^{3-2D} - 1 \tag{78}$$

Successive increments of mathematical fractal random processes are independent of the time step. Here $D = 1.5$ corresponds to a completely uncorrelated random process $r = 0$, such as Brownian motion, and $D = 1.0$ corresponds to a completely correlated process $r = 1$, such as a regular curve. Studies of various physiologic time series have shown the existence of strong long-time correlations in healthy subjects and demonstrated the breakdown of these correlations in disease; see, for example, the review by West [56]. Complexity decreases with convergence of the Hurst exponent H to the value 0.5 or equivalently of the fractal dimension to the value 1.5. Conversely, system complexity increases as a single fractal dimension expands into a spectrum of dimensions.

1. *Multifractal Spectrum*

The spectrum of fractal dimensions can be calculated in a number of ways. One way is to cover the time axis with cells of size δ such that the time is given by $t = N\delta$ and $N \gg 1$. Following Falconer [57] we can define the partition function

$$Z(q, \delta) \equiv \sum_j \mu(C_j)^{\delta} \tag{79}$$

where C_j is the jth box in the δ-coordinate mesh that intersects with the measure μ. We can construct the measure using the time series obtained from the physiologic interval data. This measure is made by aggregating the observed time intervals $\{t_j\}$, $j = 1,2,\ldots,N$, where t_j denotes the time interval between the end points of stride $j-1$ and j,

$$T(n, \delta) = \sum_{j=1}^{n} t_j \tag{80}$$

such that $T(n, \delta)$ is interpreted as a random walk trajectory. In this way we can construct the partition function in Eq. (79) using

$$\mu(C_j) = \frac{|T(j+n, \delta) - T(j, \delta)|}{\sum_{k=1}^{N-n} |T(k+n, \delta) - T(k, \delta)|} \tag{81}$$

where the integer n lags the trajectory by n steps. The typical scaling behavior of the partition function in the limit of vanishing grid scale [57] is

$$Z(q, \delta) \approx \delta^{\tau(q)} \tag{82}$$

where $\tau(q)$ is the mass exponent [58].

The mass exponent is related to the generalized dimension $D(q)$ by the relation

$$\tau(q) = (1 - q)D(q) \tag{83}$$

where $D(0)$ is the fractal or box counting dimension, $D(1)$ is the information dimension, and $D(2)$ is the correlation dimension [57,58]. The q-moment therefore accentuates different aspects of the underlying dynamical process. For $q > 0$, the partition function emphasizes large fluctuations and strong singularities through the generalized dimensions, whereas for $q < 0$, the partition function stresses the small fluctuations and the weak singularities. This property of the partition function deserves a cautionary note because the negative moments can easily become unstable, introducing artifacts into the calculation. Thus the interpretation of the trajectory approach must be judged with some caution for $q < 0$.

A mono-fractal time series is characterized by a single fractal dimension. In general, time series have a local Hölder exponent h that varies over the course of the trajectory and is related to the fractal dimension by $D = 2 - h$ [57]. Note that for an infinitely long time series the Hölder exponent h and the Hurst exponent H are identical; however, for a time series of finite length they need not be the same. We stress that the fractal dimension and the Hölder exponent are local quantities, whereas the Hurst exponent is a global quantity; consequently the relation $D = 2 - H$ is only true for an infinitely long time series. The function $f(h)$, called the multifractal or singularity spectrum, describes how the local Hölder (fractal) exponents contribute to such time series. Here h and f are independent variables, as are q and τ. The general formalism of Legrendre transform pairs interrelates these two sets of variables by the relation [58],

$$f(q) = qh + \tau(q) \tag{84}$$

The local Hölder exponent h varies with the q-dependent mass exponent through the equality

$$h(q) = -\frac{d\tau(q)}{dq} = -\tau'(q) \tag{85}$$

so the singularity spectrum can be written as

$$f(h(q)) = -q\tau'(q) + \tau(q) \tag{86}$$

where the mass exponent and its derivative are determined by data.

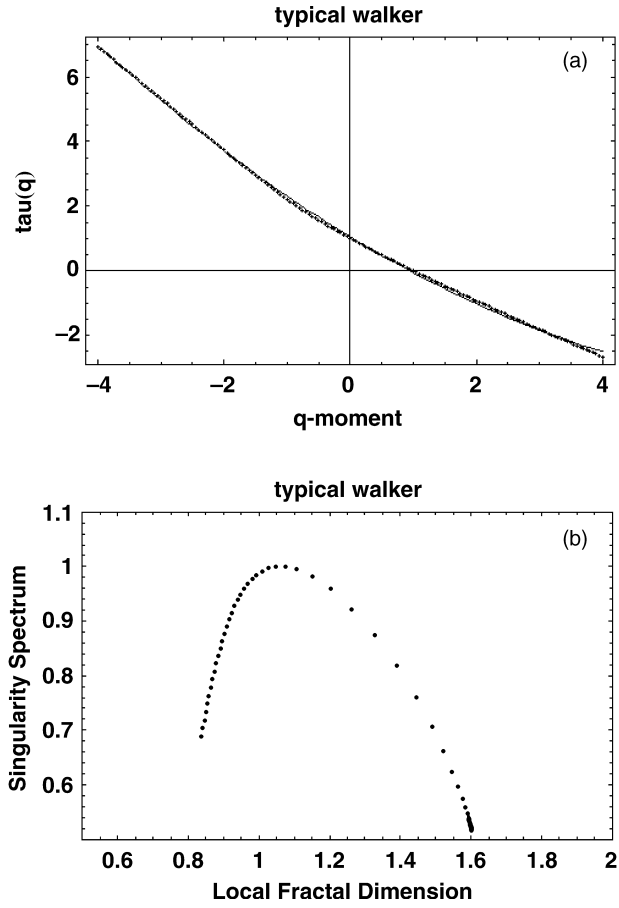

Figure 9. (*a*) The mass exponent as a function of the q-moment obtained from a numerical fit to the partition function using Eq. (87) for a typical walker. (*b*) The singularity spectrum $f(h)$ obtained from a numerical fit to the mass exponent and its derivative using Eq. (86) for a typical walker [36].

As mentioned above, a time series is mono-fractal when the mass exponent is linear in q, otherwise the underlying process is multifractal. We apply the partition function measure to numerically evaluate

$$\tau(q) = -\frac{\ln Z(q,\delta)}{\ln\delta} \tag{87}$$

and the results are depicted in Fig. 9a. Rigorously speaking, the expression for the mass exponent requires $\delta \to 0$, but we cannot do that with data, so there is

TABLE I
The Fitting Parameters for the Mass Exponent [Eq. (88)][a]

Walker	a_0	$-a_1$	a_2
1	1.03	1.26	0.13
2	0.99	1.14	0.08
3	1.05	1.32	0.14
4	1.05	1.26	0.12
5	1.00	1.12	0.07
6	1.01	1.07	0.05
7	1.02	1.17	0.09
8	1.09	1.29	0.14
9	1.02	1.14	0.08
10	1.01	1.17	0.09
Average	1.03 ± 0.03	1.19 ± 0.08	0.10 ± 0.03

[a]The column $-a_1$ is the fractal dimension for the SRV time series. In each case these numbers agree with those obtained earlier using a different method [36].

always some error in the results. The significance of that error remains to be determined. In Fig. 9 the mass exponent for a typical subject in the walking experiment [11] is shown and the individual mass exponents do not look too different from the one shown. It is clear from the figure that the mass exponent is not linear in the moment index q and therefore the SRV time series is multifractal. In Table I we record the fitting coefficients for each of the 10 SRV time series using the quadratic polynomial in the moments interval $-4 \leq q \leq 4$

$$\tau(q) = a_0 + a_1 q + a_2 q^2 \tag{88}$$

The fit to the data using Eq. (88) is indicated by the solid curve in Fig. 9a.

A second method for determining the singularity spectrum, the one we use here, is to numerically determine both the mass exponent and its derivative. In this way we calculate the multifractal spectrum directly from the data using Eq. (86). It is clear from Fig. 9b that we obtain the canonical form of the spectrum; that is, $f(h)$ is a convex function of the scaling parameter h. The peak of the spectrum is determined to be the fractal dimension, as it should. Here again we have an indication that the interstride interval time series describes a multifractal process. We stress that we are only using the qualitative properties of the spectrum for $q < 0$, due to the sensitivity of the numerical method to weak singularities.

The singularity spectrum can now be determined using the Legendre transformation by at least two different methods. One technique is to use the fitting equation substituted into Eq. (86). We do not do this here, but we note in

passing that if Eq. (88) is inserted into Eq. (85), the fractal dimension is determined by the $q = 0$ moment to be

$$h(0) = -\tau'(0) = -a_1 \tag{89}$$

The values of the parameter a_1 listed in Table I agree with the fractal dimensions obtained earlier using a scaling argument for the same data [11,36].

The multifractal behavior of time series such as SRV, HRV, and BRV can be modeled using a number of different formalisms. For example, a random walk in which a multiplicative coefficient in the random walk is itself made random becomes a multifractal process [59,60]. This approach was developed long before the identification of fractals and multifractals and may be found in Feller's book [61] under the heading of subordination processes. The multifractal random walks have been used to model various physiological phenomena. A third method, one that involves an integral kernel with a random parameter, was used to model turbulent fluid flow [62]. Here we adopt a version of the integral kernel, but one adapted to time rather than space series. The latter procedure is developed in Section IV after the introduction and discussion of fractional derivatives and integrals.

2. *Diffusion Entropy Analysis (DEA)*

So far in this section we have focused on mathematical models that generate time series with scaling properties. In Section II we introduced a simple data aggregation procedure to reveal the scaling of physiologic time series. The allometric aggregation method offered some insight into the scaling of the underlying process, but now we turn our attention to a method that can reveal both the statistical and the correlation properties of a time series. To do this, we interpret the physiologic time series as the generator of a diffusion process and replace the random elements of the right-hand side of the simple random walk in Eq. (90) with the time series data. Thus, even though we do not know the *a priori* statistical properties of the data set $\{\xi_j\}$, we can deduce them from the probability density function $p(x, t)$ for the diffusion variable $X(t)$. Note that $X(t)$ is the dynamic variable that aggregates the time series data into a "random walk" trajectory. If the time series is stationary, the scaling property of the probability density function for the diffusive process is given by Eq. (35), where δ is the scaling exponent.

We now offer a way to independently determine the scaling exponent from the time series data using the Shannon entropy for a diffusive process $p(x, t)$:

$$S(t) = -\int_{-\infty}^{\infty} p(x,t) \ln p(x,t)\, dx \tag{90}$$

Now if the probability density function satisfies the scaling condition Eq. (35) substituting this functional form of $p(x,t)$ into Eq. (90) yields

$$S(t) = -\int_{-\infty}^{\infty} \frac{1}{t^{\delta}} F\left(\frac{x}{t^{\delta}}\right) \ln\left[\frac{1}{t^{\delta}} F\left(\frac{x}{t^{\delta}}\right)\right] dx$$

using the transformation $y = \dfrac{x}{t^{\delta}}$ simplifies this equation to

$$S(t) = A + \delta \ln t \tag{91}$$

and the constant A is determined by the time-independent distribution $F(y)$

$$A = -\int_{-\infty}^{\infty} F(y) \ln F(y)\, dy$$

It is obvious from Eq. (91) that a graph of the entropy $S(t)$ versus the logarithm of the time t yields a straight line with positive slope δ. Consequently using time series data to generate a diffusive process we can construct a histogram of the probability density enabling us to numerically determine the scaling parameter using the entropy. This procedure is called diffusion entropy analysis [47] (DEA).

The theoretical scaling index for ordinary diffusion is $\delta = H = 1/2$. To test this prediction using a known data set, we generate a diffusive trajectory from Eq. (90) using a computer-generated uncorrelated Gaussian time series for 10^4 data points on the right-hand side of the equation. We consider a time series with a maximum length of 200 data points and construct a histogram from the nearly 10^4 realizations of such a time series $X(t)$ obtained using Eq. (90). The histogram constructed from the realizations of the trajectories is inserted into Eq. (90), and the resulting entropy is calculated as a function of time. Figure 10 shows that the entropy calculated this way increases linearly with the logarithm of time with a slope of 0.48, very close to the theoretical value of 0.50 one would obtain for an infinitely long time series.

Recall that fractional Brownian motion, with the distribution given by Eq. (19), satisfies the scaling relation [Eq. (35)] for the probability density. Consequently, we have the equality $\delta = H \neq 1/2$, so that the scaling exponent δ, determined by DEA, is given by the Hurst exponent H. We emphasize that this equality is not true in general, and it is quite possible that $\delta \neq H$, indicating that there is scaling in the time series, but the statistics need not be Gaussian. We examine this case now.

Consider the limit distribution first studied by Paul Lévy for processes having diverging central moments and which consequently violate the central limit

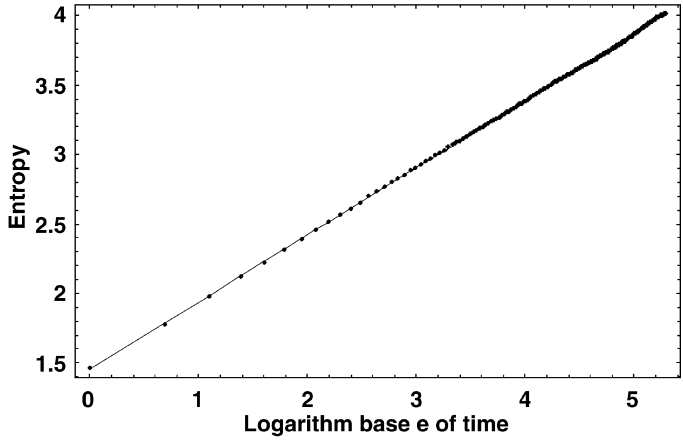

Figure 10. The entropy for an uncorrelated Gaussian random process generating random walk trajectories calculated using DEA is graphed versus the natural logarithm of the time. The data indicate a linear relationship between $S(t)$ and $ln\ t$ as predicted by Eq. (91).

theorem. The generalized central limit theorem yields the probability density for the symmetric stable Lévy process in terms of the Fourier transform of the characteristic function [63]

$$p_L(x,t) = \int_{-\infty}^{\infty} \frac{dk}{2\pi} e^{ikx} e^{-\gamma t|k|^{\alpha}} \tag{92}$$

where the Lévy index is in the interval $0 < \alpha \leq 2$ and $\gamma > 0$. The only explicit expression for the Lévy stable distribution is an infinite series whose lowest-order term is given by [64]

$$p_L(x,t) \propto \frac{t}{|x|^{\alpha+1}} \tag{93}$$

It is evident from the inverse power-law form of the probability density given by Eq. (93) that the second moment $\langle x^2 \rangle$ of the Lévy α-stable distribution diverges since $\alpha + 1 < 3$. Equally clear is the fact that the first moment for this distribution diverges for $\alpha + 1 < 2$. The first and second moments converge for $\alpha = 2$, in which case the Lévy stable distribution becomes a Gaussian distribution and the central limit theorem again applies to the time series.

We use the parameters λ and κ to scale the random walk phase-space variable x and time t in the Lévy stable distribution [Eq. (92)] and obtain after

some algebra

$$p_L(\lambda x, \kappa t) = \frac{1}{\lambda t^{1/\alpha}} p_L\left(\frac{x}{t^{1/\alpha}}, 1\right) = \frac{1}{t^{1/\alpha}} F\left(\frac{x}{t^{1/\alpha}}\right) \tag{94}$$

when the parameters are related by $\kappa = \lambda^{\alpha}$. Thus, the Lévy α-stable distribution satisfies the scaling relation in Eq. (35), so that the underlying process is fractal, but without memory. This lack of memory is a consequence of the Lévy α-stable distribution being a Markov process [63,64]. The scaling behavior of a time series described by Lévy α-stable statistics is determined using the DEA by substituting Eq. (92) into the equation for the entropy. The scaling index is determined to be $\delta = 1/\alpha$, but δ in this case is not related to a Hurst exponent H. Therefore we obtain the remarkable result that the scaling index can be determined from statistical processes even when the central moments of such processes diverge and the traditional scaling methods fail.

Using DEA, we have established that there are statistical processes for which $\delta = H$ and statistical processes for which $\delta \neq H$, both of which scale. However, there is a third class of processes for which the scaling index is a function of the Hurst exponent, but the relation is not one of their being equal. This third class is the Lévy random walk process (Lévy diffusion) introduced by Shlesinger et al. [65] in their discussion of the application of Lévy statistics to the understanding of turbulent fluid flow.

Let us distinguish between a Lévy flight and a Lévy walk. In a Lévy flight the jumps taken by the random flyer each take the same amount of time, so that the statistical properties of the trajectories are determined solely by the length of the steps. If the distribution of step lengths is inverse power law, with index less than three, then using the generalized central limit theorem the resulting distribution is Lévy [Eq. (92)]. If the step-distribution index is greater than three, the distribution converges to that of Gauss and the usual central limit theorem is recovered.

A Lévy walk, on the other hand, takes into account the fact that longer steps take longer times to complete than do shorter steps. The recognition of this simple fact ties the distribution of step sizes to the distribution of time intervals, which in the case of turbulence was determined by the fluctuations in the fluid velocity [62]. In the present example the continuum form of the Lévy walk process is described by Eq. (42), with the autocorrelation function for the random driver being given by the inverse power law Eq. (66) and W is the constant speed of the walker. The asymptotic form of the second moment for this process is

$$\langle X(t)^2 \rangle \propto \int_0^t dt_1 \int_0^t dt_2 \Phi_{\xi}(|t_1 - t_2|) = t^{2-\beta} \tag{95}$$

and in terms of the index for the autocorrelation function the Hurst exponent is

$$2H = 2 - \beta \tag{96}$$

Using the relation between the waiting-time distribution function Eq. (61) and the autocorrelation function Eq. (66), we obtain the inverse power-law waiting-time distribution

$$\psi(t) = \frac{\alpha T^{\alpha}}{(T+t)^{\alpha+1}} \tag{97}$$

where the autocorrelation index and the waiting-time index are related by

$$\beta = \alpha - 1 \tag{98}$$

Consequently, by means of the delta function $\delta(|x| - Wt)$ which ties space and time together, the resulting distribution for the diffusion process is Lévy α-stable and the scaling parameter in Eq. (98) is the Lévy index. Therefore, using Eq. (96) and the fact that $\delta = 1/\alpha$ for a Lévy α-stable process, we obtain the relation between exponents:

$$\delta = \frac{1}{3 - 2H} \tag{99}$$

Scafetta and Grigolini [47] established that the DEA scaling does, in fact, yield the scaling relation given by (99) for Lévy diffusion.

We give two examples of fractal time series. The first is fractal Gaussian intermittent noise characterized by a long-time correlated waiting-time sequence, and the second is a Lévy-walk intermittent noise. These examples were developed in an environmental context to explain the observed distribution of earthquakes in California [66].

The Gaussian intermittent noise has an autocorrelation function given by Eq. (20) and power-law index given by $2H - 2$. The statistics of this sequence is determined by a finite variance waiting time distribution function $\psi(t)$ whose form may be, for example, that of a Gaussian, exponential, or Poisson. The diffusion generated by a fractal Gaussian intermittent noise is a particular type of fractional Brownian motion and satisfies the asymptotic scaling relation between indices $\delta = H$. Figure 11A is based on a realization of this process using an exponential waiting-time distribution function. The parallel lines through the computer-generated data show the two scaling exponents, one determined by DEA, indicated by the entropy $S(t)$ minus the constant term, and the other determined directly from the second moment, denoted by $D(t)$. If the long-time correlations are destroyed by means of shuffling—that is, by

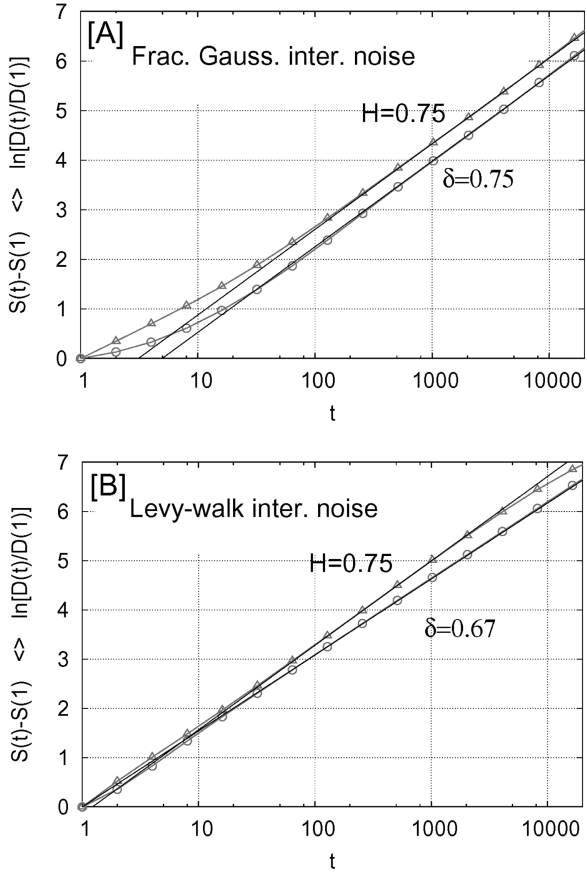

Figure 11. DEA and SDA for (*A*) a fractal Gaussian intermittent noise with $\psi(t) = \exp[-t/\gamma]$ with $\gamma = 25$ and $H = \delta = 0.75$; the fractal Gaussian relation of equal exponents is satisfied. (*B*) A Lévy-walk intermittent noise with $\psi(\tau) \propto \tau^{-\mu}$ and $\mu = 2.5$; note the bifurcation between $H = 0.75$ and $\delta = 0.67$ caused by the Lévy-walk diffusion relation [66].

randomly interchanging the positions of the elements of the sequence—the new intermittent random time series is characterized by the value $\delta = H = 0.50$. This latter result is not shown.

The Lévy-walk intermittent noise is characterized by an uncorrelated waiting-time sequence and a Lévy or an inverse power-law waiting-time distribution function such as given by Eq. (97) with $1 < \alpha < 2$. This interval for the scaling index insures that although the second moment diverges, the first moment is finite. The presence of a Lévy-walk process in a given time series can be detected by means of the asymptotic relation Eq. (99), which we refer to as

the *Lévy-walk diffusion relation* [66]. Figure 11B is based on a realization of this process using an inverse power-law waiting-time distribution function. This figure shows the scaling properties of a computer-generated random Lévy-walk intermittent noise with $\alpha = 1.5$ that has $H = 0.75$ and $\delta = 0.67$ in agreement with the Lévy-walk diffusion relation.

We stress that the Lévy-walk diffusion relation is fulfilled if the waiting times are uncorrelated, in which case any shuffling of the elements in data sequence would not alter the scaling exponents H and δ. In fact, the superdiffusion scaling exponent $0.5 < \delta < H < 1$ of a Lévy-walk intermittent noise are related to the fatness of the waiting-time inverse power-law tail, as measured by the exponent α. Contrary to a fractal Gaussian intermittent noise, this Lévy scaling does not imply a temporal correlation, or a historical memory, among events because the occurrence of future events is independent of the frequency of past events.

It should be stressed that even though the second moment for a Lévy walk is finite, the scaling index obtained from the second moment does not give the correct scaling properties of the time series. This is a word of caution regarding the application of FVSMs to determine the scaling properties of a time series. Even when the second moment has the form

$$\langle X(t)^2 \rangle \propto t^{2\mu} \tag{100}$$

this does not mean that the index so determined has any interesting implications regarding the underlying dynamics of the time series. It is only after the statistics of the time series are determined, by using DEA or some other technique, that can one begin to interpret the anomalous diffusion equation, Eq. (100).

IV. FRACTIONAL DYNAMICS

In the late nineteenth century, most mathematicians felt that a continuous function must have a derivative "almost everywhere," which means that the derivative of a function is singular only on a set of points whose total length (measure) vanishes. However, some mathematicians wondered if functions existed that were continuous, but did not have a derivative at any point (continuous everywhere but differentiable nowhere). The motivation for considering such pathological functions was initiated within mathematics and not in the physical or biological sciences, the insights of Boltzmann and Perrin notwithstanding. In 1872, Karl Weierstrass (1815–1897) gave a lecture to the Berlin Academy in which he presented functions that had the aforementioned continuity and nondifferentiability properties; consequently, these functions had the symmetry of self-similarity. Twenty-six years later, Ludwig Boltzmann, who elucidated the microscopic basis of entropy, said that physicists could have

invented such functions in order to treat collisions among molecules in gases and fluids. Boltzmann had a great deal of experience thinking about such things as discontinuous changes of particle velocities that occur in kinetic theory and to wonder about their proper mathematical representation. He had spent many years trying to develop a microscopic theory of gases and he was successful in developing such a theory, only to have his colleagues reject his contributions. Although kinetic theory led to acceptable results (and provided a suitable microscopic definition of entropy), it was based on time-reversible dynamic equations; that is, entropy distinguishes the past from the future, whereas the equations of classical mechanics do not [2]. This basic inconsistency between analytic dynamics and thermodynamics remains unresolved today, although there are indications that the resolution of this old chestnut lies in microscopic chaos.

It was assumed in the kinetic theory of gases that molecules are materially unchanged as a result of interactions with other molecules, and collisions are instantaneous events as would occur if the molecules were impenetrable and perfectly elastic. As a result, it seemed quite natural that the trajectories of molecules would sometimes undergo discontinuous changes. Robert Brown, in 1827, observed the random motion of a speck of pollen immersed in a water droplet. Discontinuous changes in the speed and direction of the motion of the pollen mote were observed, but the mechanism causing these changes was not understood.

Albert Einstein published a paper in 1905 that, although concerned with diffusion in physical systems, ultimately explained the source of Brownian motion as being due to the net imbalance of the random collisions of the lighter particles of the medium with the surface of the pollen mote. Jean Baptiste Perrin, of the University of Paris, experimentally verified Einstein's predictions and received the Nobel Prize for his work in 1926. Perrin [67], giving a physicist's view of mathematics in 1913, stated that curves without derivatives are more common than those special, but interesting ones, like the circle, that have derivatives. In fact he was quite adamant in his arguments emphasizing the importance of nonanalytic functions for describing complex physical phenomena, such as Brownian motion. Thus, there are valid physical reasons for looking for these types of functions, but the scientific reasons became evident to the general scientific community only long after the mathematical discoveries made by Weierstrass.

On the theoretical physics side, the Kolmogorov–Arnold–Moser (KAM) theory for conservative dynamical systems describes how the continuous trajectories of a particle break up into a chaotic sea of randomly disconnected points. Furthermore, the strange attractors of dissipative dynamical systems have a fractal dimension in phase space. Both these developments in classical dynamics—KAM theory and strange attractors—emphasize the importance of nonanalytic functions in the description of the evolution of deterministic nonlinear dynamical systems. We do not discuss the details of such dynamical systems herein, but refer the reader to a number of excellent books on the

subject ranging from the mathematical rigorous, but readable [68], to provocative picture books [69], to extensive applications [23].

In this section we describe some of the essential features of fractal functions starting from the simple dynamical processes described by functions that are fractal (such as the Weierstrass function) and that are continuous everywhere but are nowhere differentiable. This idea of nondifferentiability leads to the introduction of the elementary definitions of fractional integrals and fractional derivatives starting from the limits of appropriately defined sums. We find that the relation between fractal functions and the fractional calculus is a deep one. For example, the fractional derivative of a regular function yields a fractal function of dimension determined by the order of the fractional derivative. Thus, the changes in time of phenomena that are best described by fractal functions are probably best described by fractional equations of motion, as well. In any event, this latter perspective is the one we developed elsewhere [52] and discuss herein. Others have also made inquiries along these lines [70]:

> It is interesting to investigate whether fractional calculus, which generates the operation of derivation and integration to fractional order, can provide a possible calculus to deal with fractals. In fact there has been a surge of activity in recent times which supports this point of view. This possible connection between fractals and fractional calculus gives rise to various interesting questions. . . .

The separation of time scales in physical phenomena allows us to smooth over the microscopic fluctuations and construct a differentiable representation of the dynamics on large space scales and long time scales. However, such smoothing is not always possible, examples of physical phenomena that resist this approach include turbulent fluid flow [71], the stress relaxation of viscoelastic materials such as plastics and rubber [72,73], and finally phase transitions [74,75].

Metaphorically, these complex phenomena, whose evolution cannot be described by ordinary differential equations of motion, leap and jump in unexpected ways to obtain food; they unpredictably twist and turn to avoid capture, and they suddenly change strategy to anticipate environmental changes. To understand these and other analogous processes in physiology, we find that we must adopt a new type of modeling, one that is not in terms of ordinary or partial differential equations of motion. It is clear that the fundamental elements of complex physical phenomena, such as phase transitions, the deformation of plastics, and the stress relaxation of polymers, satisfy Newton's laws. In these phenomena the evolution of individual particles are described by ordinary differential equations that control the dynamics of individual particle trajectories. It is equally clear that the connection between the fundamental laws of motion controlling the individual particle dynamics and the observed large-scale dynamics cannot be made in any straightforward way.

In previous sections we have investigated the scaling properties of processes described by certain stochastic differential equations. The scaling in the system response was a consequence of the inverse power-law correlation in the fluctuations driving the system. The fractal statistics of the dynamic model in Section III are suggestive of the scaling observed in the physiologic time series presented in Section II. Of course this is not the only way the system variable, as characterized by measured time series, can manifest scaling. Another is through the internal dynamics of the system, and that is what we explore in this section. We construct a fractional Langevin equation in which the fractional derivatives give rise to the long-time memory in the system dynamics. It is determined that the solutions to such equations describe multifractal statistics, and we subsequently apply this model to a number of physiological phenomena, including cerebral blood flow and migraines.

A. Fractional Calculus

It is useful to have in mind the formalism of the fractional calculus before embarking on the interpretation of models using this formalism to explain the complexity of physiological phenomena. What we call the fractional calculus dates back to a question L'Hôpital asked Leibniz in 1695, where in a letter he asked the meaning of the expression $d^n y/dx^n$ if $n = 1/2$, that is:

> ...what if n is fractional?

Leibniz replied in part [76]:

> Thus it follows that $d^{1/2}x$ will be equal to $2\sqrt{dx : x}$.... John Bernoulli seems to have told you of my having mentioned to him a marvelous analogy which makes it possible to say in a way the successive differentials are in geometric progression. One can ask what would be a differential having as its exponent a fraction. You see that the result can be expressed by an infinite series. Although this seems removed from Geometry, which does not yet know of such fractional exponents, it appears that one day these paradoxes will yield useful consequences, since there is hardly a paradox without utility.

After 310 years of sporadic development, the fractional calculus is now becoming so sufficiently well developed and well known that books and articles are being devoted to its consequences in the physical sciences [53,77,78].

The simplest way to introduce fractional derivatives is to consider the ordinary derivative of a monomial, say the nth derivative of t^m for $m > n$:

$$\begin{aligned} D_t^n[t^m] &= m(m-1)\dots(m-n+1)t^{m-n} \\ &= \frac{m!}{(m-n)!}t^{m-n} \end{aligned} \tag{101}$$

where the operator D_t is the ordinary derivative. We can generalize the form of Eq. (101) by recognizing that the ratio of factorials can be expressed as the ratio of gamma functions:

$$D_t^n[t^m] = \frac{\Gamma(m+1)}{\Gamma(m+1-n)} t^{m-n} \tag{102}$$

We can extend these considerations to fractional derivatives by means of analogy. We define a real indexed derivative of a monomial t:

$$D_t^\alpha[t^\beta] = \frac{\Gamma(\beta+1)}{\Gamma(\beta+1-\alpha)} t^{\beta-\alpha} \tag{103}$$

where $\beta + 1 \neq 0, -1, -2, \ldots, -n$; this is, the monomial index is not integer-valued.

With this analogy we can solve the ½-derivative problem posed to Leibniz. Consider the definition (103) for $\alpha = \beta = ½$ yielding

$$\begin{aligned} D_t^{1/2}[t^{-1/2}] &= \frac{\Gamma(-1/2+1)}{\Gamma(-1/2+1-1/2)} t^{-1/2-1/2} \\ &= \frac{\Gamma(1/2)}{\Gamma(0)} t^{-1} = 0 \end{aligned}$$

since $\gamma(0) = \infty$. Thus, a particular function is effectively a constant with regard to a certain functional derivative. Consider a second example, this time with monomial index equal to zero $\beta = 0$ so that we have the ½-derivative of a constant:

$$\begin{aligned} D_t^{1/2}[1] &= \frac{\Gamma(0+1)}{\Gamma(0+1-1/2)} t^{-1/2} \\ &= \frac{1}{\sqrt{\pi t}} \end{aligned}$$

where we see that the constant is not a constant with regard to fractional derivatives. Finally, there is the ½-derivative of t, $\beta = 1$:

$$D_t^{1/2}[t] = \frac{\Gamma(1+1)}{\Gamma(1+1/2)} t^{1-1/2} = \sqrt{\frac{t}{\pi}}$$

the result obtained by Leibniz.

Another way to introduce fractional operators is by generalizing Cauchy's formula for a n-fold integration over a fixed time interval (a,t):

$$\frac{1}{(n-1)!}\int_a^t (t-\xi)^{n-1} f(\xi)d\xi = \int_a^t \int_a^{t_1} \cdots \int_a^{t_{n-1}} f(\xi_n)\, d\xi_n \cdot \cdot d\xi_1 \equiv {}_aD_t^{(-n)}[\, f(t)] \quad (104)$$

where the operator ${}_aD_t^{(-n)}[\cdot]$ denotes the n-fold integration operation. The fractional integral analogue to this equation is defined as

$${}_aD_t^{(-\alpha)}[f(t)] = \frac{1}{\Gamma(\alpha)}\int_a^t (t-\xi)^{\alpha-1} f(\xi)\, d\xi, \qquad t \geq a \quad (105)$$

where the factorial has been replaced by the gamma function, the latter having an analytic continuation into the complex domain for noninteger and nonpositive values of its argument. The corresponding fractional derivative is given by

$${}_aD_t^{(\alpha)} = \frac{d^n}{dt^n}\, {}_aD_t^{(\alpha-n)} \quad (106)$$

where $[\alpha]+1 \geq n \geq [\alpha]$ and the bracket denotes the integer value n closest to α. Consequently for $\alpha < 1/2$ we have $n = 0$. Equation (105) is the Riemann–Liouville (RL) formula for the fractional operator; it is the integral operator when $\alpha < 0$ and it is the differential operator interpreted as (106) when $\alpha > 0$.

1. *Derivative of a Fractal Function*

Richardson, in his 1926 investigation of turbulence, observed that the velocity field of the atmospheric wind is so erratic that it probably cannot be described by an analytic function [79]. He suggested a Weierstrass function as a candidate to represent the velocity field, since the function is continuous everywhere, but nowhere differentiable, properties he observed in the wind-field data. Here we investigate a generalization of the Weierstrass function in order to simplify some of the discussion:

$$W(t) = \sum_{n=-\infty}^{\infty} \frac{1}{a^n}[1 - \cos(b^n t)] \quad (107)$$

under the conditions that $b > a > 1$. The generalized Weierstrass function (GWF) satisfies the scaling relation

$$W(bt) = aW(t) \quad (108)$$

resulting from a simple shift of the index n in the summation. Equation (108) has the form of a renormalization group scaling relation [5], which can be solved by assuming a solution of the form

$$W(t) = \sum_{n=-\infty}^{\infty} A_n t^{H_n} \tag{109}$$

Inserting Eq. (109) into Eq. (108) yields the equation for the scaling index:

$$H_n = \frac{\ln a}{\ln b} - i\frac{2\pi n}{\ln b} \tag{110}$$

where the scaling exponent is seen to be complex. This exponent has been related to a complex fractal dimension in the architecture of the human lung [80], in many other physiological systems [5,23], and in earthquakes, turbulence, and financial crashes [81].

The GWF is a superposition of harmonic terms having increasing frequencies as powers of b with decreasing amplitudes as powers of $1/a$. This function has a fractal dimension D if we choose $a = b^{2-D}$, so that in terms of the fractal dimension we write the GWF as

$$W(t) = \sum_{n=-\infty}^{\infty} \frac{1}{b^{(2-D)n}}[1 - \cos(b^n t)] \tag{111}$$

The RL -fractional integral of the GWF is given by

$$W^{(-\alpha)}(t) \equiv {}_{-\infty}D_t^{(-\alpha)}[W(t)] = \frac{1}{\Gamma(\alpha)} \int_{-\infty}^{t} \frac{W(\xi)}{(t-\xi)^{1-\alpha}} d\xi \tag{112}$$

for $0 < \alpha < 1$, which after some not so straightforward analysis [23,82] yields

$$W^{(-\alpha)}(t) = \sum_{n=-\infty}^{\infty} \frac{1}{b^{(2-D+\alpha)n}} [1 - \cos(b^n t)] \tag{113}$$

Similarly the RL-fractional derivative of the GWF is given by

$$W^{(\alpha)}(t) \equiv {}_{-\infty}D_t^{(\alpha)}[W(t)] = \frac{1}{\Gamma(1-\alpha)} \frac{d}{dt} \int_{-\infty}^{t} \frac{W(\xi)}{(t-\xi)^{\alpha}} d\xi \tag{114}$$

for $0 < \alpha < 1$, which integrates to [23,82]

$$W^{(\alpha)}(t) = \sum_{n=-\infty}^{\infty} \frac{1}{b^{(2-D-\alpha)n}} [1 - \cos(b^n t)] \tag{115}$$

Consequently, we see that the fractional integral shifts the fractal dimension $D \to D - \alpha$ and the fractional derivative shifts the fractal dimension $D \to D + \alpha$.

These results can be interpreted by noticing that the fractional dimension gives information about the degree of irregularity of the function under analysis. Carrying out a fractional integral of the GWF implies decreasing its fractional dimension and therefore smooths the process, whereas carrying out the fractional derivative means increasing the fractional dimension and therefore making the process and its increments more irregular. What is most intriguing is the fact that a fractional operator acting on a fractal function yields another fractal function; the derivative does not diverge, as does an ordinary derivative of a fractal function, like that of Weierstrass. This suggests that the fractional calculus might be the appropriate method for characterizing the dynamics of complex phenomena, particularly those that are described by fractal functions.

2. *Fractional Brownian Motion*

In the previous subsection it would have been possible to extend out discussion to random processes by including random phases in the definition of the GWF:

$$W(t) = \mathrm{Re}\left\{ \sum_{n=-\infty}^{\infty} \frac{1}{a^n} \left[1 - e^{ib^n t}\right] e^{i\phi_n} \right\} \tag{116}$$

where the phase is a random quantity uniformly distributed on the interval $(0,2\pi)$. Equation (116) would be one way to introduce a random function that has the desired scaling properties and we could discuss the dynamics of this process in time using the fractional operators. An alternative approach is to start with continuous functions and that is what we do now. Consider a function defined by the Fourier transform

$$\xi(t) = \frac{1}{2\pi} \int_{-\infty}^{\infty} e^{-i\omega t} \hat{\xi}(\omega)\, d\omega \tag{117}$$

Operating on this function with the RL-fractional operator, with a lower limit of negative infinity, defines a new function

$$F_\alpha(t) \equiv {}_{-\infty}D_t^{(-\alpha)}[\xi(t)] = \frac{1}{2\pi} \int_{-\infty}^{\infty} e^{-i\omega t} (-i\omega)^{-\alpha} \hat{\xi}(\omega)\, d\omega \tag{118}$$

and the weighting in the integrand is obtained by operating on the exponential in the Fourier transform ${}_{-\infty}D_t^{(-\alpha)}[e^{i\omega t}] = e^{i\omega t}(i\omega)^{-\alpha}$. If we now interpret the function Eq. (117) as a stochastic quantity, then we can evaluate the correlation of the function Eq. (118) at two time points separated by an interval τ

$$\langle F_\alpha(t)F_\alpha^*(t+\tau)\rangle = \frac{1}{(2\pi)^2}\int_{-\infty}^{\infty} d\omega_1 \int_{-\infty}^{\infty} d\omega_2 e^{-i(\omega_1-\omega_2)t}e^{i\omega_2\tau}\omega_1^{-\alpha}\omega_2^{-\alpha}\langle\hat{\xi}(\omega_1)\hat{\xi}^*(\omega_2)\rangle \tag{119}$$

where the brackets denote an average over an ensemble of realizations of random fluctuations. If the random fluctuations correspond to a Wiener process, the average in the integrand reduces to

$$\langle\hat{\xi}(\omega_1)\hat{\xi}^*(\omega_2)\rangle = C\delta(\omega_1-\omega_2) \tag{120}$$

and C is a constant. Substituting Eq. (120) into Eq. (119) and integrating over one of the frequencies yields for the autocorrelation function

$$\langle F_\alpha(t)F_\alpha^*(t+\tau)\rangle = \frac{C}{(2\pi)^2}\int_{-\infty}^{\infty} d\omega e^{i\omega\tau}\omega^{-2\alpha} \propto \tau^{2\alpha-1} \tag{121}$$

If we make the association of the order of the fractional operator with the Hurst exponent

$$\alpha = H - 1/2 \tag{122}$$

we observe that the fractional index lies in the interval $-1/2 \leq \alpha \leq 1/2$, because the Hurst exponent is confined to the interval $0 < H \leq 1$. Therefore the solution to the fractal stochastic equation of motion

$${}_{-\infty}D_t^{(\alpha)}[F_\alpha(t)] = \xi(t) \tag{123}$$

given by Eq. (115) has the same scaling properties as the dichotomous process with the inverse power-law correlations studied in Section III.

Note that Eq. (118) is a colored noise representation of the dynamics expressed by Eq. (123). Even though the central moments of the solution to Eq. (123) scale in the present case in the same way as the moments did for the process in Section III, they are very different processes. The simplest way to see the difference is to note that the integral relation in Eq. (118) is linear so that the solution $F_\alpha(t)$ and the random fluctuations $\xi(t)$ have the same statistics,

which, by assumption, are Gaussian. Consequently the solution $F_\alpha(t)$ is a realization of fractional Brownian motion with the fractional index restricted to the indicated region. This is certainly different from the exact solution given by the series expansion for the phase-space distribution function in Eq. (74).

B. Fractional Langevin Equations

Of course, the fractional calculus does not in itself constitute a physical/biological theory; however, one requires such a theory in order to interpret the fractional derivatives and integrals in terms of physical/biological phenomena. We therefore follow a pedagogical approach and examine the simple relaxation process described by the rate equation

$$\frac{d}{dt}\Phi(t) + \lambda\Phi(t) = 0 \tag{124}$$

where $t > 0$ and the relaxation rate λ determines how quickly the process returns to its equilibrium state. The solution to Eq. (124) is given by $\Phi(t) = \Phi(0)e^{-\lambda\tau}$, which is unique in terms of the initial condition $\Phi(0)$. An alternative way of writing Eq. (124) is in terms of the anti-derivative operator

$$\Phi(t) - \Phi(0) = \lambda\left(\frac{d}{dt}\right)^{-1}\Phi(t)$$

which suggests, for its generalization, replacing the anti-derivative with the RL-fractional integral operator

$$\Phi(t) - \Phi(0) = \lambda^\alpha {}_0D_t^{(-\alpha)}[\Phi(t)] \tag{125}$$

where the lower limit of the fractional integral is zero, corresponding to the initial value problem. Operating on the left in Eq. (125) with the fractional derivative we obtain the generalization to the relaxation equation given by [83]

$${}_0D_t^{(\alpha)}[\Phi(t)] + \lambda^\alpha\Phi(t) = \frac{t^{-\alpha}\Phi(0)}{\Gamma(1-\alpha)} \tag{126}$$

and the initial value becomes an inhomogeneous term in this fractional relaxation equation of motion. Here the relaxation time is raised to the power $\alpha > 0$ in order to maintain the correct dimensionality.

Equations of the form (126) are mathematically well-defined, and strategies for solving such equations have been developed by a number of investigators, particularly in the book by Miller and Ross [84] that is devoted almost

exclusively to solving such equations when the index is rational. Here we make no such restriction and consider the Laplace transform of Eq. (126) to obtain

$$\tilde{\Phi}(s) = \frac{\Phi(0)}{s} \frac{s^\alpha}{\lambda^\alpha + s^\alpha} \tag{127}$$

whose inverse Laplace transform is the solution to the fractional differential equation. Inverting Laplace transforms such as Eq. (127) is nontrivial and an excellent technique that overcomes many of the technical difficulties, implemented by Nonnenmacher and Metzler [83], involve the use of Fox functions [53]. The solution to the fractional relaxation equation is given by the series expansion for the standard Mittag–Leffler function

$$\Phi(t) = \Phi(0) E_\alpha(-(\lambda t)^\alpha) = \Phi(0) \sum_{k=0}^{\infty} \frac{(-1)^k}{\Gamma(1 + k\alpha)} (\lambda t)^{k\alpha} \tag{128}$$

which in the limit $\alpha \to 1$ yields the exponential function

$$\lim_{\alpha \to 1} E_\alpha(-(\lambda t)^\alpha) = e^{-\lambda t}$$

as it should, since under this condition (126) reduces to the ordinary relaxation rate equation Eq. (124).

The Mittag–Leffler function has interesting properties in both the short-time and the long-time limits. In the short-time limit it yields the Kohlrausch–Williams–Watts Law from stress relaxation in rheology given by

$$\lim_{t \to 0} E_\alpha(-(\lambda t)^\alpha) = e^{-(\lambda t)^\alpha} \tag{129}$$

also known as the stretched exponential. In the long-time limit it yields the inverse power law, known as the Nutting Law,

$$\lim_{t \to \infty} E_\alpha(-(\lambda t)^\alpha) = (\lambda t)^{-\alpha} \tag{130}$$

Figure 12 displays the Mittag–Leffler function as well as the two asymptotes, the dashed curve being the stretched exponential and the dotted curve the inverse power law. What is apparent from this discussion is the long-time memory associated with the fractional relaxation process, being an inverse power law rather than the exponential of ordinary relaxation. It is apparent that the Mittag–Leffler function smoothly joins these two empirically determined asymptotic distributions.

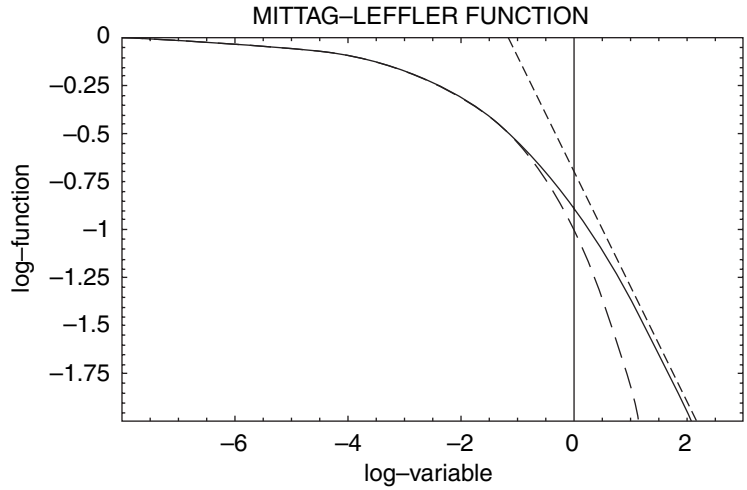

Figure 12. The solid curve is the Mittag–Leffler function, the solution to the fractional relaxation equation. The dashed curve is the stretched exponential (Kohlrausch–Williams–Watts Law), and the dotted curve is the inverse power law (Nutting Law).

We can now generalize the fractional differential equation to include a random force $\xi(t)$ and in this way obtain a fractional Langevin equation

$$ {}_0D_t^{(\alpha)}[\Phi(t)] + \lambda^\alpha \Phi(t) = \frac{t^{-\alpha}\Phi(0)}{\Gamma(1-\alpha)} + \xi(t) \tag{131} $$

The solution to this equation is obtained using Laplace transforms as done previously:

$$ \tilde{\Phi}(s) = \frac{\Phi(0)s^{\alpha-1}}{\lambda^\alpha + s^\alpha} + \frac{\tilde{\xi}(s)}{\lambda^\alpha + s^\alpha} \tag{132} $$

Note the difference in the s-dependence of the two coefficients of the right-hand side of Eq. (132). The inverse Laplace transform of the first term yields the Mittag–Leffler function as found in the homogeneous case above. The inverse Laplace transform of the second term is the convolution of the random force and a stationary kernel. The kernel is given by the series

$$ E_{\alpha,\beta}(z) \equiv \sum_{k=0}^{\infty} \frac{z^k}{\Gamma(\alpha k + \beta)}, \qquad \alpha > 0, \beta > 0 \tag{133} $$

which is the generalized Mittag–Leffler function. The function defined by Eq. (133) reduces to the usual Mittag–Leffler function when $\beta = 1$, so that both

the homogeneous and inhomogeneous terms in the solution to the fractional Langevin equation can be expressed in terms of these series.

Note that taking the average value of Eq. (131) and observing that the average of the random force is zero, we obtain

$$ {}_0D_t^{(\alpha)}[\langle\Phi(t)\rangle] + \lambda^\alpha\langle\Phi(t)\rangle = \frac{t^{-\alpha}\Phi(0)}{\Gamma(1-\alpha)} \tag{134} $$

which is clearly of the form of the fractional stress relaxation equation. The average response of the system is determined by the Mittag–Leffler function; that is, the average has a long-time memory (inverse power law).

The explicit inverse of Eq. (132) yields the solution [53]

$$ \Phi(t) = \Phi(0)E_\alpha(-(\lambda t)^\alpha) + \int_0^t (t-t')^{\alpha-1}E_{\alpha,\alpha}(-(\lambda t)^\alpha)\xi(t')\,dt' \tag{135} $$

In the case $\alpha = 1$, the Mittag–Leffler function becomes the exponential, so that the solution to the fractional Langevin equation reduces to that for an Ornstein–Uhlenbeck process

$$ \Phi(t) = \Phi(0)e^{-\lambda t} + \int_0^t e^{-\lambda(t-t')}\xi(t')\,dt' \tag{136} $$

as it should. The analysis of the autocorrelation function of Eq. (135) can be quite daunting and so we do not pursue it further here, but refer the reader to the literature [53,85]. A somewhat simpler problem is the fractional Langevin equation without dissipation.

Consider the second moment of the solution to the Langevin equation when $\lambda = 0$ giving rise to

$$ \langle[\Phi(t_1)-\Phi(0)][\Phi(t_1)-\Phi(0)]\rangle = \frac{1}{\Gamma(\alpha)^2}\int_0^{t_1} d\tau_1 \int_0^{t_2} d\tau_2 \frac{\langle\xi(\tau_1)\xi(\tau_2)\rangle}{(t_1-\tau_1)^{1-\alpha}(t_2-\tau_2)^{1-\alpha}} \tag{137} $$

Here again we take the random force to have Gaussian statistics and to be delta correlated in time:

$$ \langle\xi(\tau_1)\xi(\tau_2)\rangle = C\delta(\tau_1-\tau_2) \tag{138} $$

Inserting Eq. (138) into the expression for the autocorrelation function (137) and noting that the integral is symmetric in the times, the delta function restricts the integration to the lesser of the two times, so introducing the notation for the lesser time $t_<$ and greater time $t_>$ we obtain [53]

$$\langle[\Phi(t_>) - \Phi(0)][\Phi(t_<) - \Phi(0)]\rangle = \frac{2Ct_>^{\alpha-1}t_<^{\alpha}}{\Gamma(\alpha)^2} F\left(1; 1-\alpha; 1+\alpha : \frac{t_<}{t_>}\right) \tag{139}$$

in terms of the hypergeometric function. Note that although the statistics of the solution are Gaussian, they are also nonstationary, since the autocorrelation function depends on the lesser and the greater times separately and not on their difference.

Of course, we can also use the general expression Eq. (139) to write the second moment of the solution at time $t = t_< = t_>$,

$$\begin{aligned}\langle[\Phi(t) - \Phi(0)]^2\rangle &= \frac{2Ct^{2\alpha-1}}{\Gamma(\alpha)^2} F(1; 1-\alpha; 1+\alpha : 1) \\ &= \frac{2Ct^{2\alpha-1}}{(2\alpha-1)\Gamma(\alpha)^2}\end{aligned} \tag{140}$$

where the second equality results from writing the hypergeometric function as the ratio of gamma functions. The time dependence of the second moment [Eq. (140)] agrees with that obtained for anomalous diffusion in Section III, if we make the identification $2H = 2\alpha - 1$, where, since the fractional index is less than one, we have $1/2 \geq H > 0$. Consequently, the process described by the dissipation-free fractional Langevin equation is antipersistent.

This antipersistent behavior of the time series was observed by Peng et al. [25] for the differences in time intervals between heart beats. They interpreted this result, as did a number of subsequent investigators, in terms of random walks with $H < 1/2$. However, we can see from Eq. (140) that the fractional Langevin equation without dissipation is an equally good, or one might say an equivalent, description of the underlying dynamics. The scaling behavior alone cannot distinguish between these two models; what is needed is the complete statistical distribution and not just the time-dependence (scaling behavior) of a moment.

1. *Physical/Physiological Models*

A theoretical Langevin equation is generally constructed from a Hamiltonian model for a simple dynamical system coupled to the environment. The equations of motion for the coupled system are manipulated so as to eliminate the degrees

of freedom of the environment from the dynamical description of the system. Only the initial state of the environment (heat bath) remains in the Langevin description, where the random nature of the driving force is inserted through the choice of distribution of the initial states of the bath. The simplest Langevin equation for a dynamical system open to the environment has the form

$$\frac{dX(t)}{dt} + \lambda X(t) = \xi(t) \tag{141}$$

where $\xi(t)$ is a random force, λ is a dissipation parameter and there exists a fluctuation–dissipation relation connecting the two [86]. Of course we cannot completely interpret Eq. (141) until we specify the statistical properties of the fluctuations, and for this we need to know the environment of the system. The random driver is typically assumed to be a Wiener process—that is, to have Gaussian statistics and no memory.

When the system dynamics depends on what occurred earlier—that is, the environment has memory—Eq. (141) is no longer adequate and the Langevin equation must be modified. The generalized Langevin equation takes this memory into account through an integral term of the form

$$\frac{dX(t)}{dt} + \int_0^t K(t-t')X(t')\,dt' = \xi(t) \tag{142}$$

where the memory kernel replaces the dissipation parameter and the fluctuation–dissipation relation becomes generalized:

$$K(\tau) = \langle \xi(t+\tau)\xi(t) \rangle \tag{143}$$

Both these Langevin equations are monofractal if the fluctuations are monofractal, which is to say, the time series given by the trajectory $X(t)$ is a fractal random process if the random force is a fractal random process.

However, neither of these models is adequate for describing multifractal statistical processes as they stand. A number of investigators have recently developed multifractal random walk models to account for the multifractal character of various physiological phenomena, and here we introduce a variant of those discussions based on the fractional calculus. The most recent generalization of the Langevin equation incorporates memory into the system's dynamics and has the simple form of Eq. (131) with the dissipation parameter set to zero:

$${}_0D_t^{(\mu)}[X(t)] - \frac{t^{-\alpha}}{\Gamma(1-\mu)}X_0 = \xi(t) \tag{144}$$

Equation (144) could also be obtained from the construction of a fractional Langevin equation by Lutz [87] for a free particle coupled to a fractal heat bath, when the inertial term is negligible. The formal solution to this fractional Langevin equation is

$$X(t) - X_0 = \frac{1}{\Gamma(\mu)} \int_0^t \frac{\xi(t')dt'}{(t-t')^{1-\mu}}$$

which can be expressed in terms of the integral kernel:

$$X(t) - X_0 = \int_0^t K_\mu(t-t')\xi(t')\,dt' \tag{145}$$

As mentioned earlier, the form of this relation for multiplicative stochastic processes and its association with multifractals has been noted in the phenomenon of turbulent fluid flow [61], through a space, rather than time, integration kernel.

The random force term on the right-hand side of Eq. (145) is selected to be a zero-centered, Gaussian random variable and therefore to scale as [21]

$$\xi(\lambda t) = \lambda^{-H}\xi(t) \tag{146}$$

where the Hurst exponent is in the range $0 < H \leq 1$. In a similar way the kernel in Eq. (145) is easily shown to scale as

$$K_\mu(\lambda t) = \lambda^\mu K_\mu(t) \tag{147}$$

so that the solution to the fractional Langevin equation scales as

$$X(\lambda t) - X_0 = \lambda^{-H+\mu}[X(t) - X_0] \tag{148}$$

In order to make the solution to the fractional Langevin equation a multifractal, we assume that the parameter α is a random variable. To construct the traditional measures of multifractal stochastic processes, we calculate the qth moment of the solution (148) by averaging over both the random force and the random parameter to obtain

$$\begin{aligned} \langle |X(\lambda t) - X_0|^q \rangle &= \lambda^{(q-1)H} \langle \lambda^{q\mu} \rangle \langle |X(t) - X_0|^q \rangle \\ &= \langle |X(t) - X_0|^q \rangle \lambda^{\rho(q)} \end{aligned} \tag{149}$$

The scaling relation in Eq. (149) determines the qth order structure function exponent $\rho(q)$. Note that when $\rho(q)$ is linear in q the underlying process is monofractal, whereas when it is nonlinear in q the process is multifractal, because we can relate the structure function to the mass exponent [88]:

$$\rho(q) = 2 - \tau(q) \tag{150}$$

Consequently we have that $\rho(0) = H$ so that $\tau(0) = 2 - H$, as it should because of the well-known relation between the fractal dimension and the global Hurst exponent $D_0 = 2 - H$.

To determine the structure function exponent, we make an assumption about the statistics of the parameter α. We can always write the μ-average as

$$\langle \lambda^{q\mu} \rangle = \langle e^{qZ(\ln\lambda)} \rangle \tag{151}$$

where $Z(\ln \lambda)$ is the random variable. In this way the expression on the right-hand side of Eq. (151) is the Laplace transform of the probability density. We assume the random variable is an α-stable Lévy process in which case the statistics of the multiplicative fluctuations are given by the distribution

$$P(x,s) = \frac{1}{2\pi} \int_{-\infty}^{\infty} e^{ikz} e^{-bs|k|^{\alpha}} dk \tag{152}$$

with $0 < \alpha \leq 2$. Inserting Eq. (152) into Eq. (151) and integrating over z yields the delta function $\delta(k + iq)$, which, integrating over k, results in

$$\langle e^{qZ(\ln\lambda)} \rangle = e^{-b|q|^{\alpha}\ln\lambda} = \lambda^{-b|q|^{\alpha}} \tag{153}$$

so that comparing this result with Eq. (149) we obtain for the structure function exponent

$$\rho(q) = (q-1)H - b|q|^{\alpha} \tag{154}$$

Therefore the solution to the fractional Langevin equation corresponds to a monofractal process only in the case $\alpha = 1$ and $q > 0$; otherwise the process is multifractal. We restrict the remaining discussion to positive moments.

Thus, we observe that when the memory kernel in the fractional Langevin equation is random, the solution consists of the product of two random quantities giving rise to a multifractal process. This is Feller's subordination process. We apply this approach to the SRV time series data discussed in Section II and observe, for the statistics of the multiplicative exponent given by Lévy statistics, the singularity spectrum as a function of the positive moments

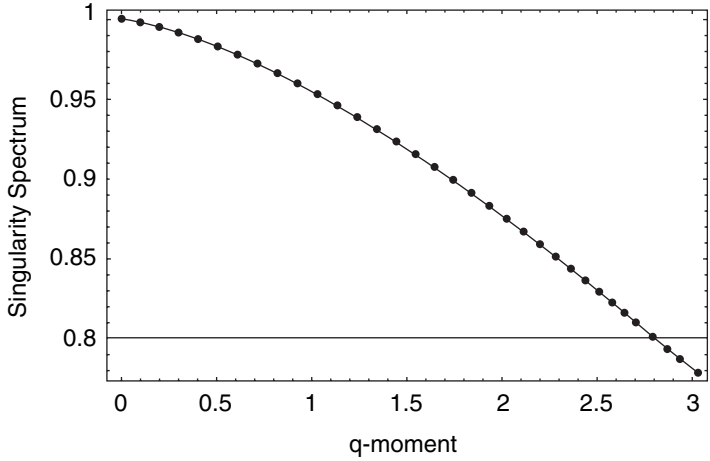

Figure 13. The singularity spectrum for $q > 0$ obtained through the numerical fit to the human gait data. The curve is the average over the 10 data sets obtained in the experiment [11].

shown by the points in Fig. 13. The solid curve in this figure is obtained from the analytic form of the singularity spectrum

$$f(q) = 2 - H - (\alpha - 1)bq^{\alpha} \tag{155}$$

which is determined by substituting Eq. (154) into the equation for the singularity spectrum [Eq. (84)], through the relationship between exponents [Eq. (150)]. It is clear from Fig. 13 that the data are well fit by the solution to the fractional Langevin equation with the parameter values $\alpha = 1.45$ and $b = 0.1$, obtained through a mean-square fit of Eq. (155) to the SRV time series data.

The nonlinear form of the mass exponent in Fig. 9a, the convex form of the singularity spectrum $f(h)$ in Fig. 9b, and the fit to $f(q)$ in Fig. 13, are all evidence that the interstride interval time series are multifractal. This analysis is further supported by the fact that the maxima of the singularity spectra coincide with the fractal dimensions determined using the scaling properties of the time series using the allometric aggregation technique.

Of course, different physiologic processes generate different fractal time series, because the long-time memory of the underlying dynamical processes can be quite different. Physiological signals, such as cerebral blood flow (CBF), are typically generated by complex self-regulatory systems that handle inputs with a broad range of characteristics. Ivanov et al. [89] established that healthy human heartbeat intervals, rather than being fractal, exhibit multifractal properties and uncovered the loss of multifractality for a life-threatening condition of congestive heart failure. West et al. [90] similarly determined that

CBF in healthy humans is also multifractal, and this multifractality is severely narrowed for people who suffer from migraines.

Migraine headaches have been the bane of humanity for centuries, afflicting such notables as Caesar, Pascal, Kant, Beethoven, Chopin, and Napoleon. However, its etiology and pathomechanism have to date not been satisfactorily explained. It was demonstrated [90] that the characteristics of CBF time series significantly differs between that of normal healthy individuals and migraineurs. Transcranial Doppler ultrasonography (TCD) enables high-resolution measurement of middle cerebral artery blood flow velocity. Like the HRV, SRV, and BRV time series data, the time series of cerebral blood flow velocity consists of a sequence of waveforms. These waveforms are influenced by a complex feedback system involving a number of variables, such as arterial pressure, cerebral vascular resistance, plasma viscosity, arterial oxygen, and carbon dioxide content, as well as other factors. Even though the TCD technique does not allow us to directly determine CBF values, it helps to clarify the nature and role of vascular abnormalities associated with migraine. In particular we present the multifractal properties of human middle cerebral artery flow velocity, an example of which is presented below in Fig. 14

The dynamical aspects of cerebral blood flow regulation were recognized by Zhang et al. [91]. Rossitti and Stephensen [92] used the relative dispersion (the ratio of the standard deviation to mean), of the middle cerebral artery flow velocity time series to reveal its fractal nature; this is a technique closely related to the allometric aggregation introduced in Section II. West et al. [93] extended this line or research by taking into account the more general properties of fractal time series, showing that the beat-to-beat variability in the flow velocity has a long-time memory and is persistent with the average scaling exponent 0.85 ± 0.04, a value consistent with that found earlier for HRV time series. They also observed that cerebral blood flow was multifractal in nature.

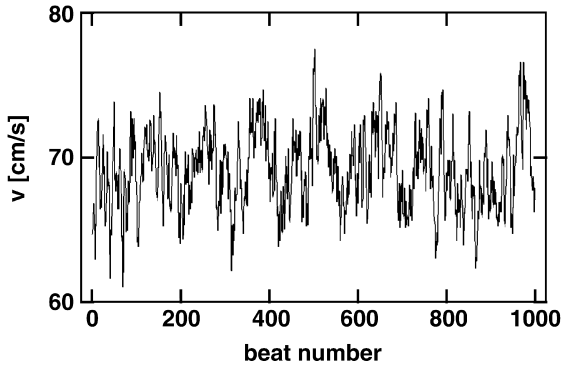

Figure 14. Middle cerebral artery flow velocity time series for a typical healthy subject [90].

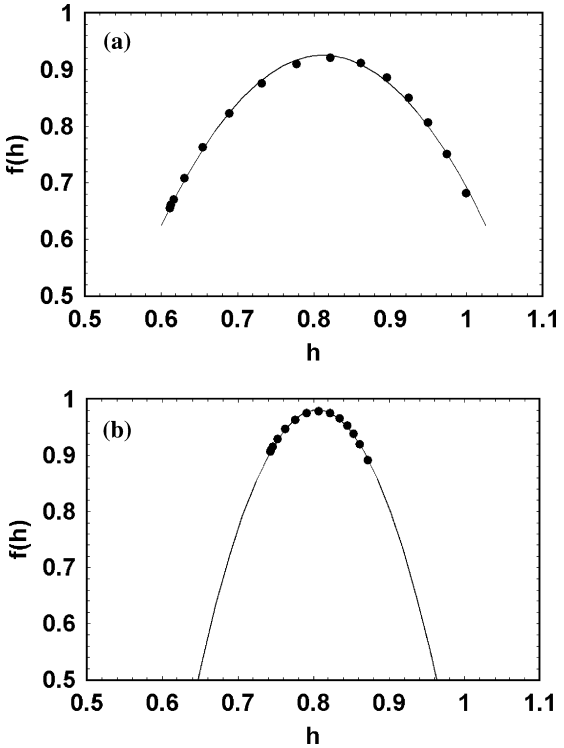

Figure 15. The average multifractal spectrum for middle cerebral blood flow time series is depicted by $f(h)$. (*a*) The spectrum is the average of 10 time series measurements from five healthy subjects (filled circles). The solid curve is the best least-squares fit of the parameters to the predicted spectrum using Eq. (157). (*b*) The spectrum is the average of 14 time series measurements of eight migraineurs (filled circles). The solid curve is the best least-squares fit to the predicted spectrum using Eq. (157). (Taken from [90].)

In Fig. 15 we compare the multifractal spectrum for middle cerebral artery blood flow velocity time series for a healthy group of five subjects and a group of eight migraineurs [90]. A significant change in the multifractal properties of the blood flow time series is apparent. Namely, the interval for the multifractal distribution on the local scaling exponent is greatly constricted. This is reflected in the small value of the width of the multifractal spectrum for the migraineurs (0.013), which is almost three times smaller than the width for the control group (0.038); for both migraineurs with and without aura the distribution is centered at 0.81, the same as that of the control group, so the average scaling behavior would appear to be the same. However, the contraction of the spectrum suggests that the underlying process has lost its flexibility. The biological advantage of

multifractal processes is that they are highly adaptive, so that in this case the brain of a healthy individual adapts to the multifractality of the interbeat interval time series. Here again we see that disease, in this case migraine, may be associated with the loss of complexity and consequently the loss of adaptability, thereby suppressing the normal multifractality of cerebral blood flow time series. Thus, the reduction in the width of the multifractal spectrum is the result of excessive dampening of the cerebral flow fluctuations and is the manifestation of the significant loss of adaptability and overall hyperexcitability of the underlying regulation system. West et al. [90] emphasize that hyperexcitability of the CBF control system seems to be physiologically consistent with the reduced activation level of cortical neurons observed in some transcranial magnetic simulation and evoked potential studies.

Regulation of CBF is a complex dynamical process and remains relatively constant over a wide range of perfusion pressure via a variety of feedback control mechanisms, such as metabolic, myogenic, and neurally mediated changes in cerebrovascular impedance respond to changes in perfusion pressure. The contribution to the overall CBF regulation by different areas of the brain is modeled by the statistics of the fractional derivative parameter, which determines the multifractal nature of the time series. The source of the multifractality is over and above that produced by the cardiovascular system.

The multifractal nature of CBF time series is here modeled using a fractional Langevin model. We again implement the scaling properties of the random force and the memory kernel to obtain Eq. (148) as the scaling of the solution to the fractional Langevin equation. Here when we calculate the qth moment of the solution we assume Gaussian, rather than the more general Lévy, statistics. Consequently we obtain the quadratic function for the singularity spectrum

$$f(q) = 2 - H - bq^2 \tag{156}$$

which can be obtained from Eq. (155) by setting $\alpha = 2$. Another way to express Eq. (156) is

$$f(h) = f(H) - \frac{b}{4}(h - H)^2 \tag{157}$$

where we have used the fact that the fractal dimension is given by $2 - H$, which is the value of the function at $h = H$.

It seems that the changes in the cerebral autoregulation associated with migraine can strongly modify the multifractality of middle cerebral artery blood flow. The constriction of the multifractal to monofractal behavior of the blood flow depends on the statistics of the fractional derivative index. As the distribution of this parameter narrows down to a delta function, the nonlocal

influence of the mechanoreceptor constriction disappears. On the other hand, the cerebral autoregulation does not modify the monofractal properties characterized by the single global Hurst exponent, presumably that produced by the cardiovascular system.

C. Fractional Diffusion Equations

The change in time of a stationary stochastic process using the conditional transition probability density $P(x,t|x',t')$ for the dynamical variable $X(t)$ to lie in the range $(x, x+dx)$ conditional on $X(t') = x'$ is given by the chain condition

$$P(x,t|x_0,t_0) = \int_{\Omega} P(x,t|x',t')P(x',t'|x_0,t_0)\,dx' \tag{158}$$

where Ω is the domain of the variate. This equation is often used as the starting equation for the analysis of Brownian motion. Here $P(x,t|x_0,t_0)$ is the probability that the process undergoes a transition from the initial value x_0 to a final value x at time t through a sequence of intermediate values. Equation (158) was introduced by Bachelier in 1900 in his Ph.D. thesis on speculation in the French stock market. The nonphysical application of this equation was probably the reason why his work went unnoticed for nearly 50 years, even though the mathematical content was equivalent to that found in the Einstein papers on diffusion published five and more years later.

The chain condition is the general description of the evolution of the probability density for an infinitely divisible stable process and the solution to which has the most general form of a Markov probability density. When the range of the variate is unbounded $\Omega = (-\infty, \infty)$ and the process under consideration has translational invariance, so the probability density is independent of the origin of the coordinate system $P(x,t|x_0,t_0) = P(x-x_0, t-t_0)$, the chain condition becomes

$$P(x-x_0,t-t_0) = \int_{\Omega} P(x-x',t-t')P(x'-x_0,t'-t_0)\,dx' \tag{159}$$

The stationary chain condition (159) is more simply expressed in terms of characteristic functions, the Fourier transform of the probability density, as the product

$$\phi(k,t-t_0) = \phi(k,t-t')\phi(k,t'-t_0) \tag{160}$$

using the convolution property of Fourier transforms. Montroll and West [64] noticed that, since the probability density resulting from the characteristic function satisfies the product form, its solution yields an infinitely divisible

distribution. The most general form of the characteristic function for infinitely divisible distributions was first obtained by Paul Lévy in 1937.

Here we merely sketch how to obtain the general solution to Eq. (160). Take the logarithm of the equation to obtain

$$\log\phi(k,t-t_0) = \log\phi(k,t-t') + \log\phi(k,t'-t_0) \tag{161}$$

from which it is clear that the characteristic function factors into a function of k, say $g(k)$, and a function of time. In order for the intermediate time to vanish from the solution, the function of time must be linear. Thus, the form of the solution to Eq. (161) is

$$\phi(k,t) = e^{g(k)t} \tag{162}$$

Since the probability density is normalizable at all times, the real part of $g(k)$ must be negative definite. In order for the characteristic function to retain the product form at all spatial scales, it must be infinitely divisible. If we scale the Fourier variable k by a constant factor b, then in order for the probability density to be infinitely divisible, $g(k)$ must be homogeneous:

$$g(bk) = b^{\alpha} g(k) \tag{163}$$

The homogeneity requirement implies that

$$g(k) = -b(\alpha)|k|^{\alpha} \tag{164}$$

where $b(\alpha)$ is a complex function dependent on the parameter α, with a positive definite real part. Thus, we have for the characteristic function

$$\phi(k,t) = e^{-b(\alpha)|k|^{\alpha}t} \tag{165}$$

The symmetric solution to the chain condition is obtained by setting the constant in the exponential to be independent of α, $b(\alpha) = b$. The most general solution is obtained using

$$b(\alpha) = b\left[1 + iC\omega(k,\alpha)\frac{k}{|k|}\right] \tag{166}$$

where C is a real parameter, $\omega(k,\alpha)$ is a real function, and the imaginary part of the coefficient determines the skewness of the distribution.

The functional form of the characteristic function in Eq. (165) gives

$$\phi(k,t) = \exp\left[-bt|k|^{\alpha}\left(1 + iC\omega(k,\alpha)\frac{k}{|k|}\right)\right] \tag{167}$$

so that the inverse Fourier transform sets the conditions $0 < \alpha \leq 2$, so that it is positive definite, $b > 0$ so that it is normalizable, and $-1 \leq C \leq 1$ indicating the degree of skewness. Finally the function $\omega(k,\alpha)$ is defined by

$$\omega(k,\alpha) = \begin{cases} \tan(\alpha\pi/2) & \text{if } \alpha \neq 1 \\ \dfrac{2}{\pi}\ln|k| & \text{if } \alpha = 1 \end{cases} \tag{168}$$

whose derivation can be found in Gnedenko and Kolmogorov [63]. The equation of evolution for the probability density is obtained by taking the time derivative of the characteristic function in Eq. (165):

$$\frac{\partial\phi(k,t)}{\partial t} = -b(\alpha)|k|^{\alpha}\phi(k,t) \tag{169}$$

The inverse Fourier transform of Eq. (169) yields

$$\frac{\partial P(x,t)}{\partial t} = -\int_{-\infty}^{\infty} b(\alpha)e^{-ikx}|k|^{\alpha}\phi(k,t)\frac{dk}{2\pi} \tag{170}$$

which Gorenflo and Mainardi [94] identify with *Lévy–Feller diffusion* through the Feller pseudodifferential operator D_{θ}^{α}, the Feller fractional derivative of order α:

$$\frac{\partial P(x,t)}{\partial t} = D_{\theta}^{\alpha}[P(x,t)] \tag{171}$$

In this notation the inverse Fourier transform of the characteristic function in Eq. (167) is Green's function for Eq. (171), but in a notation where

$$\phi(k,t;\alpha,\theta) = \exp\left[-t|k|^{\alpha}e^{i\theta\pi sign(k)/2}\right] \tag{172}$$

and the Feller pseudodifferential operator acting with respect to the spatial variable x has the Fourier representation

$$\hat{D}_{\theta}^{\alpha} = -|k|^{\alpha}e^{i\theta\pi sign(k)/2} \tag{173}$$

In the symmetric case where $C = 0$ Eq. in (167), using the convolution property of the product of Fourier amplitudes in Eq. (170), we obtain [95]

$$\frac{\partial P(x,t)}{\partial t} = \frac{b}{\pi}\Gamma(\alpha+1)\sin(\alpha\pi/2)\int_{-\infty}^{\infty}\frac{P(x',t)\,dx'}{|x-x'|^{\alpha+1}} \tag{174}$$

Note that the integral term in Eq. (174) is the Reisz fractional derivative, first applied in this context by Seshadri and West [96] and whose solution is the symmetric Lévy distribution. It is worth stressing that in the last few years the approaches based on fractional derivatives, of which Eq. (174) is an early example [95], have received an ever-increasing interest, as shown by the excellent review articles by Metzler and Klafter [97] and Sokolov et al. [78].

The symmetric Lévy distribution that solves Eq. (174) is

$$P(x,t) = \frac{1}{2\pi} \int_{-\infty}^{\infty} e^{ikx} e^{-bt|k|^{\alpha}} dk \tag{175}$$

which satisfies the scaling relation

$$P(x,t) = \gamma^{\frac{1}{\alpha}} P\left(\gamma^{\frac{1}{\alpha}} x, \gamma t\right) \tag{176}$$

as does the more general form of the Lévy α-stable distribution. From Eq. (176) it is clear that the Lévy or Lévy–Feller diffusion diffusion process has the scaling, $x \sim t^{\delta}$, with

$$\delta = 1/\alpha \tag{177}$$

as we demonstrated in Section III. This scaling is consistent with the process generated by the fluctuations of the variable ξ, as verified by numerical simulation [98].

D. Langevin Equation with Lévy Statistics

We now examine the response of a linear dissipative system to Lévy fluctuations using the ordinary Langevin equation,

$$\frac{dV(t)}{dt} + \lambda V(t) = \xi(t) \tag{178}$$

where $V(t)$ is the dynamical variable—say, the velocity of a particle—λ is the dissipation parameter, and the fluctuations are represented by a stationary differential Markov process whose statistics are assumed to be given by a symmetric Lévy distribution

$$p(\xi,t) = \frac{1}{2\pi} \int_{-\infty}^{\infty} e^{ik\xi} e^{-bt|k|^{\alpha}} \tag{179}$$

As we know, if the random force had Gaussian statistics and was delta-correlated in time, we would have an Ornstein–Uhlenbeck process. The variance of the system response would increase linearly in time for early times and be constant at late times. However, when the random force is Lévy-stable the second moment of the system response is infinite.

The linear dynamical equation can be formally integrated to yield

$$V(V(0),t) = V_0 e^{-\lambda t} + \int_0^t e^{-\lambda(t-t')}\xi(t')\,dt' \tag{180}$$

where $V_0 = V(0)$ is the initial value of the velocity variable. West and Seshadri [95] used the phase-space equations to determine the conditional probability density for this process. However, it is somewhat easier to use the characteristic function [53], given by

$$\phi(k,t|V(0)) = \int_{-\infty}^{\infty} e^{iku}P(u,t|u_0)\,du \tag{181}$$

to determine the complete dynamical properties of the system response. Another way to express the characteristic function is in terms of the solution to the Langevin equation

$$\begin{aligned}\phi(k,t|V(0)) &= \langle e^{-ikV(t)}\rangle \\ &= \exp[iku_0e^{-\lambda t}]\left\langle \exp\left[ik\int_0^t e^{-\lambda(t-t')}\xi(t')\,dt'\right]\right\rangle\end{aligned} \tag{182}$$

where $V(0) = u_0$. Doob [99] has shown that a differential Lévy process described by Eq. (179), for an arbitrary analytic function $q(t)$, satisfies the equation

$$\left\langle \exp\left[i\int_0^t q(t')\xi(t')dt'\right|\right]\right\rangle = \exp\left[-\sigma^2\int_0^t |q(t')|^{\alpha}dt'\right|\right] \tag{183}$$

Thus, the characteristic function in (182) can be evaluated to yield

$$\phi(k,t|V(0)) = \exp\left[-iku_0e^{-\lambda t}\right]\exp\left[-\sigma^2_{\alpha\lambda}(t)|k|^{\alpha}\right] \tag{184}$$

where the time-dependent "variance" is

$$\sigma^2_{\alpha\lambda}(t) \equiv \frac{\sigma^2}{\alpha\lambda}\left(1 - e^{-\alpha\lambda t}\right) \tag{185}$$

which agrees with the result obtained by Doob [99] and also by West and Seshadri [95]. The conditional probability density is then given by

$$P(u,t|u_0) = \int_{-\infty}^{\infty} \frac{dk}{2\pi} \exp\left[ik(u - u_0 e^{-\lambda t}) - \sigma_{\alpha\lambda}^2(t)|k|^{\alpha}\right] \tag{186}$$

where the Fourier transform is taken with respect to the centered variable $u - u_0 e^{-\lambda t}$. Hence, the solution to the linear Langevin equation driven by a random force with Lévy statistics has Lévy-stable statistics in the variable $u - u_0 e^{-\lambda t}$ with Lévy index α and parameter given by Eq. (185).

In the long time limit the characteristic function in Eq. (184) reduces to the asymptotic form

$$\phi(k,\infty|V(0)) = \exp\left[-\frac{\sigma^2}{\alpha\lambda}|k|^{\alpha}\right] \tag{187}$$

a characteristic function that is independent of both time and the initial state of the system. At long times the probability distribution given by the inverse Fourier transform of Eq. (187) attains the steady-state form

$$P_{ss}(u) = \frac{1}{2\pi} \int_{-\infty}^{\infty} dk e^{-iku} e^{-b|k|^{\alpha}} \tag{188}$$

where the Lévy parameter is given by $b = \sigma^2/\alpha\lambda$. Thus, the dissipation in the linear Langevin equation leads to a steady state in the presence of Lévy fluctuations. The variance of the system response is, however, infinite for all $t > 0$ and, in particular, for the steady-state distribution given by Eq. (188).

A scale-invariant biological process that has been shown to possess such Lévy statistics is the human heartbeat time series, see Peng et al. [25]. The data consist of digitized electrocardiograms of beat-to-beat heart rate fluctuations over approximately 24 hours or 10^5 beats recorded with an ambulatory monitor. The time series is constructed by recording the interval between adjacent beats as data, for example, let $f(n)$ be the interval between the n and $n+1$ beat. A great deal of variability is observed in the interbeat interval as we discussed in Section II. Peng et al. [25] graph the histogram for the differences in the beat-to-beat intervals $I(n) = f(n+1) - f(n)$ and find that this is a stationary Lévy process such as given by Eq. (188) and shown in Fig. 16. They find that the statistics of healthy and diseased (dilated cardiomyopathy) conditions are the same, that being Lévy-stable with an index $\alpha = 1.7$; however, the spectra for the two cases are quite different.

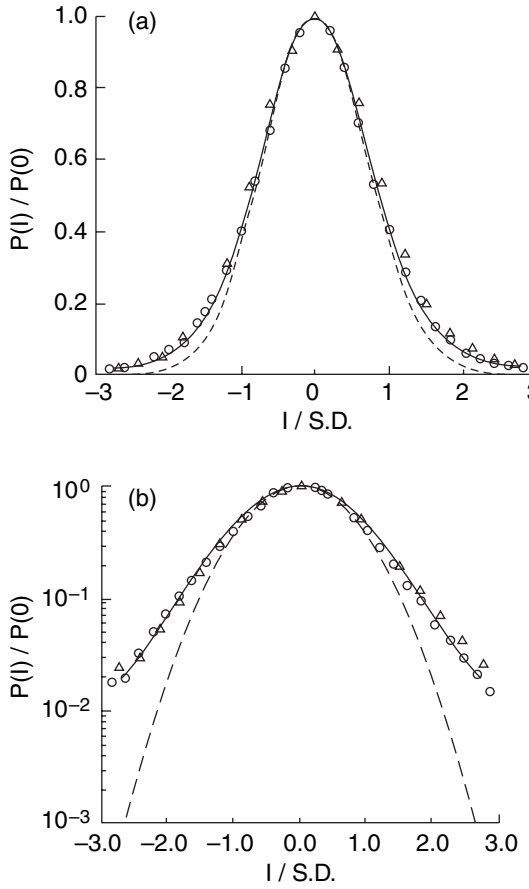

Figure 16. The histogram in the differences between interbeat intervals I for healthy (circles) and diseased (triangles) subjects $P(I)$ is the probability of finding an interbeat increment in the range $[I - \Delta I/2, I + \Delta I/2]$. To facilitate comparison, we divide the variable I by the standard deviation of the increment data and rescale the probability with P(0). In Lévy-stable distributions, α is related to the power-law exponent describing the distribution for large values of the variable, while the width of the distribution is characterized by b. Both histograms are well fitted by a Lévy-stable distribution with $\alpha = 1.7$ (solid line). The dashed line is a Gaussian distribution and is shown for comparison purposes only. Similar fits were obtained for 8 of the 10 normal subjects with heart disease. The slow decay of Lévy-stable distributions for large increment values may be of physiological importance and relate to the dynamics of the system: (*a*) linear–linear scale; (*b*) log–linear scale. (From Peng et al. [25] with permission.)

The power spectrum $S(f)$, the square of the Fourier transform of $I(n)$, yields $S(f) \sim f^{\beta}$, where $\beta = 1 - 2H$ and the mean-square level of the interbeat fluctuations increases as n^{2H}. Here again $H = 0.5$ corresponds to Brownian motion, so that $\beta = 0$ indicates the absence of correlations in the time series $I(n)$ (''white noise''). They observed that for a diseased data set, β is approximately zero in the low-frequency regime, confirming that the $I(n)$ are not correlated over long times. On the other hand, they observed that for the healthy data set, β is approximately equal to 1, indicating a long-time correlation in the interbeat interval differences. The anticorrelated property of $I(n)$ are consistent with a nonlinear feedback system that ''kicks'' the heart rate away from extremes. This tendency operates on a wide range of time scales, not on a beat-to-beat basis. The conclusion is that the different scaling pattern must be a consequence of the ordering of the differences, rather than their statistics, which is to say in the correlations produced by the underlying dynamics.

The power-law spectrum has been observed in a number of dynamical systems having chaotic solutions, see, for example, Reichl [100]. Goldberger and West suggested that the observed spectrum may be a consequence of such dynamics and that one may interpret the modifications in the inverse power-law spectrum as being indicative of pathology and therefore of diagnostic and prognostic value. Loss of heart rate variability has already been described in numerous settings, including multiple sclerosis [101], fetal distress [102], bed-rest deconditioning [103], aging [104], and in certain patients at risk for sudden cardiac death [105]. Presumably, the more severe pathologies will be associated with the greatest loss of spectral power, which we have referred to as *loss of spectral reserve* [106].

V. SUMMARY, CONCLUSIONS, AND SPECULATIONS

If one were to form a hierarchy of understanding of complex phenomena, it would surely start with physics as the most basic, expand into chemistry as large aggregates of atoms and molecules form, become biology as life is breathed into these chemical aggregates, and then form physiology as the phenomenology of human life is explored. Mathematical rigor is demanded at the base of this hierarchy, but mathematical models become less familiar and more suspect as we climb the ladder of complexity from physics to physiology. The standard in physics is the high-order accuracy to which scientists can now theoretically predict the measured value of the fine structure constant or the gravitational constant. The comfortable mathematical models that physicists rely on are missing in the studies of biomedical phenomena, and even where such models exist they do not have the degree of agreement with data that physicists have come to expect. Thus, it might seem to some that the application of mathematical concepts such as fractals, scaling, inverse power-law distributions, and the fractional calculus to physiology, such as done in this chapter, is premature.

However, unless one is willing to neglect the serious attempts that have been and are being made to apply these ideas to the understanding of physiology and medicine, and dismiss the entire activity as misguided, overviews, such as the one given herein, of how these ideas are being implemented are useful.

We have seen in Section II that physiologic time series, such as the interbeat intervals of the human heart, the interstride intervals of human gait, and the interbreath intervals in human breathing, although apparently random, do in fact have long-time memory. This combination of randomness and order has been used as the defining characteristic of complexity in this chapter. In a medical context, this complexity is encountered when attempting to understand physiological phenomena from a hotistic perspective, rather than looking at specific mechanisms. We have used the allometric aggregation technique to establish that such dynamic phenomena are complex, at least in the sense that they generate time series that are statistical fractals. The scaling behavior of such time series determine the overall properties such complex systems must have, much like the older analysis of errors and noise in physical systems. The historical view of complexity involved having a large number of variables, each variable making its individual contribution to the operation of the system and each variable responding in direct proportion to the changes in the other variables. The small differences in the contributions produced the fluctuations in the observed outcome. The linear additive statistics of measurement error or biological noise is not applicable to complex medical phenomena discussed here. The elements in complex physiologic systems are too tightly coupled, so instead of a linear additive process, nonlinear multiplicative statistics more accurately represent the fluctuations. In this chapter we examined how intersystem interactions in a generic physiologic system may give rise to the observed scaling.

The individual mechanisms giving rise to the observed statistical properties in physiologic systems are very different, so we did not attempt to present a common source to explain the observed scaling in walking, breathing, and the beating heart. On the other hand, the physiologic time series for each of these phenomena scale in the same way, so that at a certain level of abstraction the separate mechanisms cease to be important and only the relations matter and not those things being related. It is the relation between blood flow and heart function, between locomotion and postural balance, and between breathing and respiration, which are important. The thesis of complexity theory, insofar as such a theory can be said to exist, is that such relations have a common form for complex phenomena. This assumption is not so dramatic as it might first appear. Consider that traditionally such relations have been assumed to be linear, in which case their control was assumed to be in direct proportion the disturbance. Linear control theory has been the backbone of homeostasis, but fails miserably in describing, for example, the full range of HRV from the running child to the sedate senior, with all the pathologies that await them along the way.

The issue we finally address is how to control complexity. Such control is one of the goals of medicine—in particular, understanding and controlling physiologic networks in order to ensure their proper operation. We distinguish between homeostatic control and allometric control mechanisms. Homeostatic control is familiar and has as its basis a negative feedback character which is both local and instantaneous. Allometric control, on the other hand, is a relatively new concept that can take into account (a) long-term memory, (b) correlations that are inverse power law in time, and (c) long-range interactions in complex phenomena as manifest by inverse power-law distributions in the system variable. Allometric control introduces the fractal character into otherwise featureless random time series to enhance the robustness of physiologic networks by introducing either fractional Brownian motion or fractional Lévy diffusion into the control of the network.

It is not merely a new kind of control that is suggested by the scaling of physiologic time series. Scaling also suggests that the historical notion of disease, which has loss of regularity at its core, is inadequate for the treatment of dynamical diseases. Instead of loss of regularity, we identify the loss of variability with disease, so that a disease not only changes an average measure, such as heart rate, which it does in late stages, but is manifest in changes in heart rate variability at very early stages. Loss of variability implies a loss of physiologic control, and this loss of control is reflected in the change of fractal dimension—that is, in the scaling index of the corresponding time series [56].

The proper operation of physiologic processes is manifest through the scaling of appropriate time series. A measured function denoted by $X(t)$ is said to be homogeneous when the time axis being scaled by a constant γ yields the original function modified by an overall scale $X(\gamma t) = X(t)/\gamma^H$. This scaling behavior generalizes to time series when the measured function is stochastic, and the scaling relation is interpreted in terms of the probability density function rather than the dynamic function itself. This latter scaling is evident in Eq. (35).

In one of the stochastic models discussed Section III, the scaling behavior of the process of interest is a consequence of the two-point stochastic process driving the system having an inverse power-law autocorrelation function. The scaling of the autocorrelation function is only approximate, in that

$$\lim_{t\to\infty} \Phi_\xi(\gamma t) = \Phi_\xi(t)/\gamma^\beta$$

so the scaling arises asymptotically in the noise. The correlation in the noise however, gives rise to scaling in the exact solution to the phase-space equation of evolution given by Eq. (74):

$$X(\gamma t) = X(t)/\gamma^{1-\beta/2}$$

The overall scaling exponent is therefore given by

$$H = 1 - \beta/2$$

where H is the Hurst exponent for the measured time series. In Section II we argue for the ubiquity of such behavior in physiologic phenomena.

Section III steps back from physiology to review various mathematical models that can generate the fractal time series uncovered in Section II for various physiologic time series using allometric aggregation. We began with a brief discussion of simple random walks and showed how the resulting stochastic process for diffusion has a second moment that scales linearly in time. The arguments were extended to fractional random walks to explain anomalous diffusion defined by the second moment [Eq. (19)] scaling nonlinearly in time:

$$\langle X(t)^2 \rangle \propto t^{2H}$$

This leads us to one of the standard, but often inappropriate, explanations of anomalous diffusion using fractional Brownian motion with the probability density

$$p(x,t) = \frac{\exp\left[-\dfrac{x^2}{2Dt^{2H}}\right]}{\sqrt{4\pi Dt^{2H}}}$$

It is clear that this distribution function satisfies the scaling relation Eq. (35) with the scaling index given by $\delta = H$. We note that the variance calculated using fractional Brownian motion distribution is given by the equation for anomalous diffusion. However, we can see that this explanation of anomalous diffusion is not unique and there are multiple statistics that lead to this type of scaling. Consequently, we referred to all such models collectively as fractal stochastic processes and subsequently discussed alternative measures that can distinguish among them.

An alternative to the random walk model in describing diffusion is the Langevin equation, where the microscopic dynamics are linked to a macroscopic rate equation through a stochastic driving force. A simple dichotomous driver with an inverse power-law memory having an index β was shown to yield an asymptotic system response that has the scaling given by Eq. (35) with scaling index $\delta = 1 - \beta/2$. However, these mathematically generated fractal random processes are not in themselves sufficient to properly describe the physiological processes considered herein. The physiologic time series are shown to be multifractal rather than mono-fractal. An example of the multifractal character

of walking is shown in Fig. 9 and that of others (such as heartbeats) are referenced.

A way to distinguish among different ways of generating anomalous diffusion processes is by using diffusion entropy analysis (DEA), where the scaling of the probability density Eq. (35) yields a scaling of the Shannon entropy given by Eq. (91). Consequently, we determined that there are time series for which the scaling index satisfies $\delta = H$, such as fractional Brownian motion, and other time series for which $\delta \neq H$, such as the exact solution to the dichotomous Langevin equation. Also we observed that there is a third class of processes where $\delta = (3 - 2H)^{-1}$, which is valid for Lévy random walks [66] as distinct from Lévy flights.

We discussed in Section IV how the fractional calculus could embody a number of the properties so prevalent in physiologic phenomena, not the least of which being that the evolution of a fractal processes can be described by a fractional differential equation. We showed that the evolution of fractal stochastic process can be described by a fractional Langevin equation in which a fractional differential equation is driven by a stochastic force. In particular, we demonstrated that the fractional calculus could provide a description of the dynamics of an anomalous diffusion process in which the long-time memory is not part of the stochastic driver, as it was in the earlier models, but is actually part of the system's nonlocal dynamics through the fractional derivatives. The multifractal character of certain physiological time series, such as gait and cerebral blood flow, is described by fractional Langevin equations with random indices. The multifractal spectrum is shown to be related to the statistical properties of these random indices.

Finally, the fractional calculus was used to construct fractional diffusion equations. One such equation, in particular, models the evolution of the Lévy α-stable probability density describing Lévy diffusion, another mechanism for generating anomalous diffusion. It was shown that this probability density satisfies the scaling relation [Eq. (35)] with the Lévy index α such that $\delta = 1/\alpha$. The dynamics of a Lévy diffusion process, using a Langevin equation, were also considered. The probability density for a simple dissipative process being driven by Lévy noise is also Lévy but with a change in parameters. This is a possible alternate model of the fluctuations in the interbeat intervals for the human heart shown to be Lévy stable over a decade ago [25].

The well-being of the body's system-of-systems is measured by the fractal scaling properties of the various dynamic subsystems, and such scaling determines how well the overall complexity is maintained. Once the perspective that disease is the loss of complexity has been adopted, the strategies presently used in combating disease must be critically examined. Life support equipment is one such strategy, but the tradition of such life support is to supply blood at the average rate, of the beating heart, to ventilate the lungs at their average rate,

and so on. So how does the new perspective regarding disease influence the traditional approach to healing the body?

Alan Mutch, of the University of Manitoba, argues that both blood flow and ventilation are delivered in a fractal manner in both space and time in a healthy body. However, during critical illness, conventional life support devices deliver respiratory gases by mechanical ventilation or blood by cardiopulmonary bypass pump in a monotonously periodic fashion. This periodic driving overrides the natural áperiodic operation of the body. Mutch [107] speculates that these devices result in the loss of normal fractal transmission and consequently:

> . . . life support systems do more damage the longer they are required and are more problematic the sicker the patient . . . . We hypothesize that loss of fractal transmission moves the system through a critical point . . . to transform a cohesive whole to one where organ systems are no longer as well connected.

Disease as the loss of complexity is consistent with the view that complex phenomena have a multiplicity of failure modes. These failure modes result in phenomena changing character, invariably becoming simpler with an accompanying inability to carryout their function. A cascade of failures is not so much a consequence of the initiating event as it is the result of the state of the network when the event is initiated.

It is, in part, the irreversibility of failure cascades that makes them so formidable. In medicine such failure cascades may be manifest as multiple organ dysfunction syndrome (MODS) that rapidly accumulates following a minor insult; MODS is the leading cause of death in intensive care units. As Buchman [108] points out:

> Despite timely and appropriate reversal of the enticing insult . . . many patients develop the syndrome. Mortality is proportional to the number and depth of system dysfunction and the mortality of MODS after (for example) repair of ruptured abdominal aortic aneurysm is little changed despite three decades of medical progress.

One of the consequences of the traditional view of disease is what Buchman [108] calls ''fix-the-number'' imperative:

> If the bicarbonate level is low, give bicarbonate; if the urine output is low, administer a diuretic; if the bleeding patient has a sinking blood pressure, make the blood pressure normal. Unfortunately, such interventions are commonly ineffective and even harmful. For example, sepsis—which is a common predecessor of MODS—is often accompanied by hypocalcaemia. In controlled experimental conditions, administering calcium to normalize the laboratory value increases mortality.

Consequently, one's first choice of options, based on an assumed simple linear causal relationship between input and output as in homeostatsis, is probably wrong.

A number of scientists [109] have demonstrated that the stability of hierarchal biological systems is a consequence of the interactions among the elements of the system. Furthermore, there is an increase in stability resulting from the nesting of systems within systems—organelles into cells, cells into tissue, tissues into organs, and so on, up from the microscopic to the macroscopic. Each system level confers additional stability on the overall fractal structure. The fractal nature of the system suggests a basic variability in the way systems are coupled together. For example, the interaction between cardiac and respiratory cycles is not constant, but adapts to the physiologic challenges being experienced by the body.

A number of scientists have arrived at remarkably similar conclusions regarding the nature of disease that is quite different from the traditional one. Take, for example, the following observation made by Buchman [108]:

> . . . Herein, we have suggested that breakdown of network interactions may actually cause disease, and when this breakdown is widespread the clinical manifestation is the multiple organ dysfunction syndrome. If the hypothesis is correct, then network dysfunction might be expected at multiple levels of granularity, from organ systems to intracellular signal molecules. Restoration of network integrity may be a reasonable therapeutic goal, and a more permissive approach to clinical support (including algorithms that simulate biological variability) might facilitate restoration of network complexity that now appears essential to health.

Or those made by Mutch [107]:

> The layer upon layer of fractal redundancy in scale-free biological systems suggests that attack at one level does not place the organism at undue risk. But attack at vital transmission nodes can cause catastrophic failure of the system. The development of multiple organ dysfunction syndrome (MODS) in critically ill humans may be such a failure. Once devolved, death almost inevitably ensues. The similarity to concerted attack on vital Internet router nodes is evident. Patients managed by conventional non-fractal life support may sustain further unintentional attack on a devolving scale-free system due to loss of normal fractal transmission. Returning fractal transmission to life support devices may improve patient care and potentially offer benefit to the sickest of patients.

We conclude with a number of observations:

1. The empirical evidence overwhelmingly supports the interpretation of the time series analysis that complex physiologic phenomena are described by fractal stochastic processes. Furthermore, the fractal nature of these time series is not constant in time but changes with the vagaries of the interaction of the system with its environment, and therefore these phenomena are multifractal.

2. The scaling index or fractal dimension marks the system's response and can be used as an indicator of the system's state of health. Since the fractal dimension is also a measure of the level of complexity, the change in dimension with disease suggests a new definition of disease as a loss of complexity, rather than the loss of regularity [56]. This observation was first made by Goldberger and West, see, for example, Ref. [110].
3. The fractal dynamics of complex physiologic systems can be modeled using the fractional rather than the ordinary calculus because the changes in the fractal functions necessary to describe physiologic complexity remain finite in the former formalism but diverge in the latter [53].

References

1. B. B. Mandelbrot, *Fractals, Form, Chance and Dimension*, W. H. Freeman, San Francisco, 1977.
2. E. Broda, *Ludwig Boltzmann, Man-Physicist-Philosopher*, Ox Bow Press, Woodbridge, 1983.
3. B. B. Mandelbrot, *The Fractal Geometry of Nature*, W. H. Freeman, San Francisco, 1982.
4. E. Schrödinger, *What Is Life? The Physical Aspects of the Living Cell*, Cambridge University Press, London, 1943.
5. B. J. West and W. Deering, Fractal physiology for physicists: Lévy statistics. *Phys. Rep.* **246**, 1–100 (1994).
6. C. K. Peng, J. Mistus, J. M. Hausdorff, S. Havlin, H. E. Stanley, and A. L. Goldberger, Long-range anticorrelations and non-Gaussian behavior of the heartbeat. *Phys. Rev. Lett.* **70**, 1343–46 (1993).
7. B. Suki, A. M. Alencar, U. Frey, P. Ch. Ivanov, S. V. Buldyrev. A. Majumdar, H. E. Stanley, C. A. Dawson, G. S. Krenz, and M. Mishima, Fluctuations, noise and scaling in the cardiopulmonary system. *Fluctuations and Noise Lett.* **3**, R1–R25 (2003).
8. B. J. West, R. Zhang, A. W. Sanders, J. H. Zuckerman, and B. D. Levine, Fractal fluctuations in transcranial Doppler signals. *Phys. Rev. E* **59**, 3492 (1999).
9. B. J. West, A. Maciejewsk, M. Latka, T. Sebzda, and Z. Swierczynski, Wavelet analysis of scaling properties of gastric electrical activity. To appear in *Am. J. Physiol*.
10. J. M. Hausdorff, C.-K. Peng, Z. Ladin, J. Y. Ladin, J. Y. Wei, and A. L. Goldberger, Is walking a random walk? Evidence for long-range correlations in stride interval of human gait. *J. Appl. Physiol.* **78**(1), 349–358 (1995).
11. L. Griffin, D. J. West, and B. J. West, Random stride intervals with memory. *J. Biol. Phys.* **26**, 185–202 (2000).
12. J. M. Hausdorff, L. Zemany, C.-K. Peng and A. L. Goldberger, Maturation of gait dynamics: stride-to-stride variability and its temporal organization in children. *J. Appl. Physiol.* **86**, 1040–1047 (1999).
13. N. Scafetta, L. Griffin, and B. J. West, Holder exponent spectra for human gait. *Physica A* **328**, 561–583 (2003).
14. B. J. West, L. A. Griffin, H. J. Frederick, and R. E. Moon, The independently fractal nature of respiration and heart rate during exercise under normobaric and hyperbaric conditions. To appear in *Respiratory Physiol. Neurobiol.*

15. G. I. Barenblatt, *Scaling Phenomena in Fluid Mechanics*, Cambridge University Press, Cambridge, 1994.
16. J. S. Huxley, *Problems of Relative Growth*, Dial Press, New York, 1931.
17. L. R. Taylor, Aggregation, variance and the mean. *Nature* **189**, 732–735 (1961).
18. L. R. Taylor and R. A. J. Taylor, Aggregation, migration and population mechanics. *Nature* **265**, 415–421 (1977).
19. J. C. Willis, *Age and Area: A Study in Geograhical Distribution and Origin of Species*, Cambridge University Press, New York, 1922.
20. L. R. Taylor and I. P. Woiwod, Temporal stability as a density-dependent species characteristic. *J. Animal Ecol.* **49**, 209–224 (1980).
21. J. B. Bassingthwaighte, L. S. Liebovitch, and B. J. West, *Fractal Physiology*, Oxford University Press, New York, 1994.
22. Heart rate variability. *Eur. Heart J.* **17**, 354–381 (1996).
23. B. J. West, *Physiology, Promiscuity and Prophecy at the Millennium: A Tale of Tails, Studies of Nonlinear Phenomena in Life Science*, Vol. 7, World Scientific, Hackensack, NJ, 1999.
24. B. Suki, A. M. Alencar, U. Frey, P. C. Ivanov, S. V. Buldyrev, A. Majumdar, H. E. Stanley, C. A. Dawson, G. S. Krenz, and M. Mishima, Fluctuations, noise and scaling in the cardio-pulmonary system. *Fluctuations and Noise Lett.* **3**, R1–R25 (2003).
25. C. K. Peng, J. Mistus, J. M. Hausdorff, S. Havlin, H. E. Stanley, and A. L. Goldberger, Long-range anticorrelations and non-Gaussian behavior of the heartbeat. *Phys. Rev. Lett.* **70**, 1343–1346 (1993).
26. B. J. West, Physiology in fractal dimension: Error tolerance. *Ann. Biomed. Eng.* **18**, 135–149 (1990).
27. H. H. Szeto, P. Y. Cheng, J. A. Decena, Y. Chen, Y. Wu, and G. Dwyer, Fractal properties of fetal breathing dynamics. *Am. J. Physiol.* **262** (*Regulatory Integrative Comp. Physiol.* **32**), R141–R147 (1992).
28. G. S. Dawes, H. E. Cox, M. B. Leduc, E. C. Liggins, and R. T. Richards, Fractal properties of fetal breathing dynamics. *J. Physiol. Lond.* **220**, 119–143 (1972).
29. W. A. C. Mutch, S. H. Harm, G. R. Lefevre, M. R. Graham, L. G. Girling, and S. E. Kowalski, Biologically variable ventilation increases arterial oxygenation over that seen with positive end-expiratory pressure alone in a porcine model of acute respiratory distress syndrome. *Crit. Care Med.* **28**, 2457–2464 (2000).
30. W. A. Altemeier, S. McKinney, and R. W. Glenny, Fractal nature of regional ventilation distribution. *J. Appl. Physiol.* **88**, 1551–1557 (2000).
31. C. K. Peng, J. Metus, Y. Li, C. Lee, J. M. Hausdorff, H. E. Stanley, A. L. Goldberger, and L. A. Lipsitz, Quantifying fractal dynamics of human respiration: Age and gender effects. *Ann. Biomed. Eng.* **30**, 683–692 (2002).
32. J. W. Kantelhardt, T. Penzel, S. Rostig, H. F. Becker, S. Havlin, and A. Bunde, Breathing during REM and non-REM sleep: Correlated versus uncorrelated behaviour. *Physica A* **319**, 447–457 (2003).
33. C. L. Webber, Rhythmogenesis of deterministic breathing patterns, in *Rhythms in Physiological Systems*, H. Haken and H. P. Koepchen, eds. Springer, Berlin, 1991, pp. 177–191.
34. Vierordt, Ueber das Gehen des Menschen in Gesunden und kranken Zustaenden nach Selbstregistrirender Methoden, Tuebingen, Germany, 1881.
35. J. M. Hausdorff, S. L. Mitchell, R. Firtion, C. K. Peng, M. E. Cudkowicz, J. Y. Wei, and A. L. Goldberger, Altered fractal dynamics of gait: Reduced stride-interval correlations with aging and Huntington's disease. *J. Appl. Physiol.* **82**, (1997).

36. B. J. West and L. Griffin, Allometric control of human gait. *Fractals* **6**, 101–108 (1998); B. J. West and L. Griffin, Allometric control, inverse power laws and human gait. *Chaos, Solitons & Fractals* **10**, 1519–1527 (1999).
37. R. L. Marsh, D. J. Ellerby, J. A. Carr, H. T. Henry and C. I. Buchanan, Partitioning the energetics of walking and running: Swinging the limbs is expensive. *Science* **303**, January (2004).
38. B. J. West and L. Griffin, *Biodynamics: Why the Wirewalker Doesn't Fall*, John Wiley & Sons, New York (2003).
39. J. J. Collins and C. J. De Lucca, Random walking during quiet standing. *Phys. Rev. Lett.* **73**, 764–767 (1994).
40. J. W. Blaszczyk and W. Klonowski, Postural stability and fractal dynamics. *Acta Neurobiol. Exp.* **61**, 105–112 (2001).
41. G. L. Gernstein and B. Mandelbrot, Random walk models for the spike activity of a single neuron, *Biophys. J.* **4**, 41–68 (1968).
42. M. C. Teich, C. Heneghan, S. B. Lowen, T. Ozaki, and E. Kaplan, Fractal character of the neural spike train in the visual system of the cat, *Opt. Soc. Am.* **14**, 529–546 (1997).
43. A. Babloyantz and A. Destexhe, Low-dimensional chaos in an instance of epilepsy. *Proc. Natl. Acad. Sci. USA* **83**, 3515–3517 (1987).
44. P. Langevin, *C. R. Acad. Sci. Paris*, 530 (1908).
45. J. Beran, *Statistics for Long-Memory Processes*, Chapman & Hall, New York, 1994.
46. J. T. M. Hosking, Fractional differencing. *Biometrika* **68**, 165–176 (1982).
47. N. Scafetta and P. Grigolini, Scaling detection in time series: Diffusion entropy analysis. *Phys. Rev. E* **66**, 036130 (2002).
48. T. Gneiting and M. Schlather, Stochastic models that separate fractal dimension and the hurst effect. *SIAM Rev.* **46**, 269–282 (2004).
49. P. Allegrini, P. Grigolini, and B. J. West, Dynamical approach to Lévy processes. *Phys. Rev. E* **54**, 4760 (1996).
50. J. Klafter, M. F. Shlesinger, and G. Zumofen, *Phys. Today* **49**(2), 33 (1996); *Lect. Notes in Phys.* **519**, 15 (1998).
51. T. Geisel, in *Lévy Flights and Related Topics in Physics*, Proceedings, Nice, France; Editors, M. F. Shlesinger, G. M. Zaslavsky, and U. Frisch, eds., *Lecture Notes in Physics* **450**, 153 (1995).
52. M. Bologna, P. Grigolini, and B. J. West, Strange kinetics: Conflict between density and trajectory description. *Chem. Phys.* **284**, 115–128 (2002).
53. B. J. West, M. Bologna, and P. Grigolini, *Physics of Fractal Operators*, Springer, New York, 2003.
54. E. Barkai, R. Metzler, and J. Klafter, *Phys. Rev. E* **61**, 132 (2000).
55. R. Metzler and T. F. Nonnenmacher, *Phys. Rev. E* **57**, 6409 (1998).
56. B. J. West, *Where Medicine Went Wrong, Rediscovering the Path to Complexity*, to be published (2005).
57. K. Falconer, *Fractal Geometry*, John Wiley & Sons, New York, 1990.
58. J. Feder, *Fractals*, Plenum Press, New York, 1988.
59. J. F. Muzy, E. Bacry, and A. Arnedo, *Phys. Rev. E* **47**, 875 (1993).
60. B. J. West, M. Latka, M. Glaubic-Latka, and D. Latka, Multifractality of cerebral blood flow. *Physica A* **318**, 453–460 (2003).

61. W. Feller, *An Introduction to Probability Theory and Its Applications*, Vol. 2, John Wiley and Sons, New York, 1966.
62. D. Schertzer, S. Lovejoy, F. Schmitt, Y. Chigirinskays, and D. Marsan, Multifractal cascade dynamics and turbulent intermittency. *Fractals* **5**, 427 (1997).
63. B. V. Gnedenko and A. N. Kolmogorov, *Limit Distributions for Sums of Independent Random Variables*, Addison-Wesley, Cambridge, MA, 1954.
64. E. Montroll and B. J. West, An enriched collection of stochastic processes, in *Fluctuation Phenomena*, E. W. Montroll and J. L. Lebowitz, eds., North Holland Personal Library, Amsterdam, 1987; 1st ed. 1979.
65. M. Shlesinger, J. Klafter, and B. J. West, Lévy dynamics of enhanced diffusion: Applications to turbulence. *Phys. Rev. Lett.* **58**, 1100–1103 (1987).
66. N. Scafetta and B.J. West, Multiscale Comparative Analysis of Time Series and a Discussion on 'Earthquake Conversations' in California. *Phys. Rev. Lett.* **92**, 138501 (2004).
67. J. Perrin, Mouvement brownien et moleculaire culaire. *Ann. chim. Phys. VIII* **18**, 5–114; translated by F. Soddy as *Brownian Movement and Molecular Reality*, Taylor and Francis, London.
68. E. Ott, *Chaos in Dynamical Systems*, Cambridge University Press, New York, 1993.
69. R. J. Abraham and C. D. Shaw, *Dynamics-The Geometry of Behavior, Part 1* (1982), *Part 2* (1983), *Part 3* (1985), and *Part 4* (1988), Aerial Press, Santa Cruz, CA.
70. K. M. Kolwankar, Studies of Fractal Structures and Processes using Methods of the Fractional Calculus, unpublished thesis, University of Pune, 1997.
71. D. Ruelle, *Chaotic Evolution and Strange Attractors*, Cambridge University Press, Cambridge, 1989.
72. M. F. Shlesinger, Fractal time and 1/f noise in complex systems. *Ann. N.Y. Acad. Sci.* **504**, 214 (1987).
73. Y. N. Rabotnov, *Elements of Hereditary Solid Mechanics*, MIR , Moscow, 1980.
74. H. E. Stanley, *Introduction to Phase Transitions and Critical Phenomena*, Oxford University Press, Oxford, 1979.
75. P. Meakin, *Fractals, Scaling and Growth Far from Equilibrium*, Cambridge Nonlinear Science Series 5, Cambridge University Press, Cambridge, 1998.
76. This letter was translated by B. Mandelbrot and is contained in the Historical Sketches of his second book [3].
77. R. Hilfer, ed., *Applications of Fractional Calculus in Physics*, World Scientific, Singapore, 2000.
78. I. Sokolov, J. Klafter, and A. Blumen, Fractional Kinetics. *Phys. Today* **Nov**. (2002).
79. L. F. Richardson, Atmospheric diffusion shown on a distance-neighbor graph. *Proc. R. Soc. Lond. A* **110**, 709–737 (1926).
80. M. F. Shlesinger and B. J. West, Complex fractal dimension of the bronchial tree. *Phys. Rev. Lett*. **67**, 2106–2109 (1991).
81. D. Sornette, Discrete scale invariance and complex dimensions. *Phys. Rep.* **297**, 239–270 (1994).
82. A. Rocco and B. J. West, Fractional calculus and the evolution of fractal phenomena. *Physica A* **265**, 535 (1999).
83. T. F. Nonnenmacher and R. Metzler, On the Riemann-Liouville fractional calculus and some recent applications. *Fractals* **3**, 557 (1995).

84. K. S. Miller and B. Ross, *An Introduction to the Fractional Calculus and Fractional Differential Equations*, John Wiley & Sons, New York, 1993.

85. V. Kobelev and E. Romanov, Fractional Langevin equation to describe anomalous diffusion. *Prog. Theor. Phys. Suppl.* **139**, 470–476 (2000).

86. See, for example, K. Lindenberg and B. J. West, *The Nonequilibrium Statistical Mechanics of Open and Closed Systems*, VCH, New York, 1990.

87. E. Lutz, Fractional Langevin equation. *Phys. Rev. E* **64**, 051106 (2001).

88. B. Rajagopalon and D. G. Tarboton, *Fractals* **1**, 6060 (1993).

89. P. C. Ivanov, L. A. N. Amaral, A. L. Goldberger, S. Havlin, M. G. Rosenblum, Z. R. Struzik, H. E. Stanley, Multifractality in human heartbeat dynamics. *Nature* **399**, 461 (1999).

90. B.J. West, M. Latka, M.Galaubic-Latka, and D. Latka, Multifactility of cerebral blood flow. *Physica A* **318**, 453–460 (2003).

91. R. Zhang, J. H. Zuckerman, C. Giller, and B. D. Levine, *Am. J. Physiol.* **274**, H233 (1999).

92. S. Rossitti and H. Stephensen, *Acta Physiol. Scand.* **151**, 191 (1994).

93. B. J. West, R. Zhang, A. W. Sanders, J. H. Zuckerman, and B. D. Levine, Fractal fluctuations in transcranial Doppler signals. *Phys. Rev. E* **59**, 3492 (1999).

94. R. Gorenflo and F. Mainardi, Feller fractional diffusion and Lévy stable motion. Preprint 1999.

95. B. J. West and V. Seshadri, Linear systems with Lévy fluctuations. *Physica A* **113**, 2030216 (1982).

96. V. Seshadri and B. J. West, Fractal dimensionality of Lévy processes. *Proc. Natl. Acad. Sci. USA* **79**, 4051 (1982).

97. R. Metzler and J. Klafter, *Phys. Rep.* **339**, 1 (2000).

98. M. Annunziato and P. Grigolini, The Markov approximation revisited: Inconsistency of the standard quantum Brownian motion model. *Phys. Lett. A* **269**, 31 (2000).

99. J. L. Doob, *Stochastic Processes*, John Wiley & Sons, New York (1953).

100. L. E. Reichl, *The Transition to Chaos*, Springer, New York, 1992.

101. B. Neubauer and H. J. G. Gundersen, Analysis of heart rate variations in patients with multiple sclerosis. A simple measure of autonomic disturbances using an ordinary ECG. *J. Neurol. Neuosurg. Psychiatry* **41**, 417–419 (1978).

102. V. Kariniemi and P. Ammälä, Short-term variability of fetal heart rate during pregnancies with normal and insufficient placental function. *Am. J. Obster. Gynecol.* **139**, 33–37 (1981).

103. A. L. Goldberger, D. Goldwater, and V. Bhargava, Atrophine unmasks bed-rest deconditioning effect in healthy men: A spectral analysis of cardiac interbeat intervals. *J. Appl. Physiol.* **61**, 1843–1848 (1986).

104. J. L. Waddington, M.J. MacCulloch and J. E. Sambrooks, Resting heartrate variability in man declines with age. *Experientia* **35**, 1197–1198 (1979).

105. A. L. Goldberger, L. Findley, M. J. Blackburn, and A. J. Mandell, Nonliear dynamics of heart failure: implications of long-wavelength cardiopulmonary osciallations. *Am. Heart J.* **107**, 612–615 (1984); G. A. Myers, G. J. Martin, and N. M. Magrid et al. Power spectral analysis of heart rate variability in sudden cardiac death: Comparison to other methods. *IEEE Trans. Biomed. Eng.* **33**, 1149–1156 (1986).

106. A. L. Goldberger, V. Bhargava, B. J. West, and A. J. Mandell, On a mechanism of cardiac electrical stability: The fractal hypothesis. *Biophys. J.* **48**, 525–528 (1985); A. L. Goldberger and B. J. West, Applications of nonlinear dynamics to clinical cardiology. *Ann. NY Acad. Sci.* **504**, 195–213 (1987).

107. A. Mutch, Health, ''small-worlds'', fractals and complex networks: An emerging field. *Med. Sci. Monit.* **9**, MT55–MT59 (2003).

108. T. G. Buchman, Physiologic failure: Multiple organ dysfunction syndrome. Preprint.

109. G. A. Chauvet, Hierarchical functional organization of formal biological systems: A dynamical approach. I. The increase of complexity by self-association increases the domain of stability of a biological system. *Philos. Trans. R. Soc. Lond. B Biol. Sci*. **339**(1290), 425–44 (1993).

110. A. L. Goldberger, D. R. Rigney and B. J. West, Chaos and Fractals in Human Physiology, Scientific American, Feb., 42–49, (1990).